공학박사 학위논문

Transmittance characterization of guided-mode resonance filter in THz region

테라헤르츠 영역에서 유도-모드 공진 필터의 투과 특성

지도교수 전 태 인

2019년 2월

한국해양대학교 대학원

전기전자공학과

박 현 상

본 논문을 박현상의 공학박사 학위논문으로 인준함.

위원장 장 낙 원 (인)
위 원 전 태 인 (인)
위 원 서 동 환 (인)
위 원 주 양 익 (인)
위 원 장 규 하 (인)

2019년 2월 20일

한국해양대학교 대학원

Table of contents

▶ The work presented in this thesis is based on the work published in the following papers in refereed journals :

1. H. S. Bark, and T. -I. Jeon, "Dielectric film sensing with TE mode of terahertz guided-mode resonance," Opt. Express 26(26), 34547-34556 (2018).

2. H. S. Bark, and T. -I. Jeon, "Tunable Terahertz guided-mode resonance terahert filter with a varialbe grating period," Optics Express 36(22), 29353-29362 (2018).

3. H. S. Bark, and G. J. Kim, and T. -I. Jeon, "Transmission characteristics of all-dielectric guided-mode resonance filter in the THz region," Scientific Reports 8,13570 (2018).

4. T. K. Nguyen, W. T. Kim, B. J. Kang, H. S. Bark, K. Kim, J. Lee, L. Park, T. -I. Jeon, F. Rotermund, "Photoconductive dipole antennas for efficient terahertz receiver," Optics Communications 383, 50-56 (2017).

5. H. S. Bark, and T. -I. Jeon, "Pressure-dependent refractive indices of gases by THz time-domain spectroscopy," Optics Express 24(25), 29040-29047 (2016).

6. Y. B. Ji, I. -S. Moon, H. S. Bark, S. H. Kim, D. W. Park, S. K. Noh, Y. -M. Huh, J. -S. Suh, S. J. Oh, and T. -I. Jeon, "Terahertz otoscope and potential for diagnosing otitis media," Biomedical Optics Express 1201-1209 (2016).

7. H. S. Bark, J. S. Zha, E. S. Lee, and T. -I. Jeon, "Thin layer terahertz sensing using two-channel parallel-plate waveguides" , Optics Express,16738-16744 (2014).

List of Figures

테라헤르츠 영역에서 유도-모드 공진 필터의 투과 특성

박 현 상

전 기 전 자 공 학 부

한국 해양 대학교 공과 대학원

요약문

2장은 두 가지 물리적 현상을 결합된 격자의 회절과 슬래브 도파관 유도 특성을 결합하여 GMR 필터의 원리를 설명합니다. GMR 방정식으로 부터 공진 발생 예상 범위를 계산 합니다. GMR 필터는 구조적인 변화에 따라 공진 주파수가 민감하게 변경됩니다. 그 이외에 테라헤르츠 빔에 포함된 격자의 개수, 격자의 내부 모서리 곡률, 재료의 loss tangent (δ), 테라헤르츠 빔의 확산 그리고 투과율은 측정 시간 또는 GMR 필터의 구조, 제작, 실험적 측정의 오류들을 서술 하였습니다.

3장에서는 테라헤르츠 영역에서 GMR 필터를 설계하고 투과율의 특성을 조사하였습니다. 테라헤르츠 빔의 입사각과 편광에 변화에 따라 GMR 필터의 투과율의 특성을 FDFD 시뮬레이션하고 측정하였습니다. 제한된 빔 크기에서 감소된 GMR 필터의 성능은 2 개의 동일한 GMR 필터를 사용하여 완벽한 공진을 완성 하였습니다. GMR 필터와 주변 굴절률의 차이를 감소 줄이고 고차 모드 공진을 완벽히 제거 하였습니다.

4 장에서는 GMR 필터는 FDFD 시뮬레이션은 격자의 주기의 변화에 따라 공진 주파수가 이동을 잘 설명합니다. 3가지 다른 격자의 주기로 설계된 GMR 필터는 공진 주파수 위치는 주기에 크기에 따라 저주파로 이동되어 측정됩니다. 우리는 위치에 따라 격자의 주기가 변하는 마름모 모양의 GMR 필터를 설계 하였습니다. 마름모의 경사도에 따른 조절 가능한 격자의 주기 변화 범위는 결정 됩니다. GMR 필터와 TGMR 필터의 낮은 손실로 2개 필터로 독립된 공진을 측정하였습니다.

5 장에서는 설계된 mGMR 필터는 편광 변화에 따라 공진 크기가 변경 됩니다. 독립된 2 장의 mGMR 필터를 이용하여 두 개의 필터의 엇갈린 각도 변화와 편광의 변화에 따른 공진의 크기 변화 범위를 조절 가능합니다. = 90 일 때 편광에 둔감한 필터의 특성을 나타냅니다. 최종적으로 결합된 2장의 mGMR 필터는 더욱 안정화된 편광에 둔감한 필터의 특성을 나타냅니다. 테라헤르츠 영역에서 필터의 편광 특성을 조정 가능합니다.

6 장에서, mGMR 필터와 결합된 다양한 종류의 필름은 새로운 특성을 가지는 GMR 필터로 완성 됩니다. 필름의 두께, 굴절률 변화로 공진의 이동과 멀티 공진을 유도 할 수 있습니다. 또한, 필름의 loss tangent (δ)는 공진의 크기에 영향을 줍니다. mGMR 필터에 의해 생성 된 공진은 필름의 속성에 민감하게 주파수 이동과 크기로 나타납니다. 기존의 분광법보다 민감하게 물질의 굴절률, 두께 및 흡수 차이를 쉽게 감지 할 수 있습니다.

키워트 : 테라헤르츠, 유도-모드 공진; 필터; 필름 센서;

Chapter 1 Introduction

1.1 Motivation

The direction of the electromagnetic wave is determined by using the diffraction using the slit or the prism, and the lens surface using the refractive index difference. There are many studies using periodic metal patterns and repeating structures to precisely control the direction of electromagnetic waves. First, a frequency selective surface (FSS) is applied as a filter [1] or absorber [2] by selectively changing the direction of the selected frequency. Second, Metasurface [3] is non-planar, non-resonance metamaterials (MMs) [4], and you can modify the wavefront arbitrarily by adjusting the phase delay using the surface metal pattern. Third, MMs refers to composite materials that are deliberately designed to provide material properties that are not obtainable with regular materials using periodic patterns and structures. Using anisotropic materials and negative refractive index, it is possible to design an ideal lens and clock able device.

Recently, the development of THz wave generation and measurement technology has overcome THz Gab [5], extending the range of communication, image and non-destructive inspection using new THz wave. At the same time, the demand for electromagnetic technology that can operate on THz is also rapidly increasing. In a typical way of FSS structure, the guided-mode resonance (GMR) structure [6] using all the dielectrics not yet applied to the THz region has sufficient capacity. GMR structures have various advantages and disadvantages. Advantages

include the ability to design and fabricate very low loss structures from all dielectrics. It is possible to fabricate monolithically simple structure rather than complex structure with metal pattern on substrate. In addition, it is advantageous to higher power than structure using metal [7]. Disadvantages are that GMR filters are larger and bulkier than the same metal structures, but they are sufficiently digested in THz. They generally have limited field of view and bandwidth response compared to metal devices. GMR structures reinforcing the disadvantages are already reported. The GMR structure is very sensitive to structural deformation and can be converted into an advantage as a sensitive sensor.

The period of the FSS structure increases proportionally with the size of the wavelength. As the frequency increases, the size of the wavelength decreases and the size of the overall structure is reduced. However, optics include complex designs and processes involving substrate in the design of GMR structures with too small a wavelength size. On the other hand, in the micro area, there is a disadvantage that the wavelength is low and the frequency is large and the size of the device is large. However, a single material can be designed and manufactured with a simple structure.

In terms of manufacturing and design, it is small enough in the THz region, which has a relatively shorter wavelength than microwave. The complex and compact structure in the optical region can be replaced by a simple structure as the wavelength becomes larger with THz. Designed to be a few hundred micro-sized, the GMR structure can maintain a simple structure and maintain a compact size.

In terms of development, THz is a well-developed blue ocean area that can combine the technologies of both micro and optical technologies. Recent developments in THz wave generation and measurement technology have led to various demands such as waveguide and filter due to the overcoming of THz Gab. Techniques developed at different wavelengths accumulated up to now have many possibilities for application development by applying scale up and down.

The MMs that have been studied extensively in the THz region have limitations in their fabrication methods and their inability to use them at high power due to their low transmission efficiency and metal. In this paper, we first designed and fabricated a GMR filter that operates in the THz region as an all-dielectric material. GMR filters have higher Q-factor and higher transmittance than parallel waveguide [8], photonics crystal [9], and MMs filters [10]. In addition, THz has a potential to develop various devices because of its simple design and easy fabrication by using a dielectric material that has dynamic property changes. In this paper, we developed various devices using GMR structure.

1.2 Outline

Chapter 2, explains the principle of GMR filter. Resonance is measured when the diffraction wave in the grating matches the slab waveguide induction condition. The resonance expected range can be calculated from the GMR equation. The resonance frequency of the GMR filter changes sensitively to changes in the structure of the GMR filter. In addition, the errors of the structure, fabrication and experimental measurement of the GMR filter arise from the number of gratings contained in the THz beam, the inner corner curvature of the grating, the loss tangent (δ) of the material , the diffusion of the THz beam, and the measurement scan time.

In Section 3, the GMR filter was designed in the THz region and the transmittance characteristics were investigated. Transmittance characteristics of GMR filter were simulated by Finite-Difference Frequency-Domain (FDFD) simulation and measured by TDS-system according to incident angle and the polarization change of THz beam. Reduced performance at a limited beam size was overcome using two identical GMR filters. Decreasing the refractive index difference around the GMR filter and the GMR filter completely eliminates the higher-order mode resonance.

In section 4, the FDFD simulation of the GMR filter explains the resonance frequency shift according to the change of the grating period. The characteristics of a GMR filter designed with three types of grating periods are measured by moving the resonance frequency according to the grating period size. We designed a rhombic GMR filter

with varying grating periods depending on the position. Depending on the slope of the rhomb, the tunable range of the grating period is determined. The low transmittance loss of the two independent GMR and TGMR filters makes it easy to adjust the double resonance.

In Section 5, the designed mGMR filter changes the amplitude of resonance according to the polarization change. Two separate mGMR filters can be used to resize the resonance according to changes in the tilted angle. At $\alpha = 90°$, the characteristic of the filter is not sensitive to the polarization. Finally, the two combined mGMR filters represent a more stable polarization sensitive filter. The polarization characteristics of the GMR filter are tunable in the THz region.

In chapter 6, various types of films combined with mGMR filters are completed with new properties. Film thickness and refractive index change can induce resonance shift and multi resonance. Also, the loss tangent (δ) of a film affects the magnitude of the resonance. The resonance generated by the mGMR filter appears as a frequency shift and magnitude sensitive to the properties of the film. It is easier to detect the refractive index, thickness and absorption difference of a substance than conventional spectroscopy.

Chapter 2 Theory

2.1 Theory

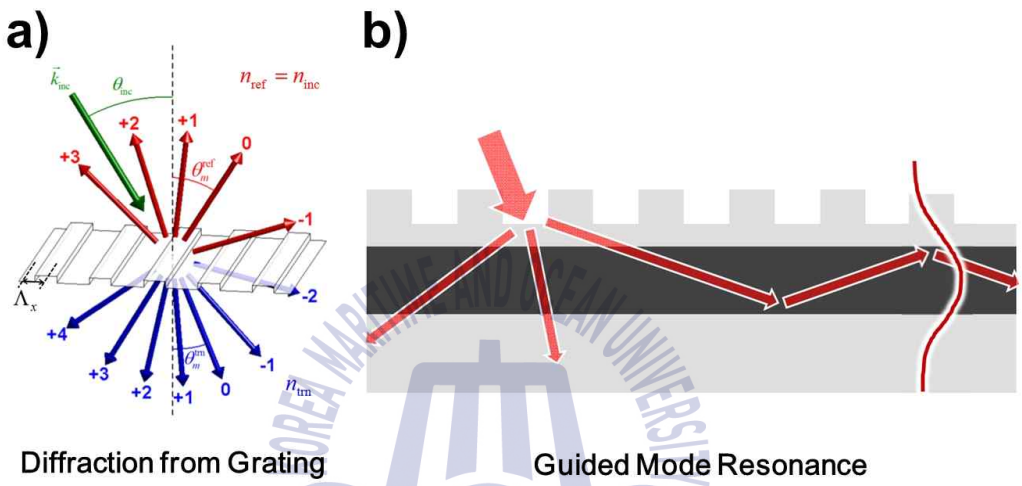

Fig. 2.1 (a) Diffraction from grating. (b) Schematic of Guided-mode resonance.

The principle of the GMR filter is described by two physical mechanisms. First, the THz wave incident on the GMR filter is diffracted by the grating. The angle of the diffraction mode is related to the wavelength and grating period. The grating equation is expressed by Equation (1). Equation (1) can only predict the direction of the mode, and the amount of power is not predicted [11].

$$n_{avg}\sin\theta_m = n_{inc}\sin\theta_{inc} - m\frac{\lambda_0}{\Lambda} \quad (1)$$

n_{avg} is the grating average refractive index, n_{inc} is the incident refractive index, Λ is the period, and λ_0 is the wavelength. The angle of incidence inc and m th diffraction mode m can be determined by

the grating equation.

$$\theta_c = \sin^{-1}\left(\frac{n_2}{n_1}\right) \tag{2}$$

When the refractive index is larger than the surrounding material and the incident angle is larger than the critical angle, it is totally reflected. Equation (2) represents the critical angle.

$$n_{inc} \leq \left|\frac{\beta_m}{\kappa_0}\right| < n_{avg} \tag{3}$$

Secondly, the slab waveguide can occur only when the dielectric constant is larger than the surrounding media and the slab dielectric constant is small. Is expressed by Equation (3).

$$\frac{\beta_m}{\kappa_0} = n_{avg}\sin\theta_m \tag{4}$$

Equation (4) is the transfer constant, and it can be changed from the equation (1) to the grating condition [12].

$$n_{inc} \leq \left| n_{inc}\sin\theta_m - m\frac{\lambda_0}{\Lambda}\right| < n_{avg} \tag{5}$$

The condition of the diffraction and the slab waveguide generated by the grating is expressed by Equation (5). It is possible to predict the resonance generation range of the designed GMR filter by mode.

2.1.1 Resonance region

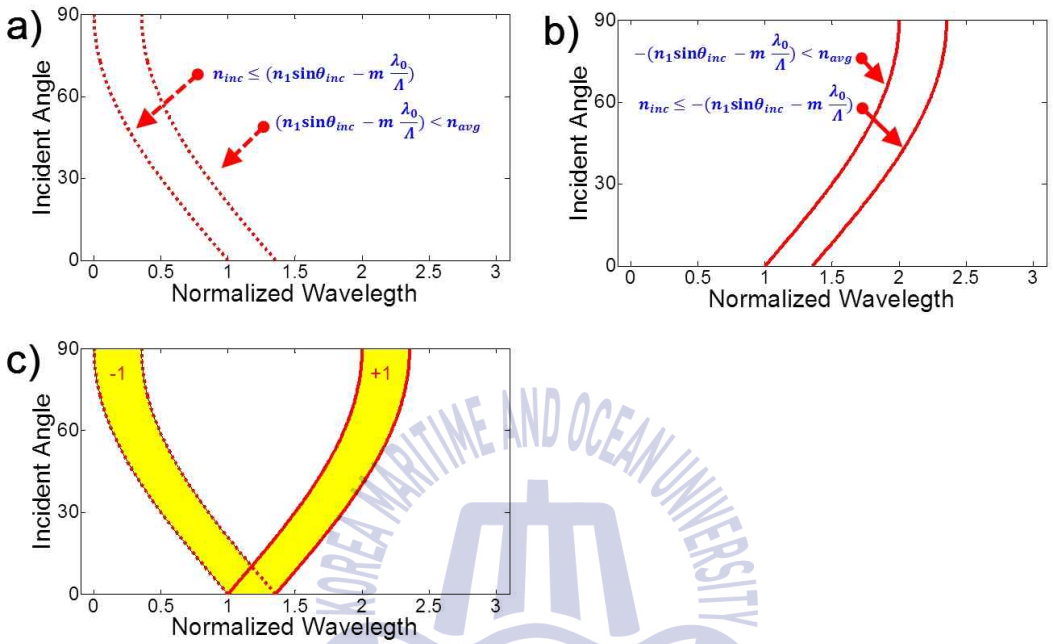

Fig. 2.2 (a) Resonant region at m = -1. (b) The resonance region at m = -1. The equation is the boundary of the resonance region (c) Resonance region according to incident angle.

The GMR filter equation (5) is divided into the range when the absolute value is positive (+) and when the absolute value is negative (-).

$$n_{inc} \leq -n_{inc}\sin\theta_m + m\frac{\lambda_0}{\Lambda} < n_{avg} \tag{6}$$

When the absolute value is a positive number, it can be expressed by Equation (6). Equation (6) can be divided into + and - modes. When m is positive, the negative refractive index is not physically present. So m = -1, -2, -3 ... is negative. Figure 2.2 (a) shows the range of

resonance occurring in the negative mode (m = -) according to the incident angle of the beam.

$$n_{inc} \leq n_{inc}\sin\theta_m - m\frac{\lambda_0}{\Lambda} < n_{avg} \tag{7}$$

When the absolute value is a negative number, it can be expressed by Equation (7). Equation (7) can be divided into + and - modes. When m is negative, the negative refractive index is not physically present. So m = 1, 2, 3 ... is positive. Figure 2.2 (b) shows the range of resonance occurring in the negative mode (m = +) according to the incident angle of the beam.

2.1.2 GMR filter modes

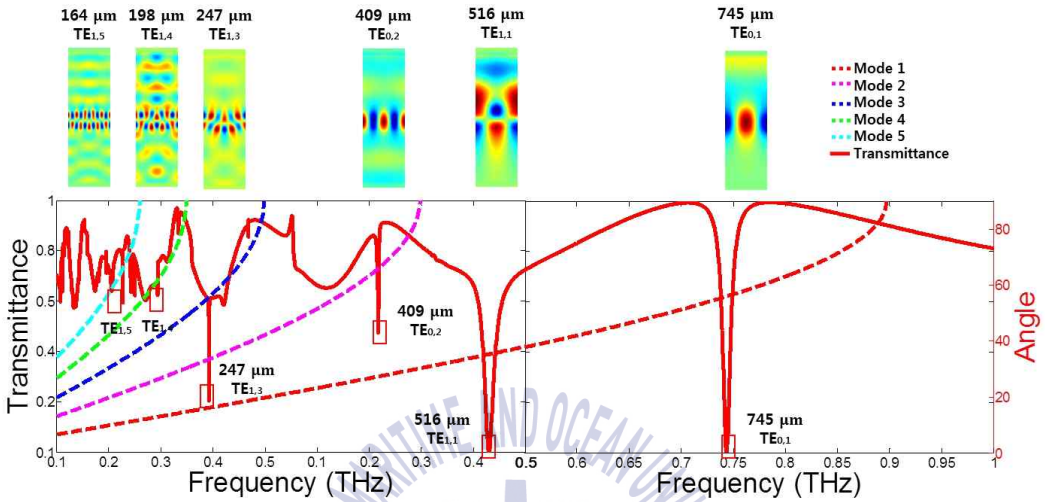

Fig. 2.3 The GMR filter transmittance characteristic frequency region at 0.1 ~ 1 THz. The dotted line is the diffraction angle according to the frequency of each diffraction mode. The red dotted line is m = 1, the purple dotted line is m = 2, the blue dotted line is m = 3, the green dotted line is m = 4 and the light blue dotted line is m = 5. Below the figure is the electric field distribution of GMR filter classified into diffraction mode and guided mode.

Figure 2.3 shows the high-order mode resonance and field distribution induced in the GMR filter by Finite-Difference Time-Domain (FDTD) simulation. The diffraction angles of the grating are indicated by red, green, blue, and blue dash lines depending on the mode.

In the first diffraction mode (m = 1), two strong resonances appeared. Two resonances are induced in the GMR filter in TE_0 and TE_1 modes. Slab waveguide mode and grating diffraction mode are denoted as $TE_{0,1}$ and $TE_{1,1}$, respectively.

The resonance occurs in the second diffraction mode (m = 2) and is field-distributed to the GMR filter in the TE_0 mode. $TE_{0,2}$. Field distributions of $TE_{1,3}$, $TE_{1,4}$, $TE_{2,4}$, and $TE_{1,5}$ in the resonance generated in the GMR filter are shown.

2.2 Dimensional & measurement errors

2.2.2 Dimensional difference

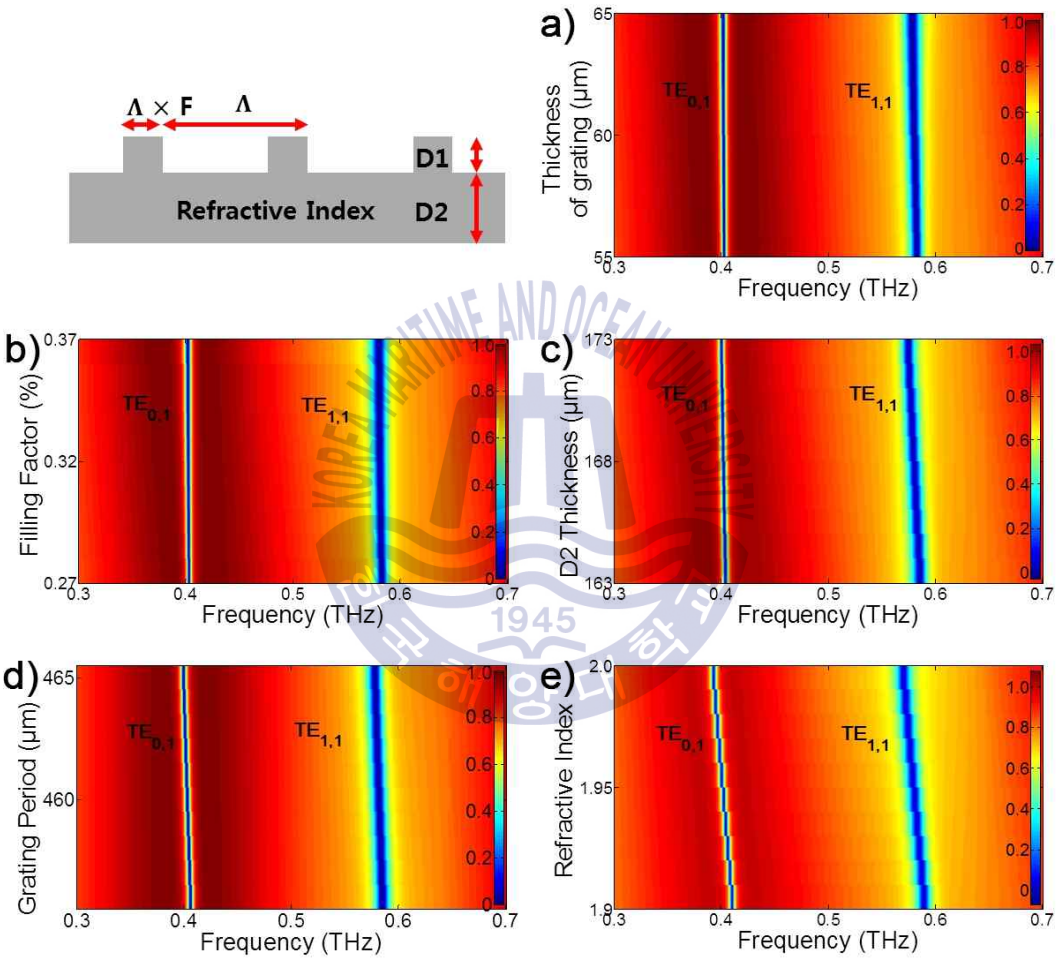

Fig. 2.4 The inserted figure is a schematic of the GMR filter. (D1 = 60 ㎛, Filing Factor = 0.32 %, D2 = 168 ㎛, grating period = 460 ㎛, and refractive index = 1.95). (a) grating thickness change 55 ~ 65 ㎛. (b) Filling factor change 0.27 ~ 0.37 %. (c) Change in thickness of D2 163 ~ 173 ㎛. (d) Grating period change 455 ~ 465 ㎛. (e) Refractive index change 1.9 ~ 2.0.

Figure 2.4 simulates the frequency shift of the resonance according to

the structural difference of the GMR filter. The designed GMR filter has a structural difference of less than 1 ㎛ with the fabricated GMR filter. GMR filters made from dielectrics are sensitive to material or structural changes. The GMR filter was fabricated with the following characteristics: D1 = 60 ㎛, Filing Factor = 0.32 %, D2 = 168 ㎛, grating period = 460 ㎛, and refractive index = 1.95.

Figure 2.4 (a) shows the transmittance characteristics according to the thickness change (55 ~ 65 ㎛) of the grating. Figure 2.4 (b) shows the transmittance characteristics according to the changing factor (0.27 ~ 0.37 %). Figure 2.4 (c) shows the transmittance characteristics according to the thickness variation (163 ~ 173 ㎛) of D2. Figure 2.4 (d) shows the transmittance characteristics according to the grating period variation (455 ~ 465 ㎛). The fabricated GMR filter has less than 1 ㎛ errors. The designed and fabricated GMR filter structure difference are very small. Figure 2.4 (e) is the transmittance characteristic according to the refractive index change (1.90 ~ 2.00). Since the refractive index of the most sensitive material in the GMR filter is a fixed constant, it does not cause a large error.

2.2.2 Inner rounded corner

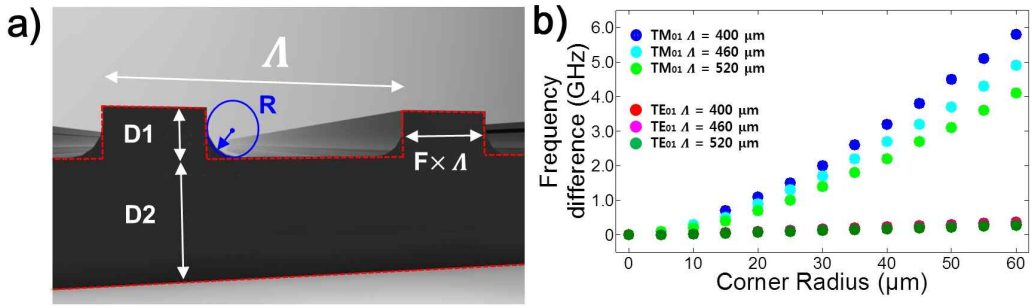

Fig. 2.5 (a) Cross-sectional schematic of the GMR filter (D1 = 60 ㎛, Filing Factor = 0.32 %, D2 = 168 ㎛, grating period = 460 ㎛, and refractive index = 1.95). The blue circle is the inner curvature R in the groove. (b) Resonance frequency difference between rectangular inner corner radius (R = 0) and rounded inner corner radius.

Figure 2.5 (a) is a cross-sectional schematic of the GMR filter with an electron microscope. Ideally designed rectangular gratings are difficult to implement mechanically. The grating structure is manufactured by an etching process (manufactured by Buysemi Co.), and the inner edge of the grooves has a round-shaped manufacturing error. The GMR filter has the largest error at the inner edge of the grooves. The difference of GMR filter with rounded corner radius was simulated for TE and TM modes.

Since the inner edge of the GMR filter groove is not a perfect circle shape, the radius of the rounded corner inside the grating can not be precisely defined. However, the structural error variable is defined as a constant-ring arc and is marked with "R" in Figure 2.5 (a). R = 0 for ideal direct gratings, and R is changed from 0 to 60 ㎛.

The resonance frequency difference was simulated for the $TE_{0,1}$ and $TM_{0,1}$ modes of the GMR filter. In the $TE_{0,1}$ mode, the difference in resonance frequency is small as R increases. However, in $TM_{0,1}$ mode, the frequency difference of resonance increased exponentially with increasing R. The frequency difference between the measured and simulated $TE_{0,1}$ modes is 0.1, 0.1, and 0.1 GHz at 400, 460 and 520 ㎛, respectively. The frequency differences in the measured and simulated $TM_{0,1}$ modes are 11.2, 6.5, and 6.1 GHz at 400, 460 and 520 ㎛, respectively. Figure 2.5 (a) is an error due to the curvature R inside the grating. In the TM mode, there is a difference between the measured value and the resonant frequency of the FDFD simulation.

2.2.3 Number of grooves

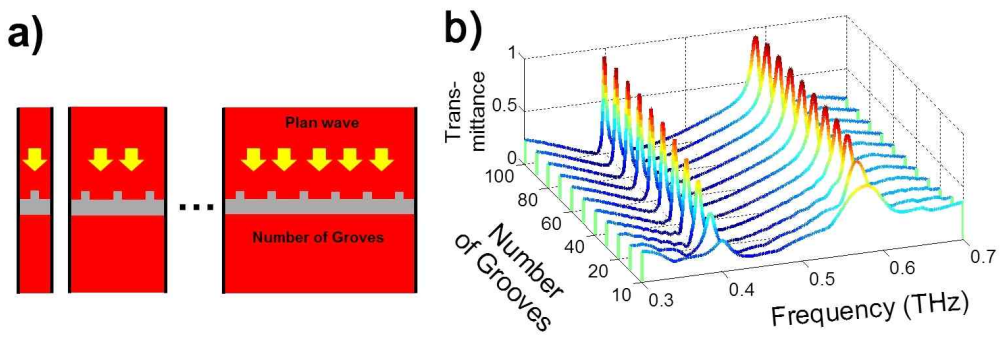

Fig. 2.6 a) FDTD simulation schematic with increasing groove number (D1 = 60 ㎛, Filing Factor = 0.32 %, D2 = 168 ㎛, grating period = 460 ㎛, and refractive index = 1.95). (b) 3-D graph of resonance characteristics change according to the number of grooves (5 ~ 100) in TE mode.

The transmittance characteristics are simulated by FDFD according to the number of grooves of GMR filter. To simplify the periodic structure, the unit cell method is used. Periodic structure was repeated by using period boundary condition (PBC) on both sides of the pattern of one repetition cycle. It is advantageous to simplify repetitive structure by using PBC. However, it is not possible to calculate the transmittance characteristics according to the number of grooves.

Figure 2.7 (a) shows a schematic of the Finite-Difference Time Frequency-Domain (FDTD) simulation for calculating the transmittance characteristics of a GMR filter according to the number of grooves. The boundaries of the FDTD simulation space were Perfect Matched Layer (PML). The transmittance characteristics of the finite number of

grooves were calculated. We simulated a sufficiently long time to react sufficiently to multiple of the THz beam passing through the GMR filter. In addition, there is enough free space in the upper and lower sides of the designed GMR filter by a multiple of the wavelength to eliminate possible errors in the simulation.

Figure 2.6 (b) shows the transmittance characteristics as the number of grooves increases from 5 to 100. As the number of grooves increases, the Q-factor and the resonant depth increase. From a sufficient number of grooves, the Q-factor and resonance depth converge at a constant rate. The number of suitable grooves can be determined in the GMR filter.

2.2.4 Loss tangent (δ)

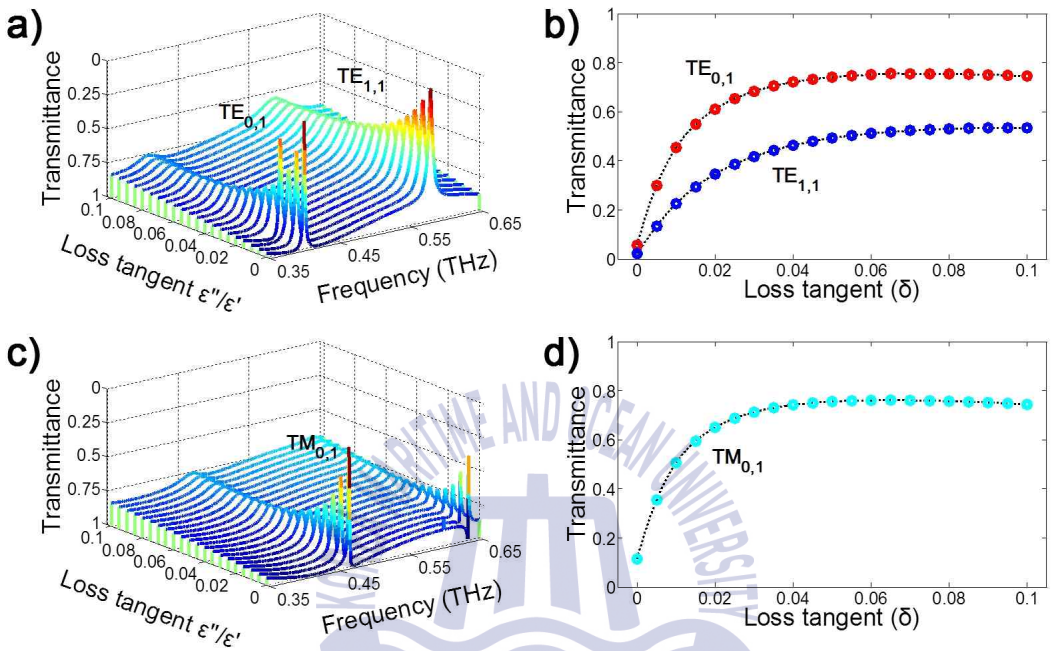

Fig. 2.7 The depth of resonance as the loss tangent (δ) (a) of a material changes from 0 to 0.1 (D1 = 60 ㎛, Filing Factor = 0.32 %, D2 = 168 ㎛, grating period = 460 ㎛, and refractive index = 1.95). a) Simulation with TE mode. b) Comparison of $TE_{0,1}$ and $TE_{1,1}$ transmittance. (c) Simulation with TM mode; (d) $TM_{0,1}$ Transmittance.

All dielectric GMR filters are sensitive to the properties of the material and produce a narrow and strong resonance. However, the measured resonance depth is not close to zero. In Figure 2.6, as well as the number of grooves, the loss tangent (δ) of the material is also a major factor in reducing the depth of resonance. The reduction of the wave induced by the loss tangent (δ) causes a decrease in the depth of the resonance.

The structure of the simulated GMR filter is D1 = 60 ㎛, Filing Factor

= 0.32 %, D2 = 168 ㎛, grating period = 460 ㎛, and refractive index = 1.95. Transmittance is expressed according to the change of loss tangent (δ) of material from 0 to 0.1 in TE and TM mode.

Figure 2.6 (a) shows the transmittance characteristics as the loss tangent (δ) increases in the TE mode. Figure 2.6 (b) shows that the TE0,1 mode has a change in depth of resonance that is less sensitive to loss tangent (δ). Figure 2.7 (c) shows that the transmittance decreases as the loss tangent (δ) increases in TM mode. In Figure 2.7 (d), when the loss tangent (δ) value is greater than 0.06, the decrease in transmittance decreases as the absorption of material increases, and the depth of resonance almost disappears.

2.2.5 Expender of beam

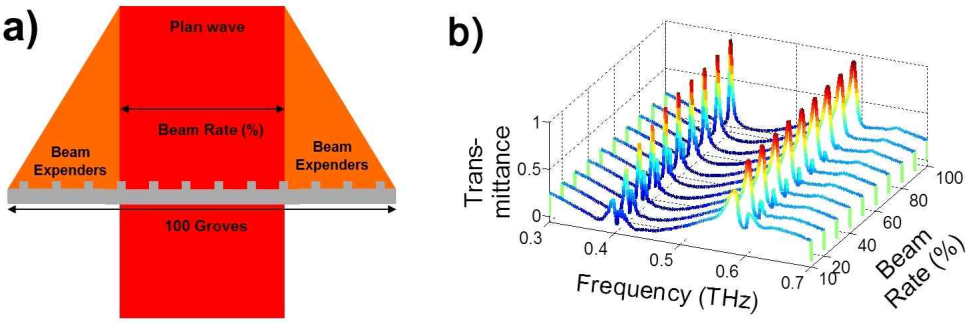

Fig. 2.8 (a) Schematic of FDTD simulation with beam spread. (D1 = 60 ㎛, Filing Factor = 0.32 %, D2 = 168 ㎛, grating period = 460 ㎛, and refractive index = 1.95). (b) Characteristics of resonance and side lobe with beam spread ratio.

The time domain system (TDS-system) generates the THz beam by the current flow generated in the semiconductor by the fs-laser pulse arriving at the SI-GaAs. A silicon lens and a 90-axis parabolic mirror designed to make the THz beam run parallel to a certain width were used. However, a beam having a Gaussian distribution is spread as the propagation distance becomes longer. In Figure 2.8, FDTD simulations of resonance errors with beam expender ratio.

Figure 2.8 (a) is a schematic of a plane wave and a fuzzy beam on both sides of the GMR filter. The transmittance according to the ratio of the plane of the beam was simulated. 100 grooves were fixed and both ends were removed by using PML at corners and at the interface. The transmittance according to the input of a parallel wave and a spreading beam at a ratio of 10 to 100 % of the groove width of 100

was calculated. A small resonance (side lobe) occurred along the main resonance depending on the ratio of beam expense. As the ratio of the plane wave decreases, the ratio of the beams that are not vertically incident through the GMR filter becomes higher and the side lobe appears.

Figure 2.5 (b) shows the side lobe size that is generated by the beam expense ratio. The spread of a small proportion of the beam does not appear at the main resonance. As the beam expender ratio increases, the side robe becomes larger and larger. To minimize the side lobe, the GMR filter was placed in the most parallel part of the beam between the two parabolic mirrors. Nonetheless, in the measured transmittance a small resonance due to the spread of the beam is measured.

2.2.6 Scan time

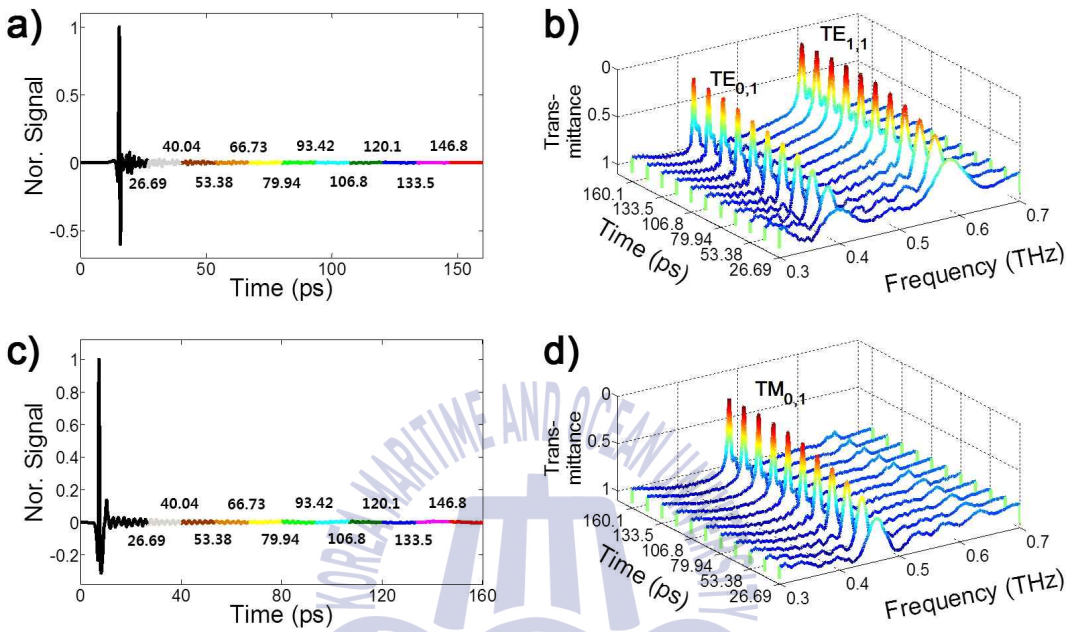

Fig. 2.9 Time domain pulse signal and transmittance measurement according to scan length (D1 = 60 ㎛, Filing Factor = 0.32 %, D2 = 168 ㎛, grating period = 460 ㎛, and refractive index = 1.95). (a) TE mode pulse. (b) 3-D graph of TE mode transmittance. (c) TM mode pulse. (d) 3-D graph of TM mode transmittance.

The pulse signal includes various frequency spectra in a short time signal. The oscillation behind the pulse transmitted through the GMR filter contains the component of the resonance. The oscillation included in the length of the measured time affects the measurement result. The oscillation behind the pulse gradually disappears. The resonance characteristics according to the measurement time length were analyzed experimentally.

The signal was measured at 160 ps at 1200 data in 20 ㎛ step. After

160 ps, the reflected pulse appears on the photoconductive antenna (PCA), and the oscillation of the signal after 133 ps is completely eliminated. Figures 9 (a) and 9 (b) compute the pulse signal and the transmittance according to the length of time measured in the TE mode. Zero padding technique improves the resolution of the spectrum. Figures 9 (c) and 9 (d) compute the pulse signal and the transmittance according to the length of time measured in the TM mode.

In the TE and TM mode, the longer the measurement time, the better the resonance characteristics and the less the oscillation of the spectrum around the resonance frequency.

Chapter 3 Characterization of guided-mode resonance (GMR)

3.1 Introduction

The thin metallic or dielectric pattern on a frequency-selective surface (FSS) can reflect and transmit specific electromagnetic fields. For this reason, the FSS has been commonly used in applications at microwave frequencies, for example, as the screen on a microwave oven [13], in antenna radomes [14], and communication filters [15], and also in the optical region, as filters [16] and polarizers [17]. Recently, metallic THz MMs, which used slits to enhance THz field, have been introduced for high THz transmission in a specific frequency band. These THz MMs were fabricated only by metal. A typical FSS uses MMs, which have a thin and repetitive metallic pattern on their dielectric surface, have been widely studied recently. MMs for THz frequencies have been suggested as ideal choices for good performance filters, sensors [18-20] and absorbers [21] due to their high Q-factor [22-24]. However, creating metal patterns is a complicated process with high cost. At the same time, there is also high reflective loss due to the high refractive index of the metal. This high reflection loss limits the applications of MMs. Meanwhile, polarizers [25] and modulators [26] for THz frequencies have been studied and applied in many fields, including imaging [27], sensing [18-20], and communication systems [28, 29]. Carbon nanotubes and nanowires [30, 31], parallel-plate waveguide [32] and MMs [33] have been used to make polarizers and modulators which operate in the THz region. But because the devices are also

complicated to fabricate and suffer high refraction loss, it has limitations in applications.

However, we suggest the GMR filter as an alternative to overcome these problems. The main function of a GMR filter is to select a narrow frequency region, which can exhibit a very high Q-factor. In this paper, an all-dielectric GMR filter operating in the THz region is proposed for the first time. The GMR filter is a combination of a grating on the filter surface and the slab waveguide of the filter substrate. The propagation of a THz wave through the structures has been studied, for example, as metal gratings [34], grooves [35], and slab waveguide [36]. However, the characteristics of an all-dielectric GMR filter in the THz region have not been reported. Unlike MMs, an all-dielectric material such as quartz is efficient for THz transmission measurements, because of the lower refractive index and absorption [37]. For these reasons, strong TM and TE resonance modes are detected. Furthermore, the designed GMR filter has an incident THz beam angle dependent THz tunable resonance filter, a rotating GMR filter angle dependent THz polarizer, and the refractive indices of the incident material dependent modulator. The measurement results agreed very well with results from the simulations.

3.2 GMR filter

3.1.1 GMR filter & setup

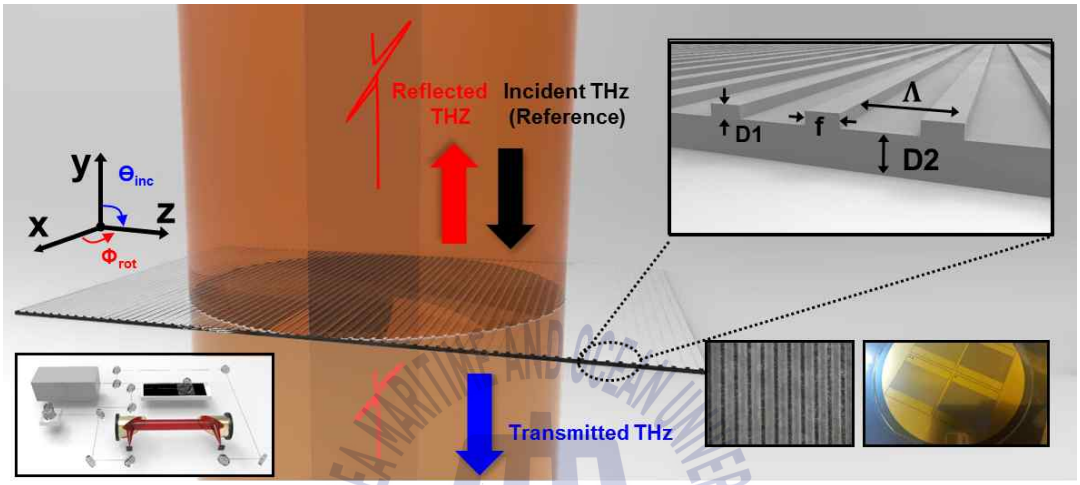

Fig. 3.1 Schematic diagram of the experimental configuration. GMR filter has a width of 30 mm and length of 30 mm, and total groove number of 65. The separation (Λ ×F) between each of the grooves is 148 μm (D1 = 60 μm, D2 = 168 μm, Λ = 460 μm, and filling factor = 32%).

Figure 3.1 is a schematic of THz-TDS system [38]. THz-TDS system was used to measure the transmittance characteristics of the GMR filter. In a THz-TDS system with a broadband spectrum using a photoconductive antenna (PCA), parallel beams can be transmitted using silicon lenses and parabolic mirrors. GMR filters made of all-dielectric material were installed and measured in the beam path. In order to fabricate a GMR filter operating in THz region, an all-dielectric material requires several characteristics. First, a material with low refractive index and loss tangent (δ) properties in the THz region can be fabricated with a high-performance resonant filter. Second, the

strength of the dielectric material should be high. The GMR filter in THz region is designed with a thickness of several hundred microns and a grating pattern size of tens of micros. Materials with low strength are difficult to process for tens or hundreds of microns. Material suitable for GMR filter is quartz. The GMR filter (prepared using an etching method by Buysemi Co.) has a groove height (D1) of 60 ㎛, a substrate thickness (D2) of 168 ㎛, a grating period (Λ) of 460 ㎛ and a filtering factor (F). The spacing between the grooves ($\Lambda \times$F) is 148 ㎛. The THz beam is incident on the GMR filter (+y-direction). Figure 3.1 shows a schematic diagram of the experimental setup for THz transmittance measurements through a GMR filter.

3.2.2 FDFD simulation

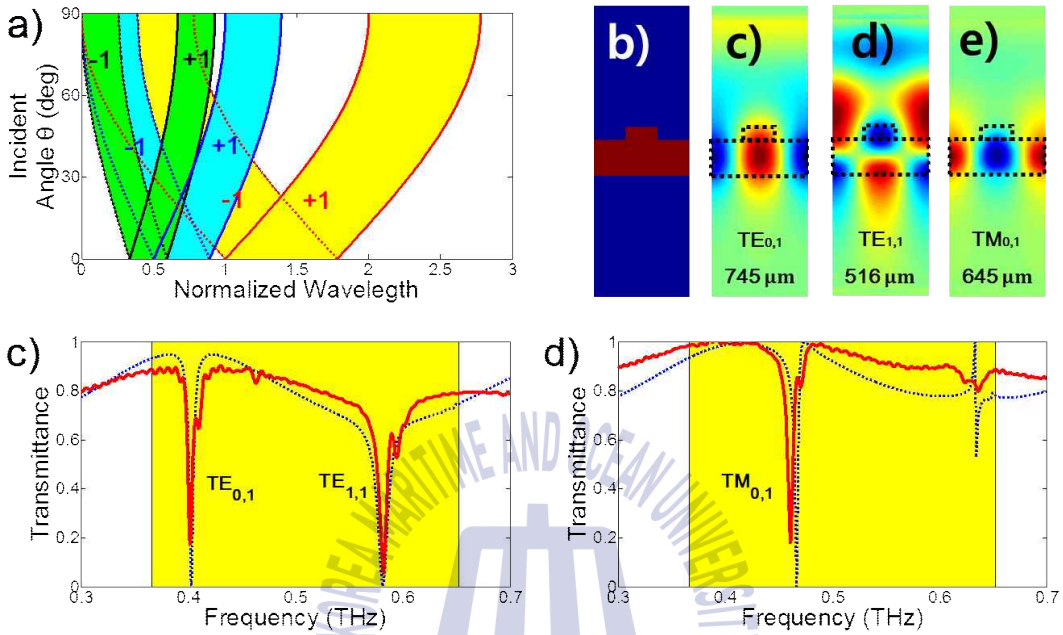

Fig. 3.2 (a) Regions of resonance in the GMR filter. According to diffraction mode m = 1 (yellow), m = 2 (blue), and m = 3 (green), respectively. (b) GMR design and map of refractive index. (c) The field distributions of resonances Electric field of the $TE_{0,1}$ mode; (d) the $TE_{1,1}$ mode; (e) Magnetic field of the $TM_{0,1}$ mode. Black dashed lines are outlines of the structure, with the three unit cells illustrated. (f) Transmittance of TE mode; (g) Transmittance of TM mode. Measurement (red solid line) and Simulation (blue dot line) using an FDFD simulation when the incident angle is zero.

Figure 3.2 (a) shows the resonance generation range according to the angle change of the incident beam and the diffraction mode from the equation (5) in which the diffraction and guide conditions are combined in the GMR principle. A single resonance is measured when the THz beam is perpendicular to the surface of the GMR filter (θ_{inc} = 0). The diffraction angle including the angle of incidence is divided into two

directions as $\theta_{1+} = \theta_1 + \theta_{inc}$ and $\theta_{1-} = \theta_1 - \theta_{inc}$. The beam diffracted in two directions by the beam incident angle appears as two split resonances. As the incident angle increases, the spacing of the separated resonance ranges increases. The yellow, sky blue, and green regions in Figure 3.2 (a) represent the resonance generation regions in the diffraction mode m = ± 1, 2, 3 from the grating structure.

A GMR filter was designed to operate around the THz center frequency of 0.4 THz, which has a wide spectrum of the wide band generated from the THz source. (D1) of 60 ㎛, a core thickness (D2) of 168 ㎛, a grating period (Λ) of 460 ㎛ and a filling factor (F) of 32 %. The spacing between the grooves ($\Lambda \times F$) is 148 ㎛ and is made of quartz with a high strength and a low refractive index of 1.95.

In the TE mode where the direction of the THz beam is parallel to the grating direction, two strong resonances are measured at 0.402 (745 ㎛) and 0.581 (516 ㎛) THz. Figures 3.3 (c) and 3.3 (d) show E-filed of the GMR filter derived from TE_0 and TE_1 modes. In the TM mode where the direction of the THz beam and the grating direction are perpendicular, one strong resonance is measured at 0.466 THz and the TM_0 mode is induced. The TE and TM mode resonance was calculated as 0.334 (898 ㎛) - 0.667 (582 ㎛) THz for the first diffraction (m = ± 1). The resonance is expressed as $TE_{0,1}$, $TE_{1,1}$, and $TM_{0,1}$ in the guide mode and diffraction mode order. In the TE and TM mode, the transmittance using FDFD simulation agrees well with the simulation.

3.2.3 GMR filter with dimension

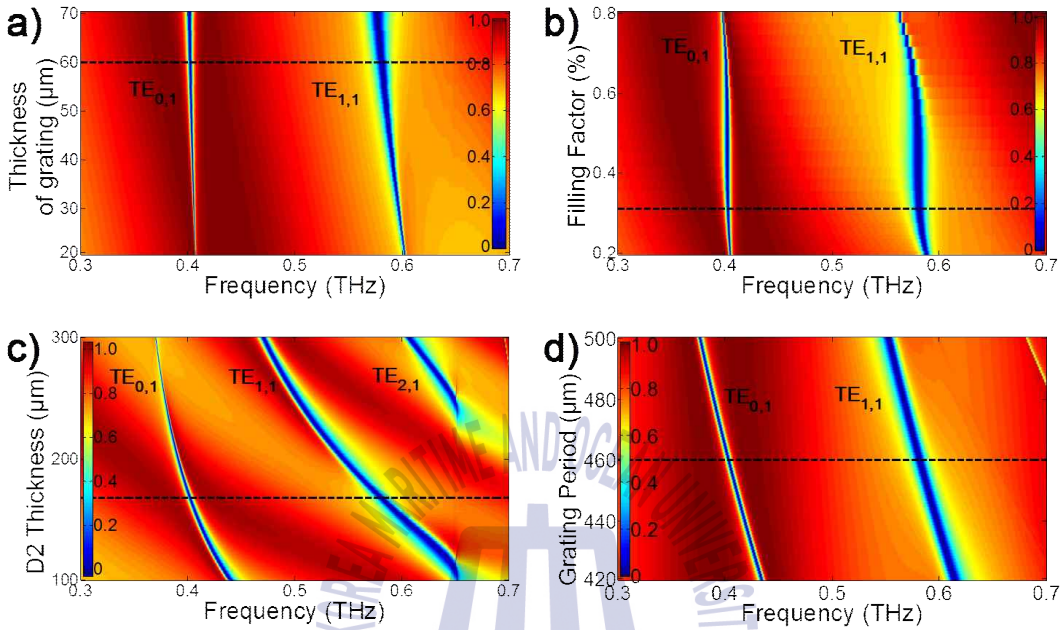

Fig. 3.3 Simulation according to the structure change of GMR filter. (a) groove high D1 = 20 ~ 70 ㎛. (b) Filing factor 20 ~ 80 %. (c) D2 thickness D2 = 100 ~ 300 ㎛. (d) groove period = 400 ~ 520 ㎛. black dot line indicate D1 = 60 ㎛, Filling factor 32 %, D2 = 168 ㎛, A = 460 ㎛.

Figure 3 shows the resonance characteristics according to the GMR filter structure change. Figure 3.3 (a) shows the change in resonance characteristics with respect to the grating height. As the thickness of the grating of the GMR filter increases, the average refractive index difference between the grooved and unfilled portions within one cycle increases. The difference in the average refractive index greatly affects the Q-factor. Thin-walled gratings have a reduced average refractive index difference and thicker gratings have an increased

average refractive index difference, resulting in a resonance with a changed Q-factor size.

Figure 3.3 (b) shows the resonance characteristics according to the ratio of grooves to one period of grating (filing factor). The overall resonance characteristics are uniform, and the resonance gradually disappears when the ratio of the foaming factor is high or low.

Figure 3.3 (c) shows that the change of the thickness (D2) of the core of the GMR filter changes the induced guide mode condition and induces a higher mode. Thickness of Core Thickness The GMR filter produces long wavelength (low frequency) and high order mode field distributions. On the contrary, the thickness of the thinned core has a short wavelength (high frequency) field distribution in the GMR filter. The core thickness increase of the GMR filter is caused by addition of the resonance mode resonance at the limit point of the resonance frequency generation range 0.66 7 THz. Figure 3.3 (d) shows that the size of the resonant wavelength varies with the grating period (Λ) of the GMR filter. When the grating period increases, it moves to a long wavelength (low frequency). When the grating period is small, the resonance moves to a short wavelength (high frequency).

3.2.4 GMR filter with refractive index

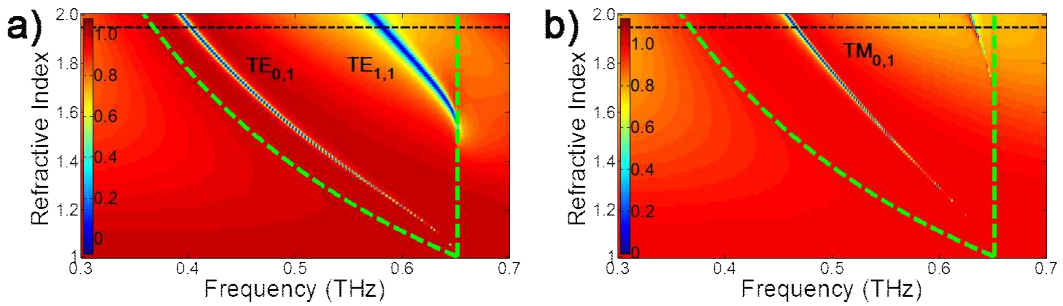

Fig. 3.4 FDFD simulation with Refractive index variation of GMR filter. The dotted lines indicate 1.95, which are the refractive indices of quartz in the THz region, respectively. The vertical color bars indicate the intensity of the electric field. (a) TE mode; (b) TM mode. Green dashed line region of resonance in the GMR filter.

Figure 3.4 (a) and (b) show the FDTD simulation map in TE and TM mode with resonance shift and higher order mode resonance according to the refractive index change of the GMR filter. The change in the refractive index of the GMR filter implies a change in the guide mode condition. A frequency induced in the higher order mode occurs. When the refractive index increases, the resonance frequency induced in the GMR filter moves to the low frequency. When the refractive index decreases, the resonance frequency induced in the GMR filter moves to the high frequency. As the refractive index of the GMR filter increases, a higher mode resonance appears at 0.667 THz, which is the limit of the resonance frequency generation range.

3.3 GMR filter with Teflon plate

3.3.1 Resonance region & filed

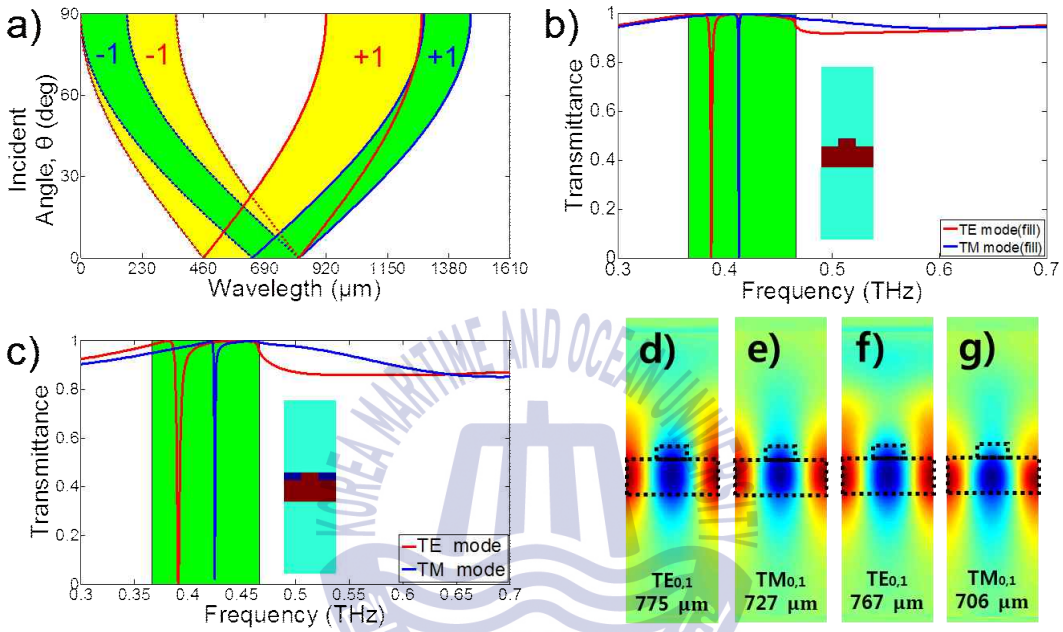

Fig. 3.5 GMR filter with incident material. (a) Regions of resonance according to the incident angle when the different incident material is air (yellow) and Teflon (green), respectively. (b) FDFD simulation of TE and TM modes when the incident material is Teflon. (c) incident material is Teflon without grating. (d) electric filed in GMR filter.

In Figure 3.5 (a), the GMR structure is described by equation (5), which is a combination of diffraction and guide conditions. The diffraction angle changed according to the change of the incidence angle of the beam determines the resonance occurrence range again. A single resonance is measured when the THz beam is perpendicular to the surface of the GMR filter ($\theta_{inc} = 0$). The diffraction angle including the angle of incidence is expressed in two directions as $\theta_1 + = \theta_1 + \theta_{inc}$

and $\theta_{1-} = \theta_1 - \theta_{inc}$. The beam diffracted in two directions appears as two split resonances, each satisfying the GMR condition. The resonance range increases as the incidence angle increases. The yellow region and the green region in Figure 3.5 (a) indicate the respective resonance occurrence regions according to the incident angles of the beam when the refractive indexes surrounding the GMR filter are 1.0 (air) and 1.4 (Teflon).

The diffraction direction and the guide condition changed by the difference of the refractive index of the GMR filter and the incident material change the resonance occurrence range. The resonance frequency shifts with the change of the refractive index of the GMR filter, and it occurs and disappears. It shows diffraction direction and guide condition changed by difference of refractive index of GMR filter and incident material. Experimentally, it is difficult to change the refractive index of the material constituting the GMR filter. However, it is possible to create a relative refractive index difference by combining the material above and below the GMR filter.

Figure 3.5 (b) changes the refractive index of the material above and below the GMR filter to 1.4, which is larger than 1.0, and reduces the refractive index difference surrounding the GMR filter and the GMR filter. The changed diffraction directions and guide conditions reduced the resonance generation range to 0.366 ~ 0.467 THz. In the TE and TM modes, strong resonances occur at 0.397 (775 ㎛) and 0.413 (727 ㎛), and Figure 3.5 (d) and (e) show the field distribution. The $TE_{1,1}$ mode does not appear as a reduction in the resonance occurrence range. For experimental convenience, FDFD simulations were performed

by combining plates on both sides of the GMR filter and changing the incident refractive index except for the grating. In the TE and TM modes, strong resonances occur at 0.391 (767 ㎛) and 0.425 (706 ㎛), and Figure 3.5 (f) and (g) show the field distribution. Compared to the simulation filled up to the grating, the Q-factor decreased slightly and the resonance frequency shifted to low frequency, but $TE_{1,1}$ mode was completely eliminated due to reduction of resonance occurrence range.

3.3.2 Refractive index of incident material

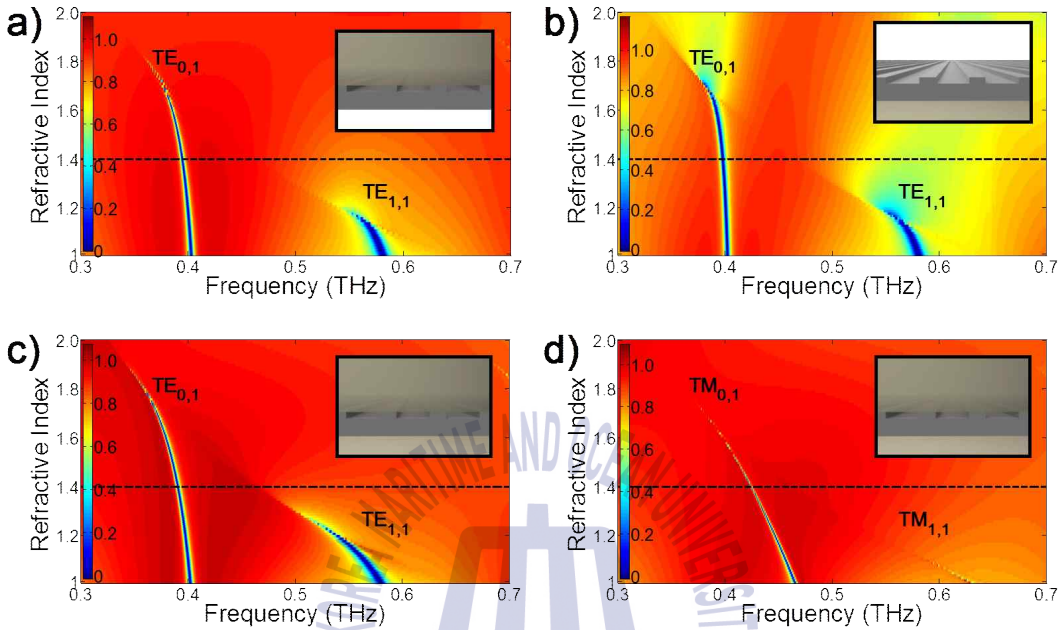

Fig. 3.6 Transmittance FDFD simulation with change of refractive index (1.0 ~ 2.0) around GMR filter (a) Upper side; (b) Below side; (c) Both side in TE modes; (d) Both side in TM modes. black dot line indicate Teflon (n = 1.4)

The diffraction direction and the guide condition changed by the difference of the refractive index of the material surrounding the GMR filter and the GMR filter are reduced in the resonance occurrence range. High-order mode resonance that deviates from the resonance occurrence range is not generated. Figure 3.6 shows the change of the resonance due to the difference of the refractive index difference between the GMR filter and GMR filter by FDFD simulation. In Figure 3.6 (a) and (b), as the refractive index increases in one direction of the material surrounding the GMR filter, it can be confirmed that the

resonance of $TE_{1,1}$ is blurred. However, low transmittance and transmission characteristics are not good.

Figure 3.6 (c) and (d) show the resonance changes in TE and TM modes with the increase in the refractive index of both materials surrounding the GMR filter. Due to the reduction in refractive index difference, the resonance generation range is gradually reduced. As the resonance occurrence range decreases, the $TE_{1,1}$ mode resonance deviates from the generation range and disappears at the Rayleigh anomaly boundary. When the refractive index difference is less than 0.55, the $TE_{1,1}$ mode is completely reduced. The $TM_{1,1}$ mode, which has the same characteristics even in the TM mode and has a relatively large difference in relative refractive index, is extinguished as the relative refractive index difference is reduced.

3.3.3 Polarization with Teflon plate

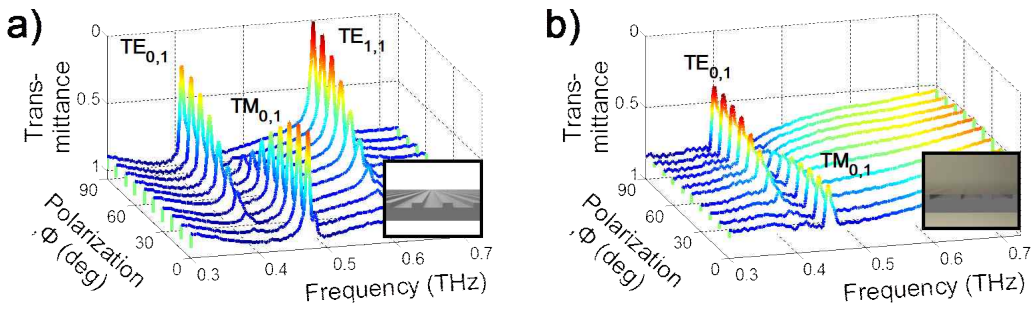

Fig. 3.7 (a) Measurement of transmittance according to the polarization with a single GMR filter. (b) Measurement when the material around the GMR filter is Teflon.

Since the GMR structure having a grating period only in the 1-D direction is asymmetric in the x-z plane, the resonance according to the mode changes depending on the polarization from 0° to 90°, which is sensitive to the polarization of the incident beam.

Figure 3.7 (a) shows the transmittance measurement according to the polarization. TE and TM mode resonance occurs and disappears according to the polarization. If the angle is 0°, only TM mode resonance exists because the direction of grating and the polarization of the THz beam are perpendicular. As the polarization increases, the resonance depth of the TM mode decreases and two resonances of the TE mode appear parallel to the polarization of the THz beam. Figure 3.7 (b) shows that the refractive index difference of the material surrounding the GMR filter and the GMR filter is reduced when Teflon is bonded to both sides of the GMR filter. To remove multiple reflections from the Teflon plate in the measurement, a sufficiently thick 3 cm thick Teflon was combined. The $TE_{1,1}$ mode resonance was

not measured at the transmittance according to the polarization from 0° to 90°. Although Teflon has a low in the THz region, the reduced resonance depth and transmittance were measured over lossless conditions due to the thick thickness of 3 cm.

3.3.4 Incident angle with Teflon plate

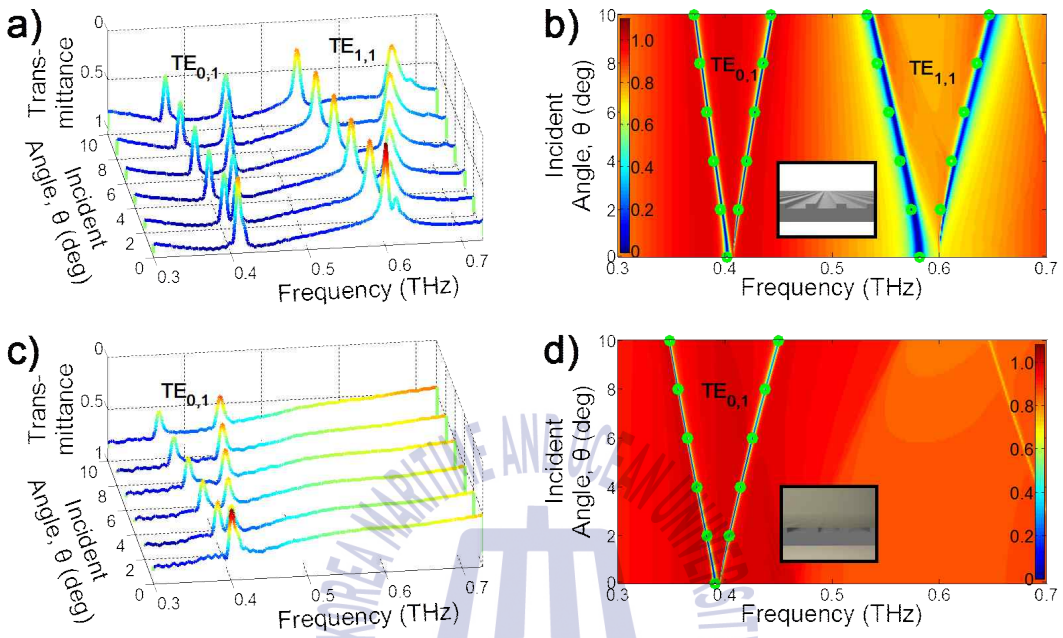

Fig. 3.8 (a) Measured in TE mode according to incident angle. (b) FDFD simulation. (c) Measurement when the material around the GMR filter is Teflon. (d) FDFD simulation when the material around the GMR filter is Teflon. Green dots represent measured data.

Figure 3.5 (a) shows the combination of the diffraction direction and the guide condition in the GMR condition (5). A single resonance is measured when the THz beam is perpendicular to the surface of the GMR filter ($\theta_{inc} = 0$). The diffraction angle including the angle of incidence is expressed in two directions as $\theta_1 + = \theta_1 + \theta_{inc}$ and $\theta_1 - = \theta_1 - \theta_{inc}$. The beam diffracted in two directions appears as two split resonances, each satisfying the GMR condition. Figures 3.8 (a) and 3.8 (b) show the measured transmittance as the angle of incidence of the

TE mode with the beam direction parallel to the grating is changed from 0° to 10° in the GMR filter. The two $TE_{0,1}$ and $TE_{1,1}$ mode resonances are separated into two resonant modes, respectively, as the incident angle increases.

Figure 3.8 shows the results of FDFD simulation and measurements of resonance shifts according to the incident angles of the THz beam. Figure 3.8 (b) and (d) show the 2D image simulation results, and the green dots show the measured resonance frequency. Measurements and simulations are in very good agreement. Depending on the angle of incidence, the resonance frequency can be shifted by a tunable filter.

Figure 3.8 (c) shows that Teflon bonded on both sides of the GMR filter reduces the refractive index difference of the material surrounding the GMR filter and the GMR filter. The $TE_{1,1}$ mode resonance is removed from the transmittance according to the incident angle of the beam from 0° to 10°, and only the $TE_{0,1}$ mode is split into two resonances

3.4 Two GMR filters

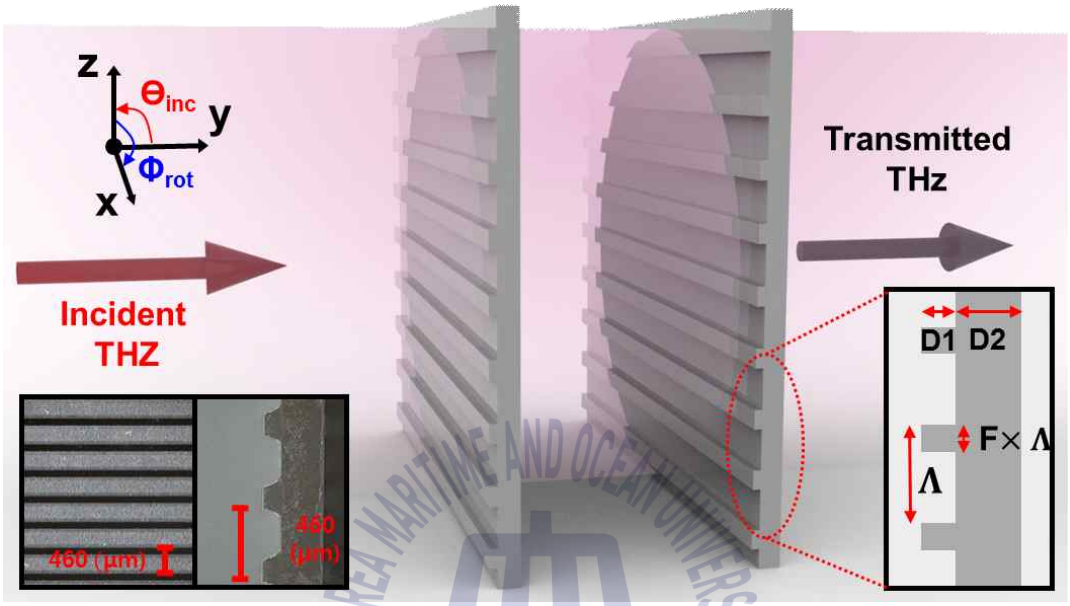

Fig. 3.9 A schematic diagram of the experimental setup using two GMR filter.

The number of grooves included in the limited THz beam is limited. Two GMR filters were placed in parallel to increase the number of grooves in the limited THz beam size. In order to eliminate mutual interference and multiple reflections of two GMR filters, they were placed between two parabolic mirrors with a distance of 8 cm. Figure 3.5 shows a schematic diagram of a simple experimental setup for measuring transmittance through the same two GMR filters.

3.4.1 Number of grooves

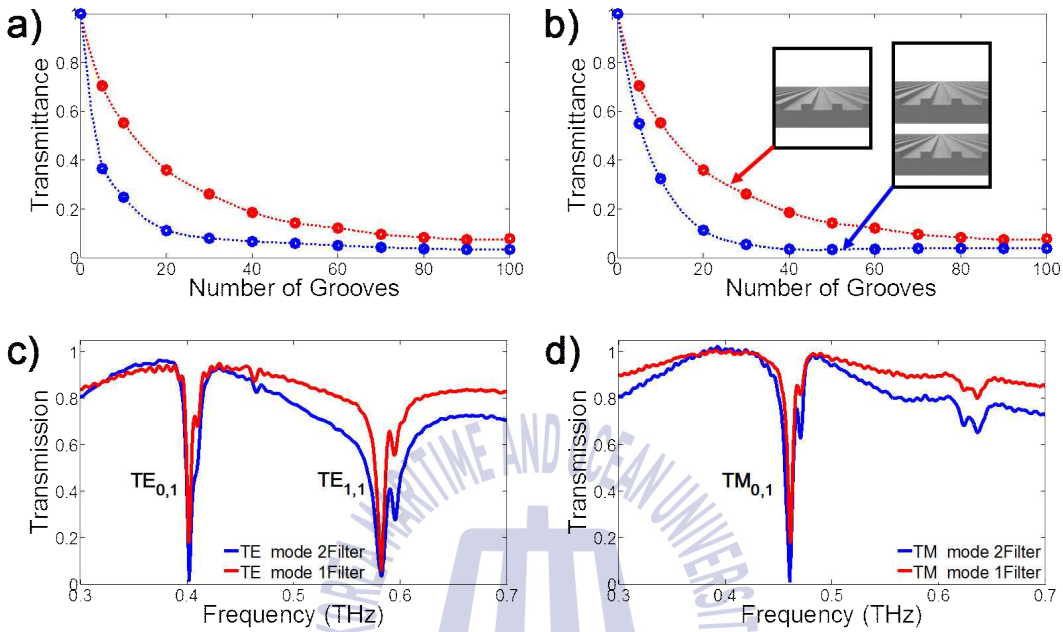

Fig. 3.10 Perfect resonance with two GMR filter. (a) Transmittance with various numbers of grooves for $TE_{0,1}$ and $TE_{1,1}$ modes. (b) Comparison of $TE_{0,1}$ modes for one and two GMR filters with various numbers of grooves. Transmittance measured with one and two GMR filters; (c) TE mode; (d) TM mode

Figure 2.7 shows the number of grooves and the depth of resonance to obtain a GMR filter [39]. In Figure 3.6 (a), $TE_{0,1}$ and $TE_{1,1}$ mode resonance were calculated using FDTD simulation with respect to the number of grooves. As the number of grooves increases, the transmittance of the two modes converges to zero, and the transmit resonance of $TE_{1,1}$ mode converges faster than the transmit resonance of $TE_{1,0}$ mode.

The generated THz beam diameter has a Gaussian distribution with a

diameter of 20 mm. Only a limited number of grooves can be included in the THz beam. Two identical GMR filters increase the groove number in the limited beam size. Figure 3.6 (b) compares the transmittance at a $TE_{0,1}$ mode resonance frequency through one or two GMR filters. Using two GMR filters, we show that the transmittance is convergent to zero at a limited beam size. The perfect resonance measured in the TE and TM mode using two GMR filters was measured.

3.4.2 Characteristics of two GMR filters

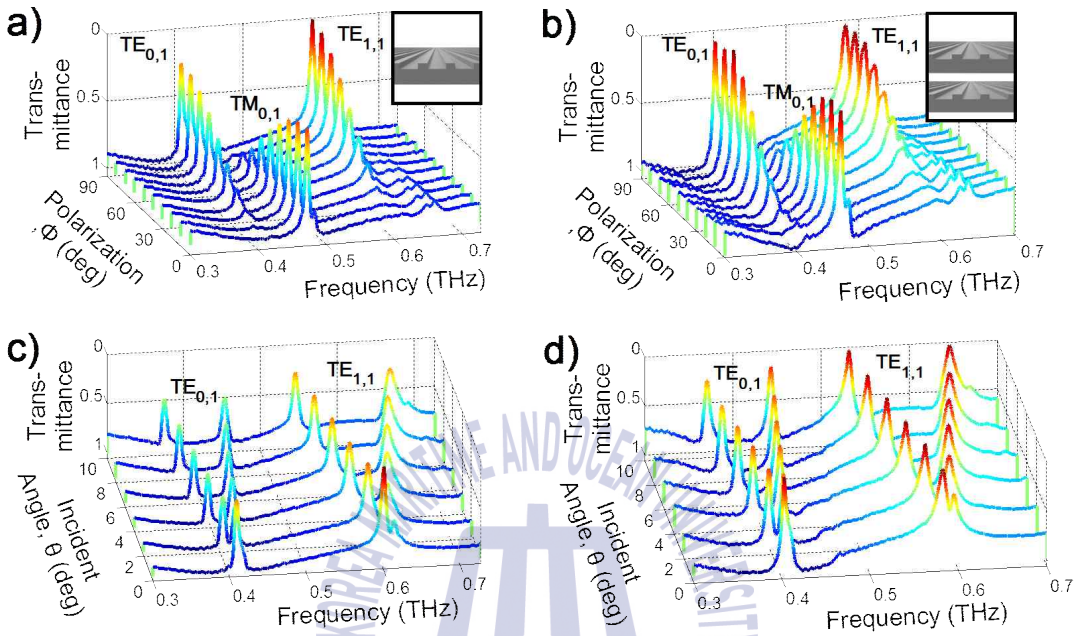

Fig. 3.11 (a) Measurement according to the polarization using GMR filter. (b) The polarization using two GMR filter. (c) Measurement according to Incident angle with a GMR filter (b) Incident angle with two GMR filter.

The perfect resonance was measured using two GMR filters. Figure 3.11 (a) and (b) show the characteristics of Transmittance according to the polarization of the GMR filter. The depth of the resonance does not converge to zero completely due to the loss tangent (δ) of the material and number of grooves that are not sufficient in the limited THz beam size.

Figure 3.11 (b) shows the total resonance measured by increasing the number of grooves in two GMR filters in a THz beam with a limited beam size. The polarization efficiency exceeds 96.9, 96.3 and 92.9 %

for $TE_{0,1}$-, $TE_{1,1}$- and $TM_{0,1}$-polarized wavelength, respectively. When the polarization increases, a superposition of the resonance of the TM and TE modes is obtained. When the polarization is 45°, the transmittance exhibits about 50 % TM and 50 % TE mode resonance at the same time. When the polarization is 90°, only the TE mode resonance is left, and the TM mode resonance, which occurs when the polarization is 0°, disappears gradually and does not exist when the polarization is 90°.

Figures 3.11 (c) and (d) show the resonance shifts according to the angle of incidence. The isolated resonance at the incident angle of the beam is reduced in depth, and the depth of the resonance is reduced by the number of restricted grooves and the loss tangent(δ) of the material. Figure 3.7 (d), measured using two GMR filters, measured the enhanced resonance.

3.5 Conclusions

The GMR The GMR filter is a useful device to overcome the disadvantages of metallic FSSs in the THz frequency region. For example, a MMs, with a metal pattern on a dielectric substrate, has a large reflection loss due to the metal pattern. This low transmission efficiency restricts its applications. However, the designed GMR filter can reduce reflection and attenuation losses because it is made of an all-dielectric material, such as quartz. It can also be made from other dielectric materials without metal patterns on the surface, including Teflon, silica, Polyethylene, etc., which have a low refractive index and low absorption coefficient in the THz region.

The main parameters determining the resonance frequency are the refractive index, grating period, and thickness of the GMR filter, which are determined by the filter itself. These parameters determine the resonance frequency by changing the diffraction angle and length within the filter. However, other parameters such as the incident angle of the THz wave and the refractive index of the incident material change the GMR conditions as shown in Equation (2). We studied all of the parameters to determine the transmission characteristics of the GMR filter in the THz region for the first time. We also demonstrated that the limited resonance depth due to the finite grating periods was overcome by using two identical GMR filters. By performing the filtering process twice, it was possible to obtain almost the same effect as an infinite grating period filter. We were able to obtain a Q-factor of up to 74.4 for the $TM_{0,1}$ mode. Because the Q-factor achieved by

the GMR filter is higher than that for THz MMs, it can be used to replace applications currently using MMs. Also, we obtained polarization efficiencies of up to 96.9 % for the $TE_{0,1}$ mode when the filter was rotated to 90° . It was found to be a very good THz polarizer. Meanwhile, wave guiding within the filter can only be achieved when the effective dielectric constant of the guided mode is greater than that of the incident material and less than that of the filter. Therefore, the positions of the TE mode resonances are separated when the incident angle is increased. Furthermore, if the GMR filter is inserted between Teflon plates, the frequency range in which the resonance exists can be reduced. As a result, the $TE_{1,1}$ mode can be perfectly removed. This provides a good THz frequency modulator.

In conclusion, because the proposed GMR filter has a high Q-factor, tunable filter, good polarizer, and good modulator characteristics, it has potential for THz applications in spectroscopy, display, image sensor, and biomedical technologies in the future.

Chapter 4 Tunable guided-mode resonance (TGMR)

4.1 Introduction

The study of filters that operate in the THz region is an important research topic because the data can be utilized in many fields, including THz communication [28, 29], sensor [18-20], and image applications [27]. Recently, THz filters using parallel-plate waveguide (PPWG) [35, 40, 41], grooves [35] and MMs [42-48] have been actively studied. Various filters, from bandpass to band rejection, can be implemented by passing a THz beam through a photonic crystal with a periodic array, which is on one surface of a PPWG [41]. Since the propagation direction of the THz beam is the same as the array direction of the photonic crystal, it is possible to obtain various filters with excellent characteristics. However, doing so requires precise alignment of the THz beam and the PPWG, and it also requires enough space to couple the THz beam to the waveguide.

At the same time, filters using MMs have been extensively studied in the microwave [49] to the optical [50] domains. Because the filter size in the THz region is smaller than that of the microwave region and larger than that of the optical region, MMs in the THz region are relatively easier to fabricate in terms of size. Although making a metal pattern on dielectric materials still requires a complex process, THz filters using MMs have the advantage of easy alignment because they are positioned perpendicular to the direction of the THz beam.

A tunable THz filter that can change the resonance frequency without having to replace samples is a very important THz device. Generally, three mechanisms have been used to make tunable THz filters [51]. The first one is a tuning circuit. In MMs, the electromagnetic behavior can be expressed as an equivalent circuit consisting of induction (L), capacitance (C), and resistance (R) elements. Typically, the resonance frequency, which is controlled by the capacitance with voltage [43, 44] and a structural gap [45], can be represented as a parallel LC or tank RLC circuit. The second approach is material tuning. Tunable devices can be obtained by controlling the properties of materials, such as permittivity, permeability and conductivity. Tunable THz resonance studies have realized material tuning using temperature [46], optical beam power [47], and magnetic field [15]. The third mechanism is geometrical tuning. When a part of the filter device is geometrically moved, the resonance is shifted due to a change in phase inversion [8] or structural deformation [52]. Using the relative positions of photonic crystals [9] and PPWG [8] have been reported as methods to obtain a tunable THz filter. Specifically, the PPWG obtained 6.28 GHz/㎛ resolution by controlling the gap of the PPWG [8]. Although tunable THz filters using PPWG have good resolution, they still have spatial size and alignment problems. The first and second mechanisms have been applied to many MMs. Because it modulates the metal pattern electronically, it has the advantage of being able to quickly tunable the resonant frequency. However, because the metal patterns on the dielectric material reflect the

incident THz beam, metal patterns reduce transmittance and increase manufacturing cost.

Many optically tunable filters using GMR have been studied using the first and second mechanisms, for example, by adjusting incident angle [53, 54], polarization [55], temperature [56], and beam power [57]. We propose a new tunable THz notch filter using the geometrical tuning method with a Tunable Guided-Mode Resonance (TGMR) filter composed of an all-dielectric material like quartz. The resonance frequency can be changed continuously by moving the position of the TGMR filter with respect to the incident THz beam. Also, it is easy to align the TGMR filter because the THz beam direction is perpendicular to the filter, like most MMs setups The TGMR filters based on dielectric materials have high transmission rates and high Q-factors with low loss, but tunable speeds have physical speed limits.

4.2 Design of TGMR filter

4.2.1 Grating period

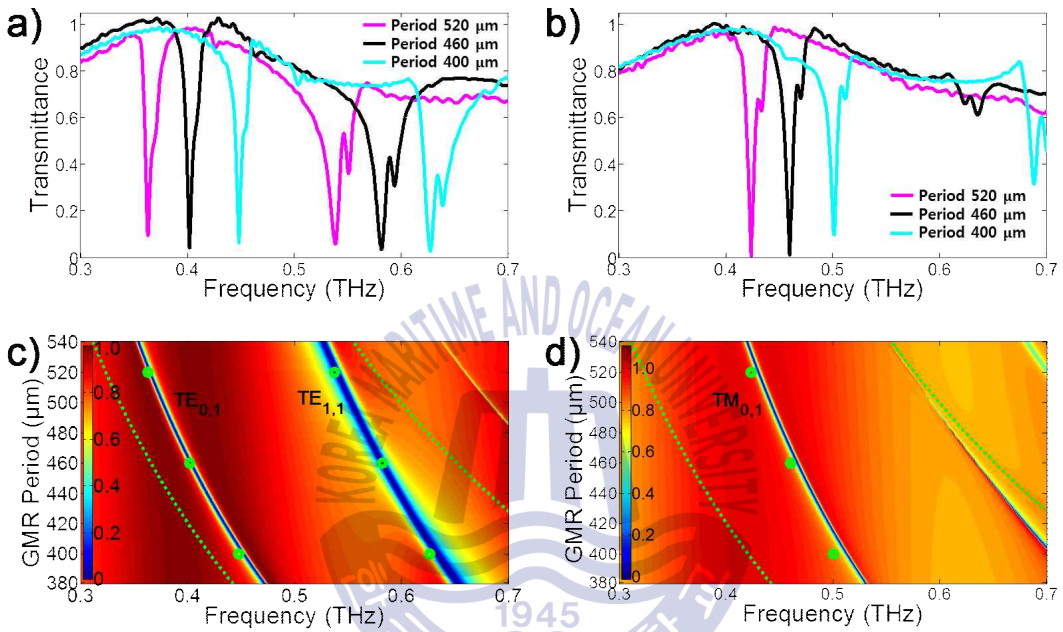

Fig. 4.1 Transmittance measurement for 400, 460, and 520 ㎛ grating periods. (a) TE mode; (b) TM mode. Simulation image of resonance frequency shift according to grating period. The dots and dashed lines indicate the measured resonance frequencies and the boundary of the region where the first mode resonance exists, as shown in Fig. 1. (c) TE mode; (d) TM mode.

The structural change of the GMR filter is sensitive to filter characteristics. In particular, the change in the grating period and the change in the size of the corresponding wavelength change the resonance of the designed GMR filter. A GMR filter (prepared using an etching method by Buysemi Co.) was fabricated using quartz, a low

refractive index and hard material. The GMR filter was fixed with a groove height (D1) of 60 ㎛, a substrate thickness (D2) of 168 ㎛, and a filing factor (f) of 32 %. The GMR filter was fabricated with a uniform period of 30 mm×30 mm with grating periods of 510 ㎛ (Sample-1), 460 ㎛ (Sample-2) and 400 ㎛ (Sample-3). Figures 4.3 (a) and 4.3 (b) show the measured transmissivity of the TE and TM modes for the grating cycle. Two strong resonances $TE_{0,1}$ and $TE_{1,1}$ in the TE mode and $TM_{0,1}$ and $TM_{1,1}$ modes in the TM mode were measured. Figure 4.3 shows the known frequency variation according to the grating period of the GMR filter.

Figures 4.1 (c) and 4.1 (d) show the FDFD simulation map according to the grating period for the TE and TM modes of the GMR filter. The dotted green line indicates the range of resonance generated by the grating period. The $TM_{1,1}$ mode in Figure 4.1 (d) moves to the resonance range boundary and disappears as the grating period increases. Two identical GMR filters were used to create the perfect resonance. The two GMR filters removed interference and multiple reflections with a distance of 8 cm. Since the THz beam between the parabolic mirrors is not a perfectly balanced wave like the simulation, a small side-lobe resonance was measured next to the measured resonance as shown in Figure 2.5. Figures 4.3 (a) and 4.3 (b) show the perfect resonance of the two GMR filters according to the grating period change using a filter.

The resonance frequencies of $TE_{0,1}$ mode measured at grating periods of 510 ㎛ (sample-1), 460 ㎛ (sample-2) and 400 ㎛ (sample-3) are 0.363, 0.402 and 0.448 THz, respectively. The GMR equation is

proportional to the grating period and the wavelength, so the resonant frequency shifts to high frequency as the period decreases.

4.2.2 Design of TGMR filter

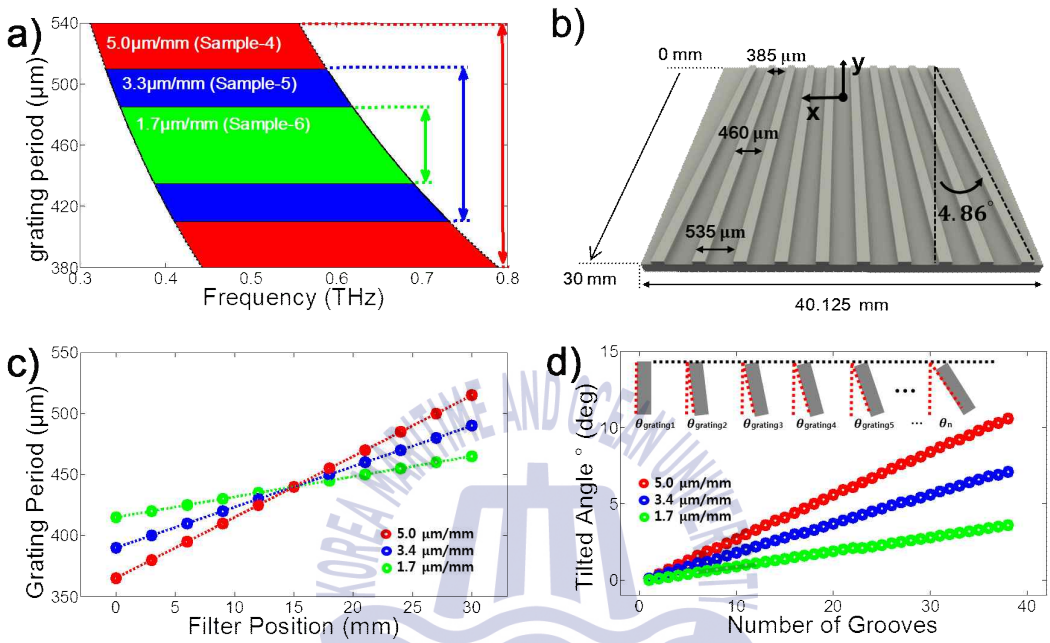

Fig. 4.2 (a) The region where resonance of the first mode exists according to frequency and grating period. The vertical arrows indicate the grating period ranges of Sample-4, Sample-5 and Sample-6. (b) Schematic diagram of TGMR filter (sample-4). Each grating pattern consists of a groove height (D1) of 60 ㎛, substrate thickness (D2) of 168 ㎛, and a filling factor (F) of 32 % as shown in the insert figure. The number of grooves is 76. The grating period gradually increases from top to bottom, from 385 ㎛ to 535 ㎛. The grating period in the middle is 460 ㎛. The last and first grooves are tilted by $\pm 11^{\circ}$ from the center groove, respectively. (c) The grating period changes with the filter position. (d) The tilted angle of the grating with increasing grating number in TGMR.

The green, blue, and red regions in Figure 4.2 (a) represent the grating period variance and resonance dominant ranges of each TGMR. The

green, blue, and red regions have grating period variation ranges of 435 ~ 485 ㎛, 410 ~ 510 ㎛, and 385 ~ 535 ㎛. When the grating period becomes large, the resonance frequency range moves to the low frequency, and when the grating period becomes small, it moves to the high frequency. The GMR structure shifts the resonant frequency range according to the grating period.

The period change of the GMR filter is operated by a TGMR filter. Figure 4.2 (b) shows a schematic diagram of a TGMR filter in which the grating period varies linearly with the position of the TGMR filter. It is designed as a trapezoidal shape with a difference in the size of the upper grating period and the lower grating period. Figure 4.2 (c) shows three TGMR filters of 150 ㎛, 100 ㎛, and 50 ㎛, respectively, which differ in the size of the upper grating period and the lower grating period. The grating period in the center of the TGMR was designed to be the same as 460 ㎛. A TGMR filter that is larger than the limited THz beam width includes a total of 76 grooves. The TGMR filter with a height of 30 mm was fabricated with 5.0 ㎛/mm (sample-4), 3.4 ㎛/mm (sample-5) and 1.7 ㎛/mm (sample-6). The number of gratings increases symmetrically from the center of the TGMR. Figure 4.2 (d) shows the slope of the grating due to the periodic change from the center. The insertion figure in Figure 4.2 (d) shows the error that occurs due to the accumulation of the grating slope due to the large gap at the bottom where the grating period is large as the number of gratings increases. The incident beam has a constant height and includes a change in the grating period, and the grating period changes according to the position of the TGMR filter.

4.2.3 Determination of spacing metal slit

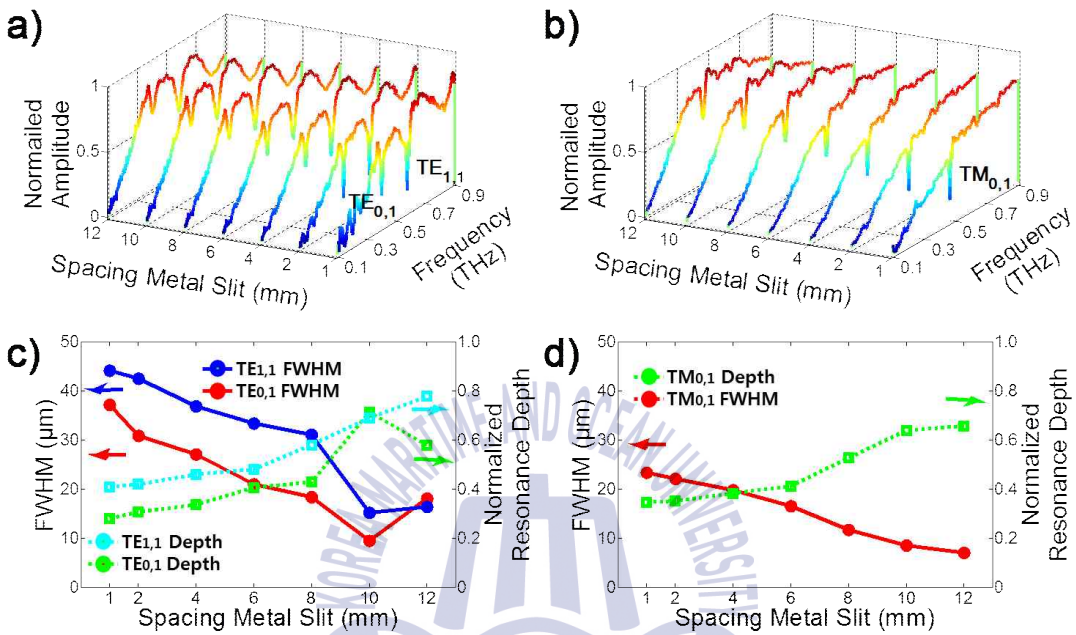

Fig. 4.3 The normalized amplitude of spectrum near the resonant frequency of the TGMR filter due to the change in spacing metal slit . (a) TE mode; (b) TM mode. Change of resonant depth and half width according to change of spacing metal slit . (c) TE mode; (d) TM mode.

The THz beam is transmitted including the grating period variation of the designed TGMR filter. A spacing metal slit was used to reduce the height of the transmitted THz beam and to reduce the variation of the grating period. The THz beam width through the metal slit is equal to the spacing metal slit . It is important that the optimal spacing metal slit does not increase the resonance distortion due to the noise and periodic changes in the transmittance. Therefore, the width of the THz beam passing through the TGMR filter was adjusted by controlling the

spacing metal slit . Figures 4.5 (a) and 4.5 (b) compare the spectra around the normalized resonance with the spacing metal slit. The 3-D graph shows the change in resonance depth and half width (FWHM) according to spacing metal slit in TE and TM modes, respectively.

Figure 4.5 (c) shows the resonance depth and resonance width in two modes $TE_{0,1}$ and $TE_{1,1}$ in the TE mode, depending on the spacing metal slits. As the spacing metal slit increases, the depth of resonance decreases and the FWHM of resonance increases. As the spacing metal slit increases, the fluctuation range of the grating period is too large in the width of the THz beam, so that the resonance depth is reduced and FWHM of resonance is widened. As the spacing metal slit becomes narrower, the resonance of the TGMR becomes larger and the half-width becomes narrower. However, as shown in Figure 4.5 (a), when the spacing metal slit is narrowed to 1 mm, the THz beam width is too small to measure noise. Figure 4.5 (d) shows the resonance depth and resonance width in one mode $TM_{0,1}$ in the TM mode, depending on the spacing metal slits. As the metal slit gap increases, the depth of resonance decreases and the FWHM of resonance increases.

4.3 TGMR filter

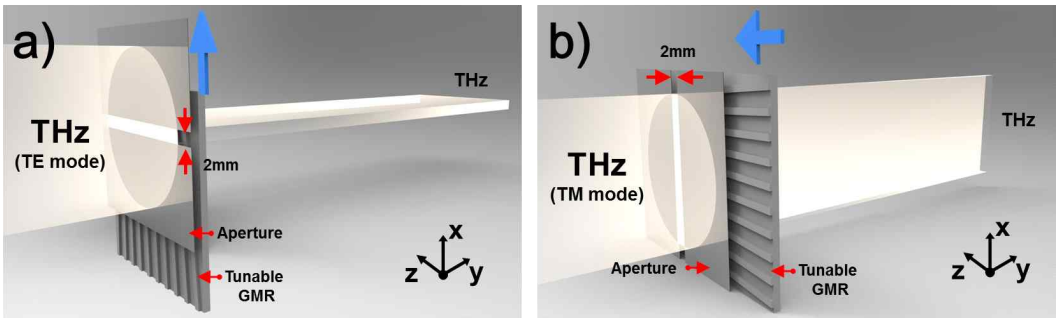

Fig. 4.4 Schematic diagram of the TGMR filter setup for (a) TE mode; (b) TM mode.

Figure 4.4 is a schematic diagram for measuring the resonance frequency displacement in the TE and TM mode of the TGMR. The TGMR filter was placed behind a spacing metal slit with 2 mm . The position of the TGMR filter is shifted in the direction of + x (TE mode) or + z (TM mode) at intervals of 2 mm from the top of the TGMR filter with a short grating period. The TGMR grating cycle was moved at precise intervals using a small motorized mobile stage. The resonance frequency displacement was measured according to the grating period change between metal slits.

Figure 4.4 (a) shows that the metal slit is located perpendicular to the polarization direction of the THz beam and the TGMR filter is positioned in parallel for the TE mode measurement. In Figure 4.4 (b), the slit is positioned parallel to the beam direction and the TGMR filter is positioned vertically to measure the TM mode resonance. Due to scattering at the edge of the TGMR filter, TE and TM mode measurements were taken at 2 mm intervals from 3 mm to 27 mm.

4.3.1 TGMR filter with 5.0 ㎛/mm

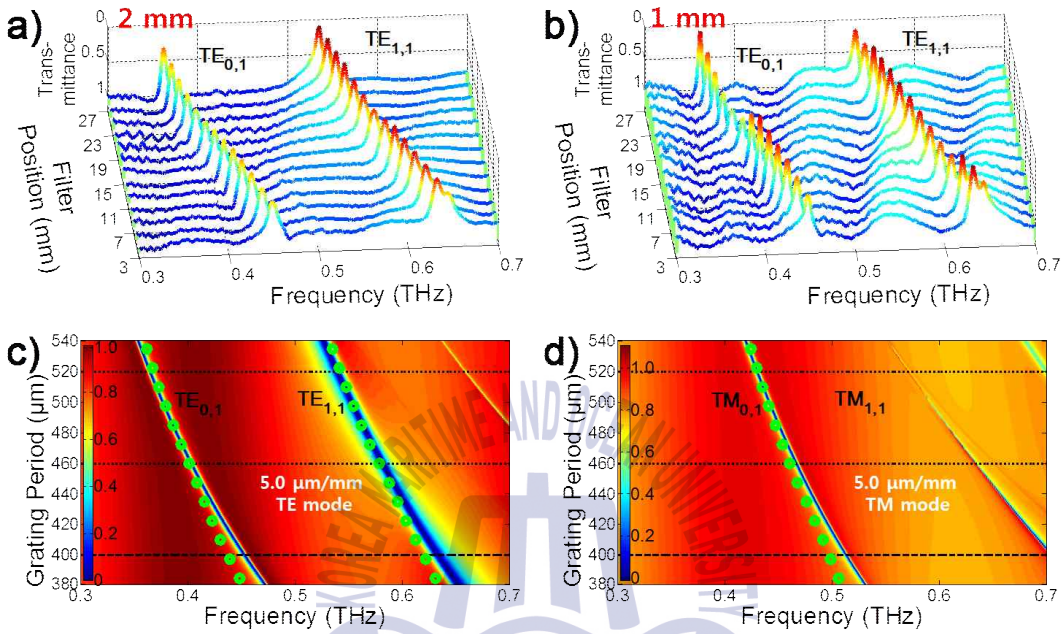

Fig. 4.5 Measurement of transmittance using TGMR filter (Sample-4). (a) 2 mm slit and TE mode. (b) 1 mm slit and TM mode. TGMR Measurement of resonance frequency changes with filter position and FDFD simulation according to grating period. (c) $TE_{0,1}$ and $TE_{1,1}$ modes; (d) $TM_{0,1}$ mode.

Figure 4.5 shows the resonant movement of the TGMR filter of Sample-4 (5.0 ㎛/mm) according to the position shift. Figures 4.5 (a) and 4.5 (b) show the measured transmittance in TE and TM modes, respectively. Figures 4.5 (c) and 4.5 (d) map the FDFD simulation results for resonance frequency shifts due to changes in the grating period. The resonance frequency measured in the TE and TM mode is indicated by the green dot. Figure 4.8 (c) shows that the resonance movements of $TE_{0,1}$ and $TE_{1,1}$ for the TGMR filter movements in the

TE mode are 86.6 and 96.2 GHz, respectively, and the resonant frequency shift ratios for the travel distance are 3.6 and 4.0 GHz/mm. Figure 4.7 (d) shows that the $TM_{0,1}$ resonance shift is 81.8 GHz for the TGMR filter movement in the TM mode, and the resonant frequency shift ratio for the travel distance is 3.4 GHz/mm.

4.3.2 TGMR filter with 3.4 ㎛/mm

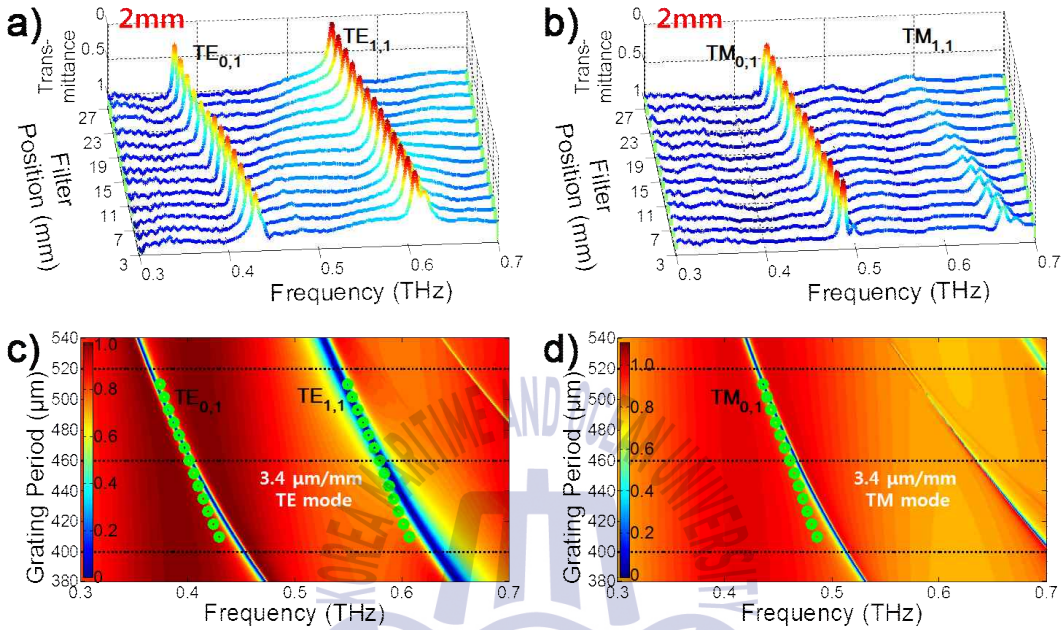

Fig. 4.6 Measurement of transmittance using 2 mm slit and TGMR filter (Sample-5). (a) TE mode; (b) TM mode. TGMR Measurement of resonance frequency changes with filter position and FDFD simulation according to grating period. (c) $TE_{0,1}$ and $TE_{1,1}$ modes; (d) $TM_{0,1}$ mode.

Figure 4.6 shows the resonant motion of the Sample-5 (3.4 ㎛/mm) TGMR filter with respect to its positional displacement. Figures 4.8 (a) and 4.8 (b) show the measured transmittance in TE and TM modes, respectively. Figures 4.6 (c) and 4.6 (d) map the FDFD simulation results for resonance frequency shifts due to changes in the grating period. The resonance frequency measured in the TE and TM mode is indicated by the green dot. Figure 4.8 (c) shows that the resonance movements of $TE_{0,1}$ and $TE_{1,1}$ for the TGMR filter movement in the TE

mode are 55.2 and 57.6 GHz, respectively, and the resonant frequency shift ratios for the travel distance are 2.3 and 2.4 GHz/mm. Figure 4.8 (d) shows that the $TM_{0,1}$ resonance shift is 50.1 GHz for the TGMR filter movement in the TM mode and the resonant frequency shift ratio for the travel distance is 2.1 GHz/mm.

4.3.3 TGMR filter with 1.7 ㎛/mm

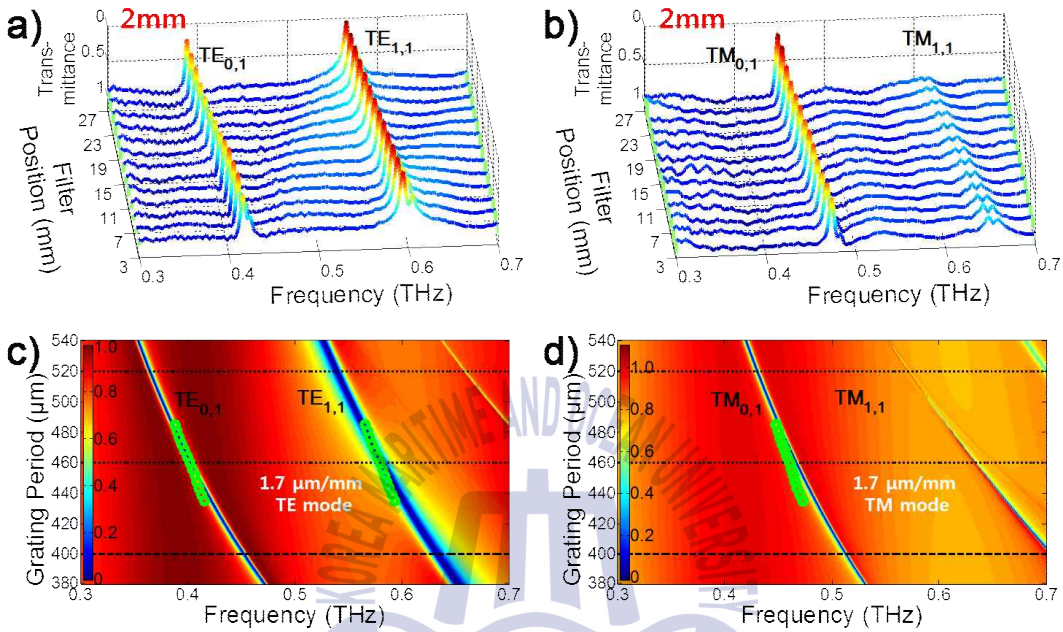

Fig. 4.7 Measurement of transmittance using 2 mm slit and TGMR filter (Sample-6). (a) TE mode. (b) TM mode. TGMR Measurement of resonance frequency changes with filter position and FDFD simulation according to grating period. (c) $TE_{0,1}$ and $TE_{1,1}$ modes and (d) $TM_{0,1}$ mode.

Figure 4.7 shows the resonant movement of the TGMR filter of Sample-6 (1.7 ㎛/mm) with respect to the displacement. Figures 4.7 (a) and 4.7 (b) show the measured transmittance in TE and TM modes, respectively. Figures 4.7 (c) and 4.7 (d) map the FDFD simulation results for resonance frequency shifts due to changes in the grating period. The resonance frequency measured in the TE and TM mode is indicated by the green dot. Figure 4.8 (c) shows that the resonance movements of $TE_{0,1}$ and $TE_{1,1}$ for the TGMR filter movements in the

TE mode are 27.5 and 28.0 GHz, respectively, and the resonance frequency shift ratios for the travel distance are 1.1 and 1.2 GHz/mm, respectively. Figure 4.9 (d) shows the resonance shift of $TM_{0,1}$ for the TGMR filter movement in the TM mode is 24.9 GHz and the resonant frequency shift ratio for the travel distance is 1.0 GHz/mm.

4.3.2 Frequency shift depend on resonance modes

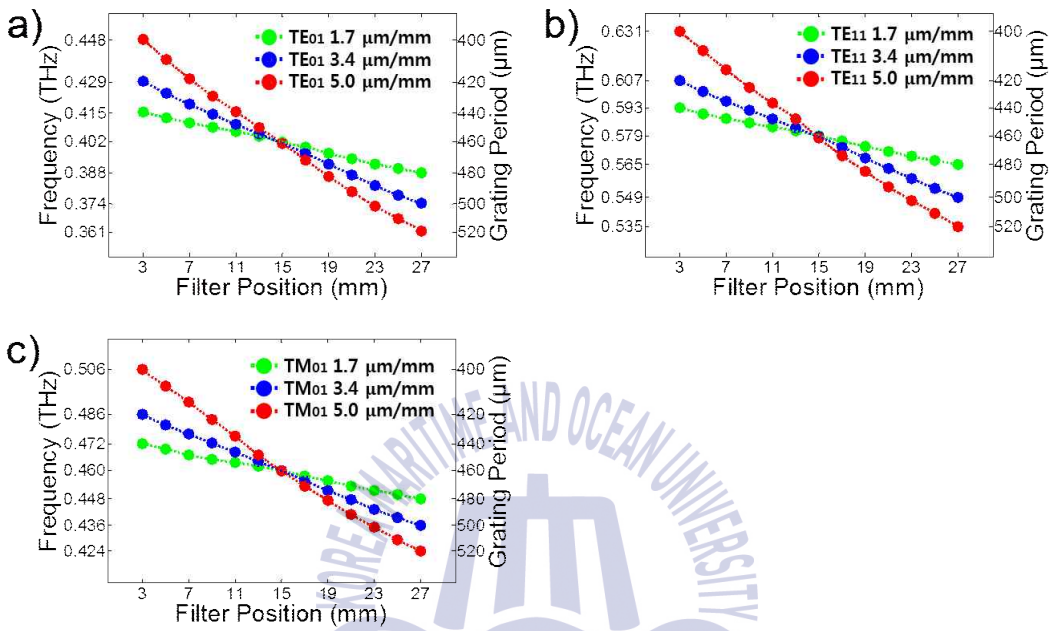

Fig. 4.8 Measured resonance frequency shift according to the TGMR filter movement for (a) $TE_{0,1}$ mode; (b) $TE_{1,1}$ mode; and (c) $TM_{0,1}$ mode. The frequency and grating period scales on the y axis indicate the end points of each data.

Figures 4.8 (a) ~ 4.9 (c) show the resonant frequency shift in the $TE_{0,1}$, $TE_{1,1}$, and $TM_{0,1}$ modes for the fabricated TGMR filters (Sample-4 (5.0 ㎛/mm), Sample-5 (3.4 ㎛/mm), and Sample-6 (1.7 ㎛/mm)).

Figure 4.9 (a) The frequency shifted by 3 to 27 mm position in $TE_{0,1}$ mode is 86.6, 55.2 and 27.5 GHz, respectively, according to Sample 4-6. The rate of change of motion is 0.72, 0.69 and 0.69 GHz/㎛. Figure 4.9 (b) In the $TE_{1,1}$ mode, the frequency shifted according to the position change of 3 to 27 mm is 96.2, 57.6 and 28.0 GHz respectively

according to Sample 4-6. The rate of change of motion is 0.80, 0.72 and 0.70 GHz/㎛. Figure 4.9 (c) The frequency shifted according to the position change of 3 to 27 mm in $TM_{0,1}$ mode is 81.8, 50.1 and 24.9 GHz respectively according to Sample 4-6. The rate of change of motion is 0.68, 0.63 and 0.62 GHz/㎛.

The TGMR filter can easily change the resonance frequency by position shift, and it can replace various GMR filters designed by resonance in one. Also, it is a design that can easily change tunable resonance moving range and precision according to period change rate. All-dielectric GMR filters are resonance tunable designs that are sensitive to the stoichiometry of structures and materials. GMR filters made of all dielectric materials can operate at high power and have very low absorption and high transmittance in the THz range.

4.4 GMR filter and TGMR filter

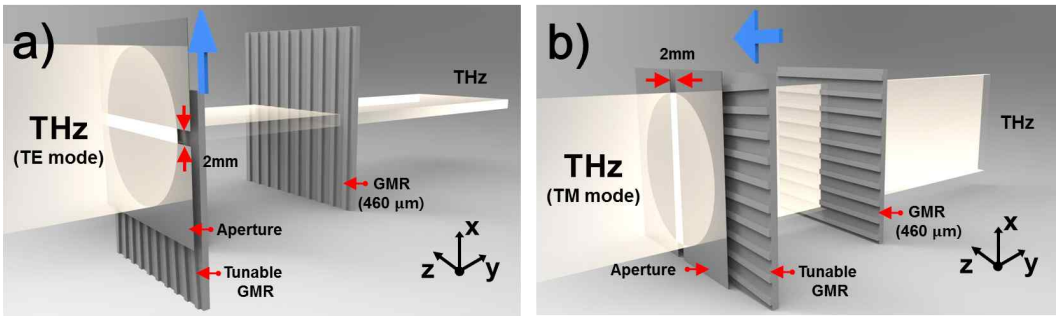

Fig. 4.9 Schematic diagram of the TGMR and GMR filter setup for (a) TE mode; (b) TM mode measurement.

The THz beam passing through the GMR filter has a high transmittance except for the resonance frequency. Low transmission loss can induce strong resonance using two identical GMR filters. If two GMR filters pass through different structures, the two resonances derived from the first filter and the second filter occur independently.

Figure 4.9 is a schematic diagram for measuring the resonance frequency displacement in the TE and TM mode according to the period variation of the TGMR filter among the two GMR filters. The TGMR filter was placed behind a fixed 2 mm metal slit. The position of the TGMR filter changes in the direction of + y (TE mode) or + x (TM mode) at intervals of 2 mm from the top of the TGMR filter with a short grating period. The TGMR grating cycle was moved at precise intervals using a small motorized mobile stage. The resonance frequency displacement was measured according to the grating period change between metal slits. In addition, Sample-2 (460 μm) with a

uniform grating period was placed at a distance of 8 cm from the TGMR in the same beam path as the TGMR filter, and a fixed resonant frequency was generated.

Figure 4.9 (a) shows that the metal slit is positioned perpendicular to the polarization direction of the THz beam and the TGMR filter is positioned in parallel for the TE mode measurement. In Figure 4.9 (b), the slit is positioned parallel to the beam direction and the TGMR filter is positioned vertically to measure TM mode resonance. Due to scattering at the edge of the TGMR filter, TE and TM mode measurements were taken at 2 mm intervals from 3 mm to 27 mm.

4.4.1 Dual resonance with TGMR filter

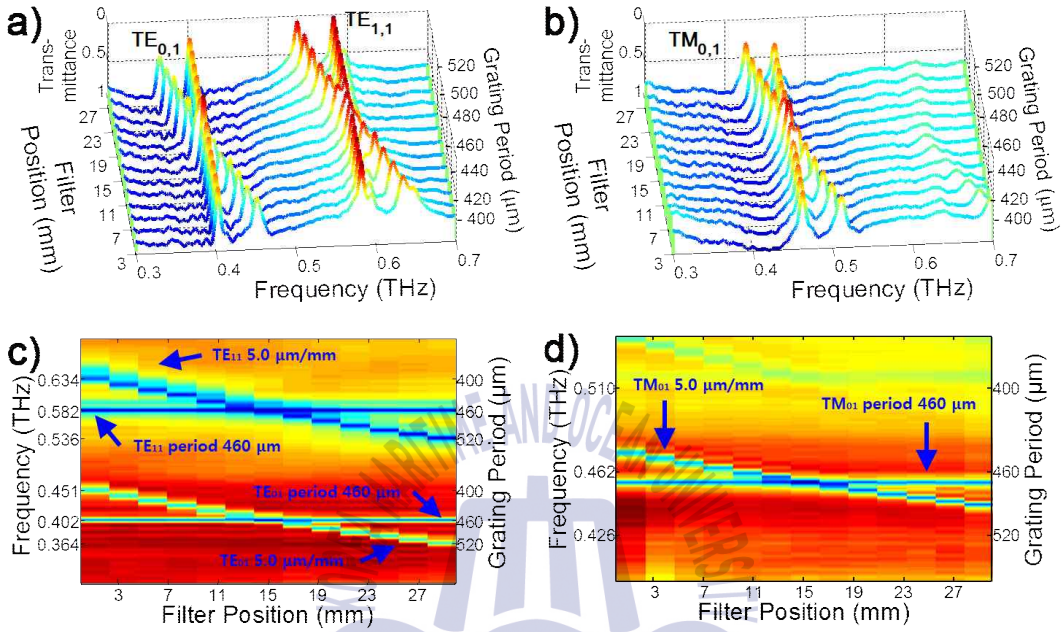

Fig. 4.10 Transmittance measurement using TGMR and GMR filters for (a) TE mode; (b) TM mode. Measured resonance frequency shift with movement of the TGMR filter for (c) TE modes ($TE_{0,1}$ and $TE_{1,1}$); (d) $TM_{0,1}$ mode. The frequency and grating period on the y axis indicate the end points of each data.

Figure 4.10. (a) and 4.10. (b), the first TGMR filter moves from the high-frequency region to the low-frequency region as the grating period increases. Figure 4.10. (a) The total resonant frequency shift of the TGMR filter is 87, 98 and 84 GHz for the $TE_{0,1}$, $TE_{1,1}$ and $TM_{0,1}$ modes, respectively. The tunable range of the TGMR is the same as that of the TGMR filter as shown in Figure 4.7 (c) and 4.7 (d), which means that resonance occurs independently.

Figures 4.10 (c) and 4.10 (d) show the map of the resonance frequency

shift passing through two filters, Smaple-4 (5.0 ㎛/mm) and Sample-2 (460 ㎛), in TE and TM mode. In the second GMR filter, fixed resonance was measured at 0.402, 0.582 and 0.463 THz for $TE_{0,1}$, $TE_{1,1}$ and $TM_{0,1}$ due to the uniform grating period of Sample-2 (460 ㎛). Independent resonance through two GMR filters with high transmittance of GMR filter appears well. The first TGMR filter with different frequencies and the two resonances derived from the second filter occur independently and are measured at the same time. When two TGMR filters and GMR filters have the same structure, strong resonance is measured.

4.5 Conclusions

Compared to the THz transmittance characteristics of a MMs, the all-dielectric GMR filter has many advantages. Fabricating MMs with metal patterns on the surface of a dielectric material involves a complicated process and high cost. Furthermore, the
MMs has high reflection loss because of the high refractive index of metal. The resulting low transmittance limits the application of MMs. In contrast, an all dielectric GMR filter has a simple low cost process with low reflection loss.

In this research, we first demonstrate a tunable THz resonance using a TGMR filter which continuously changes its grating period. The resonance frequency can be selected by simply moving the filter with respect to a metal slit of 2 mm. The proposed method in this study is a much simpler and quicker method of changing the resonant frequency than replacing GMR filters with different grating periods. Furthermore, by simultaneously using a TGMR and GMR filter, the design allows tunable dual resonance for the TE and TM modes, with a tunable resonant frequency and a fixed resonance frequency.

In conclusion, because the proposed TGMR filter has a tunable resonance frequency, it has potential for THz applications in spectroscopy, modulators, image sensors, and filters for THz communications in the future.

Chapter 5 Polarization Insensitive GMR filter

5.1 Introduction

The GMR principle has been applied to devices such as filter [58], sensor [59, 60], polarizer [55], reflector [61], and various tunable [53-57] devices from Micro wave to Optic wave domain. In particular, the THz wave has a wavelength sufficiently larger than that of Optic and sufficiently smaller than that of Micro. The simple structure of a microwave and the miniaturized advantages of an optic wave can be applied in the THz domain by using GMR principles with new fabrication methods and structures. GMR filters fabricated from all-dielectric materials show lower refractive index and higher transmittance than MMs. It is monolithic in structure, simple to induce strong reaction from dielectric, and can be used stably at higher power than metal. Because of the advantages of this GMR filter, it shows potential as various filters. In particular, a band-pass filter [58], a notch filter [62], an angular tolerant filter [63], and a polarization-insensitive grating filter (PIGF) using GMR filters have been reported for various purposes. Some applications, such as high-density wavelength division multiplexer, and polarization sensitive filters require polarization insensitive characteristics that are adapted to electromagnetic waves with arbitrary polarization states.

The resonance frequency position of the one-dimension (1-D) GMR filter is very sensitive to the direction of beam polarization. 1-D polarization insensitive filters have been classified into oblique-incident

and normal-incident types according to the direction of the beam. Lacour and Niederer have developed oblique incident type polarization insensitive characteristics in which the resonance frequency of TE and TM modes is not changed according to the properties of the filling factor effect [64] and the depth effect filling factor [65]. Also, polarization insensitive filters fabricated as normal incident types have been reported. Fu used a grating and four-film stack [66], and Wu fabricated a polarization-insensitive filter with a normal incident type using a binary blazed grating [67]. Some polarization insensitive filters have resonant Q-factor differences in TE and TM modes and are applicable with dual-bandwidth or narrow-band filters. In addition, Alasaarela proposed a polarization insensitive filter using the rectangular profile and sinusoidal profile [68].

Polarization insensitive properties can be easily designed in a lattice structure with a symmetric two-dimensional (2-D) period than a 1-D structure. A grating with a 2-D period on the GMR filter can be divided into rhombic [69], rectangular [70-72], and circular [73, 74]. Gratings with 2-D periods have two orthogonal directions [75], two orthogonal directions, and doubly periodic gratings [75, 77]. The GMR circular grating filters (CGFs) [78, 79] have a TE and TM mode polarization direction at all positions of the GMR filter, and two resonances of the TE and TM mode exhibit polarization insensitive characteristics.

We designed the monolayer guided-mode resonance (mGMR) filter and investigated the transmittance characteristics according to the polarization. By combining two GMR filters, GMR filter, which can be

converted into two characteristics of modulation filter and Polarization insensitive filter, is completed. As a modulation filter, it is possible to control the resonance magnitude according to the polarization according to the tilted angle ($\triangle n$), and to adjust the resonance magnitude variation range according to the polarization. As the polarization insensitive filter, when the tilted angle (α) between two GMR filters increases, the resonance size change and the resonance frequency change due to the polarization become smaller. The tilted angle of the two separated GMR filters was found to be Polarization Insensitive filter characteristics in the vertical direction The size of the resonance was formulated, and the relationship constants were obtained from the experimental results. Finally, a more stable polarization insensitive filter was completed using a GMR filter with two GMR filters connected vertically.

5.2 mGMR filters

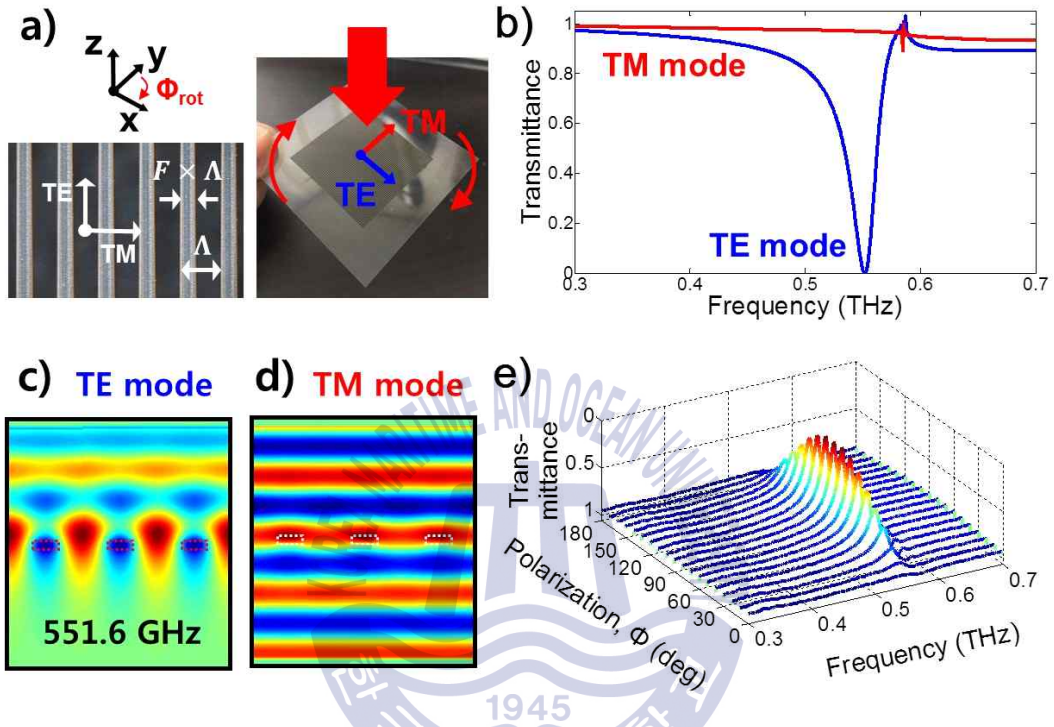

Fig. 5.1 Resonance properties of mGMR filter. (a) Microscope picture of mGMR filter. GMR filter has width of 50 mm and length of 50 mm. The linearly polarized THz beam enters the mGMR filter to a diameter 25 mm (refractive index = 1.75, D1 = 75 ㎛, grating period (Λ) = 510 ㎛, and filling factor = 32 %). (b) FDFD simulation depend on modes. (c) Electric field of the TE mode at 0.552 THz. (d) Magnetic field of the TM mode. (e) Measured transmittance according to the polarization.

Figure 5.1 (a) shows a schematic of a mGMR filter. PET film (n = 1.75) can be cut to make mGMR filter easily. Two mGMR filters were fabricated using a 75 ㎛ thick PET film at 510 ㎛ intervals (prepared by L2K Co. using femto-second laser machining (FSLM)). The TE mode is a blue arrow direction component that matches the polarization

direction of the beam and the grating direction. The TM mode is a red arrow direction component in which the polarization direction of the beam is perpendicular to the grating direction.

Figure 5.1 (b) shows the results of the TE and TM mode FDFD simulation through the mGMR filter. In the TE mode, the mGMR filter is completely blocked, and conversely, the mGMR filter is well transmitted in the TM mode. The transmittance efficiency is as high as 99.9%. The resonance occurs and disappears according to the direction of the mGMR filter and the incident beam. Figures 5.1 (c) and 5.2 (d) show the electric field and magnetic field distribution at a resonance frequency of 0.552 THz. It is divided into mGMR filter and two vector components of TE mode (z-axis) and TM mode (x-axis), which intercept according to the polarization direction of the incident beam.

Figure 5.1 (e) shows the transmittance of the mGMR filter and beam polarization direction. When the mGMR filter rotates from 0° to 90° , the transmittance decreases (resonance depth increase). Conversely, when beam polarization increases from 90° to 180° , the transmittance increases (resonance depth decrease). The resonance frequency was measured at 0.550 THz between resonance range 0.473 ~ 0.588 THz. Figure 5.1 (e) shows the resonance characteristics of the mGMR filter with respect to the polarization change, repeating the generation and disappearance of the resonance once every 180° with the cosine cycle.

5.3 Polarization Insensitive GMR filter

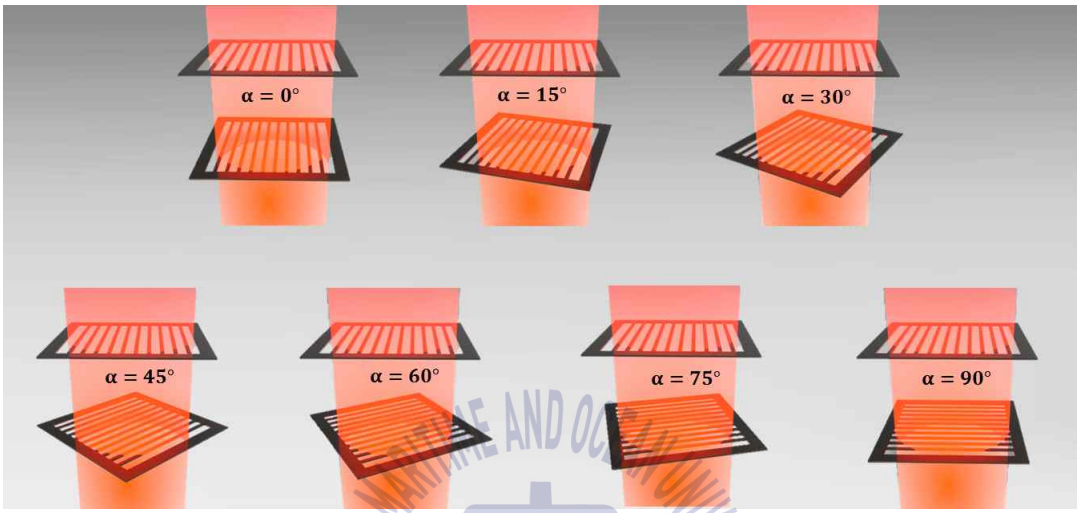

Fig. 5.2 Transmittance characteristic according to the polarization. The two mGMR filters are 8 cm apart from each other.

Figure 5.2 shows the tilted angles (α) = 0°, 15°, 30°, 45°, 60°, 75° and 90° of two mGMR filters. The first mGMR filter was fixed to the TE mode in such a way that the direction of the beam was in the same direction as the grating direction. A second mGMR filter was placed 8 cm behind to remove the effect between the two GMR filters. Based on the first mGMR filter, the second mGMR filter rotates clockwise by 90° to adjust the tilted angle (α) of the two mGMR filters.

5.3.1 Tilted angle (α) of two mGMR

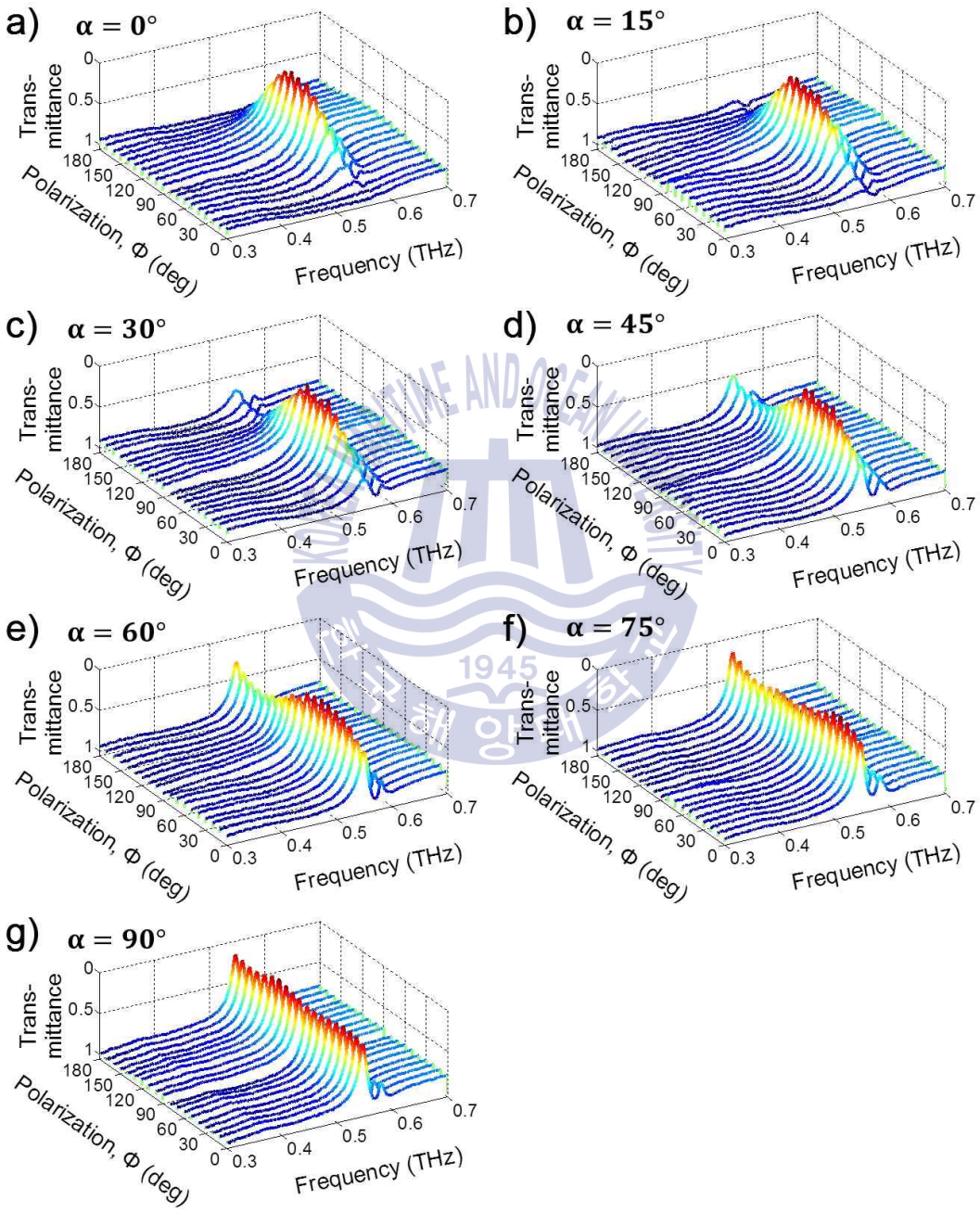

Fig. 5.3 Measurement of transmittance according to tilted angle α of two mGMR filters. (a) α = 0° , (b) α = 15° , (c) α = 30° , (d) α = 45° , (e) α = 60° , (f) α = 75° , and (g) α = 90° Schematic diagram of two mGMR filters separated by 8 cm.

Figure 5.3 shows a three-dimensional graph of the transmittance measured as a function of the tilted angle (α) of two mGMR filters. The resonance changes of one mGMR filter were measured for tilted angles of 0° , 15° , 30° , 45° , 60° , 75° and 90° at 10° intervals from 0° to 180° . Figure 5.3 (a) shows that when the grating directions of two mGMR filters match, the tilted angle is α = 0° . The resonance generation and extinction at the resonance frequency according to the polarization change are the same as the resonance change and the cycle of the mGMR filter. The size of the resonance cuts the transmittance close to zero in the blocking TE mode, and the transmittance close to 1 was measured in the transmitted TM mode. Figures 5.3 (b) - 5.3 (g) show the 3-D graphs of the tilted angle (α) of two mGMR filters and the magnitude of the resonance magnitude change according to the polarization change. As the tilted angle (α) increases, the depth variation width of the resonance decreases and converges to a constant resonance size. Figure 5.3 (g) shows the resonance amplitude of the two mGMR filters at the maximum Tilted angle α = 90° . The resonance magnitudes of the maximum and minimum values of the upper and lower layers of the mGMR filter are matched when the Tilted angle α = 90° of the two mGMR filters. The opposite is also true. Polarization insensitive filter characteristics which does not cause constant resonance depth change according to polarization change are shown.

5.3.2 Formula model and fitting lines

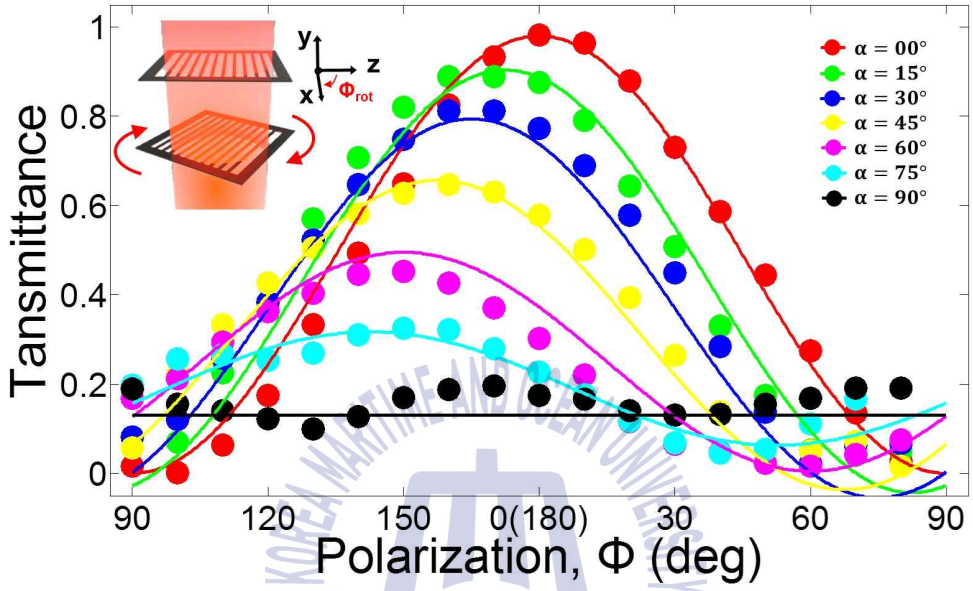

Fig. 5.4 Transmittance change at resonant frequency (0.550 THz) with changing tilted angle and the polarization of two mGMR filters. Dots are the measurement result. The solid line is a fitting line using the formulated Equation (3). The conceptual diagram inserted at the top left shows the tilted angle of two mGMR filters.

The occurrence and disappearance of the resonance according to the polarization change of the mGMR filter is explained by Malus's law.

$$I = I_0 \cos^2\theta$$

In Figure 5.2 (e), the measured transmittance at the resonance frequency according to the polarization change is expressed by Equation (2).

$$T_\alpha = a_1 \times \cos^2(\Phi + \alpha) + a_2$$

In Equation 2, the value of the constant a_1, which means the resonance

depth, is the resonance depth measured in the mGMR filter. a2 is the value of the offset constant. The loss tangent (δ) of the mGMR filter and a finite number of grooves yielded a value of a1 = 0.94. Φ is the polarization change, and α is the tilted angle of the mGMR filter.

Figure 5.4 shows the variation of resonance depth according to the tilted angle and the polarization change of two mGMR filters in Figure 5.3. The modified model is able to express the magnitude of resonance change with tilted angle and the polarization change. The sum of the resonances due to the polarization is expressed by Equation (3).

$$fitline = b_1 \times (T_0 + T_\alpha) + b_2$$

The fitting constants b_1 and b_2 were calculated from measured values according to the Tilted angle change in Figure 5.4. b_1 has a constant value of 0.5, and b_2 has a linearly changing value according to the tiled angle ($b_2 = 0.0039 \times \alpha$). The models modeled according to the tilted angle and the polarization change of two mGMR filters agree well with the measured values. When the tilted angle $\alpha = 90°$, the sum of the resonance depth was 0.82 and the constant value was measured.

5.4 Combined Two mGMR filter

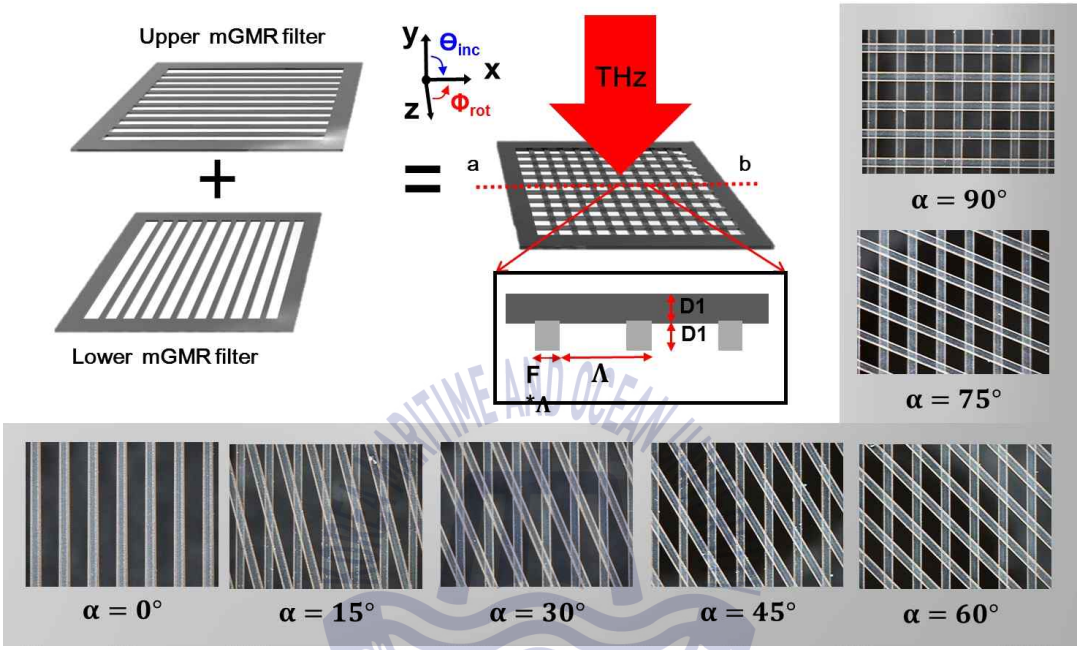

Fig. 5.5 Schematic of two mGMR filters combined. The filter has a width of 50 mm and a length of 50 mm. The linearly polarized THz beam is input to the GMR filter with a diameter of 25 mm (refractive index = 1.75, D1 = 75 ㎛, Λ = 510 ㎛ and filing factor = 32 %).

Figure 5.5 (a) is a schematic diagram showing a simple structure and a tilted angle (α) by combining two mGMR filters. The combined upper layer mGMR filter was fixed in the TE mode direction consistent with the polarization direction of the THz beam. Based on the combined mGMR filter, the combined mGMR filter was rotated clockwise and the tilted angle (α) was rotated from 0° to 90° by 15° . Figure 5.5 (c) is a photograph taken with an electron microscope when the tilted angle (α) is 0° , 15° , 30° , 45° , 60° , 75° , 80° and 90° .

5.4.1 Tilted angle (α) of two mGMR

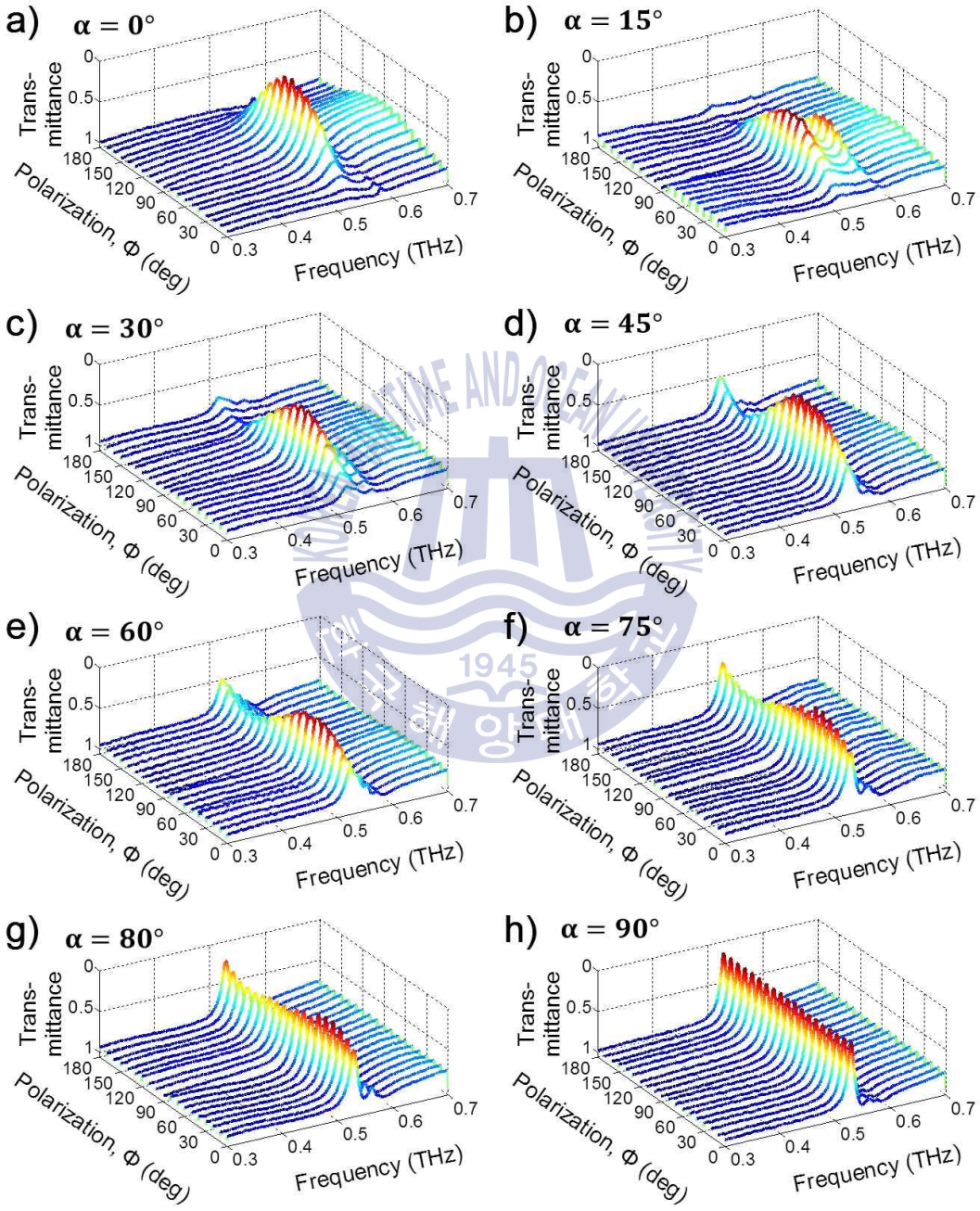

Fig. 5.6 Measurement of transmittance according to tilted angle α of two mGMR filters. (a) α = 0° , (b) α = 15° , (c) α = 30° , (d) α = 45° , (e) α = 60° , (f) α = 75° , (g) α = 80° , and (h) α = 90° Schematic diagram of two combined mGMR filters.

Figure 5.6 shows a three-dimensional graph of transmittance characteristics measured according to the tilted angle (α) and polarization change of the combined mGMR filter. Tilted angle (α) Measures the resonance change of one period by 0° , 15° , 30° , 45° , 60° , 75° , 80° , and 90° .

Figure 5.6 (a) shows that when the grating direction of the coupled mGMR filter is matched (α = 0°). The resonance occurs and disappears according to the change of polarization, and as the grating thickness increases, the resonant frequency shifts to low frequency The half width increased.

Figure 5.6 (b) - 5.6 (h) shows a 3-D graph of the resonance depth according to the tilted angle (α) and polarization changes. Combined mGMR filter When the relative angular difference is large, the variation width of resonance depth decreases and converges to a constant resonance depth. Conversely, the smaller the tilted angle (α), the greater the half-width of the resonance. Figure 5.8 (b) also shows the resonance side-loop resonance when the tilted angle α = 15° .

Figure 5.8 (h) shows the same resonance depth at the polarization change at the tilted angle α = 90° for the combined mGMR filter. A GMR filter with two mGMR filters coupled to one another exhibits a polarization independent filter characteristic with the same resonance to the change in polarization.

5.4.2 Formula model and fitting lines

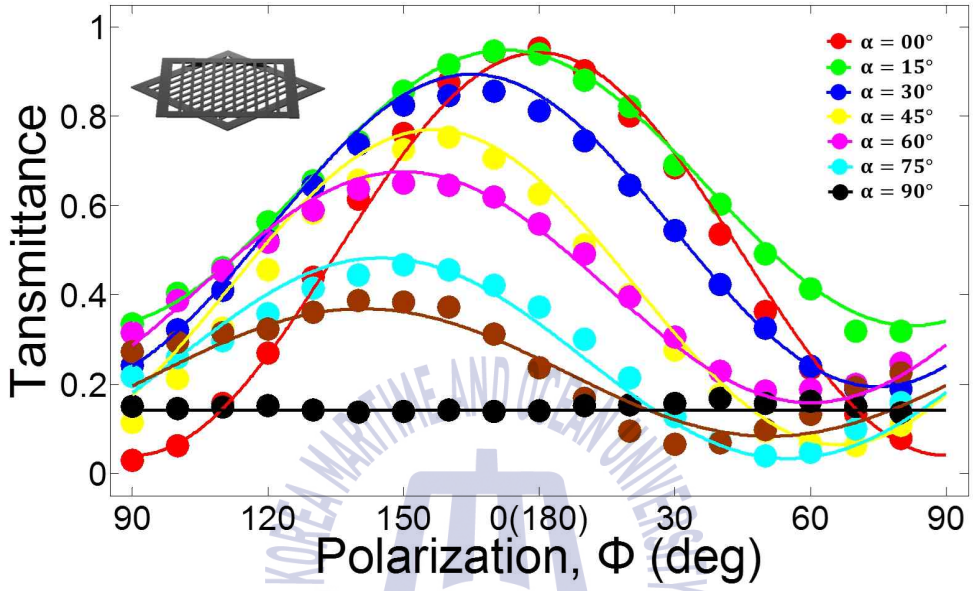

Fig. 5.7 Transmittance change with changing tilted angle and polarization of two mGMR filters. Dots are the measurement result. The solid line is a fitting line using the formulated Equation (3). The conceptual diagram inserted at the top left shows the tilted angle of two mGMR filters.

The fitting constants b_1 and b_2 were calculated from the measured values according to the tilted angle changes in Figure 5.6. b_α is has a linearly changing value according to the tiled angle ($b_1 = 0.0061 \times \alpha$). b_2 has a constant value of zero. In the coupled GMR filter, the model modeled according to the tilted angle and polarization change of the two mGMR filters agree well with the measured values. When $\alpha = 90°$, the sum of the resonance depth is 0.82, which is a constant value. The resonance depth according to the polarization change of the GMR

filter is the same, and the resonance frequency is measured at 0.529 THz which is moved to the low frequency.

5.4.3 Compare PI GMR filters

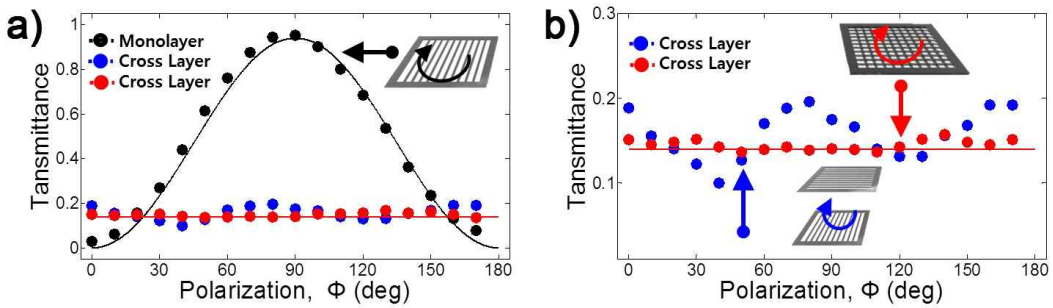

Fig. 5.8 (a) Transmittance due to change in polarization. The black dot indicates mGMR. (b) Transmittance due to change in polarization and tilted angle (α). The blue dot indicates the case where two mGMR filters are separated by 8 cm and the red dot is a structure in which two mGMR filters are combined.

Figure 5.8 shows the change in resonance depth due to the polarization change of the two separated mGMR filters and the coupled mGMR filters. The mGMR filter shows the change of resonance occurrence and extinction according to polarization in TE and TM mode. On the other hand, it has a uniform resonance depth according to the polarization change of 8 cm and exhibits a resonance depth difference of less than ~ 5.0 %. In the finally coupled mGMR filter, the uniform resonance depth due to the polarization change is more uniformly measured to be less than ~ 0.16 %. Figure 5.8 shows resonance depth uniformity and polarization independent GMR filter characteristics that are more stable than the two separated mGMR filters.

5.4.4 Field distribution of PI GMR fitler

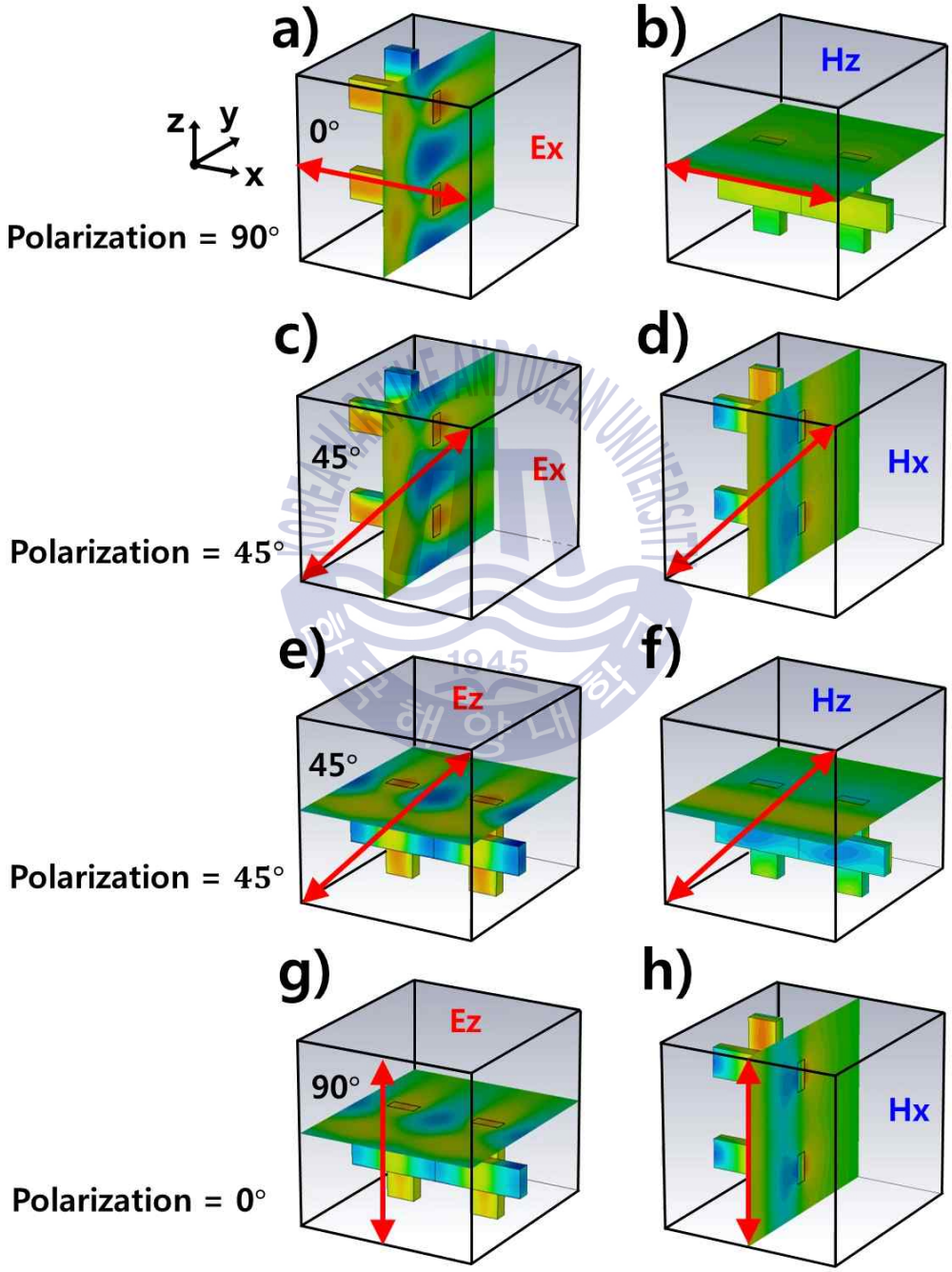

Fig. 5.9 Filed distribution of upper and lower gratings by THz beam polarization. (a) and (b) THz beam polarization = 0° , (c – f) THz beam polarization = 45° , (g) and (h) THz beam polarization = 90° and Transmittance with the 8 unit cells illustrated.

Figure 5.9 shows the field distribution of the GMR filter using CST simulation according to the polarization 0° , 45° , and 90° of the incident beam on the combined mGMR filter. As in Figure 5.9, the TE mode component that blocks the resonance frequency and the TM mode that the resonance frequency passes are divided into two vector components. Figure 5.9 (a) is E-fied in upper mGMR filter and 5.9 (b) is H-fied in lower mGMR filter. Polarization = 90 ° and the induced resonant frequency field is checked. The upper mGMR filter operates in TE mode and the lower mGMR filter operates in TM mode.

On the other hand, in Figure 5.9 (g) and 5.9 (h), the upper mGMR filter with the beam direction and grating direction vertical at the polarization = 0° operates in TM mode. The TE mode operates on the lower mGMR filter where the beam direction and the grating direction are parallel, and the induced resonance frequency electric filed is confirmed.

In Figure 5.9 (c – f), the electric field corresponding to TE mode at the polarization = 45 ° has both vector components in the x- and z-axis directions and both TE and GMR filters operate in TE mode. when the polarization is 90° and 0° , Both the electric field and the magnetic field of the resonance frequency appear. In a combined mGMR filter, resonance appears in all polarization directions of the THz beam.

5.4.5 CST simulation

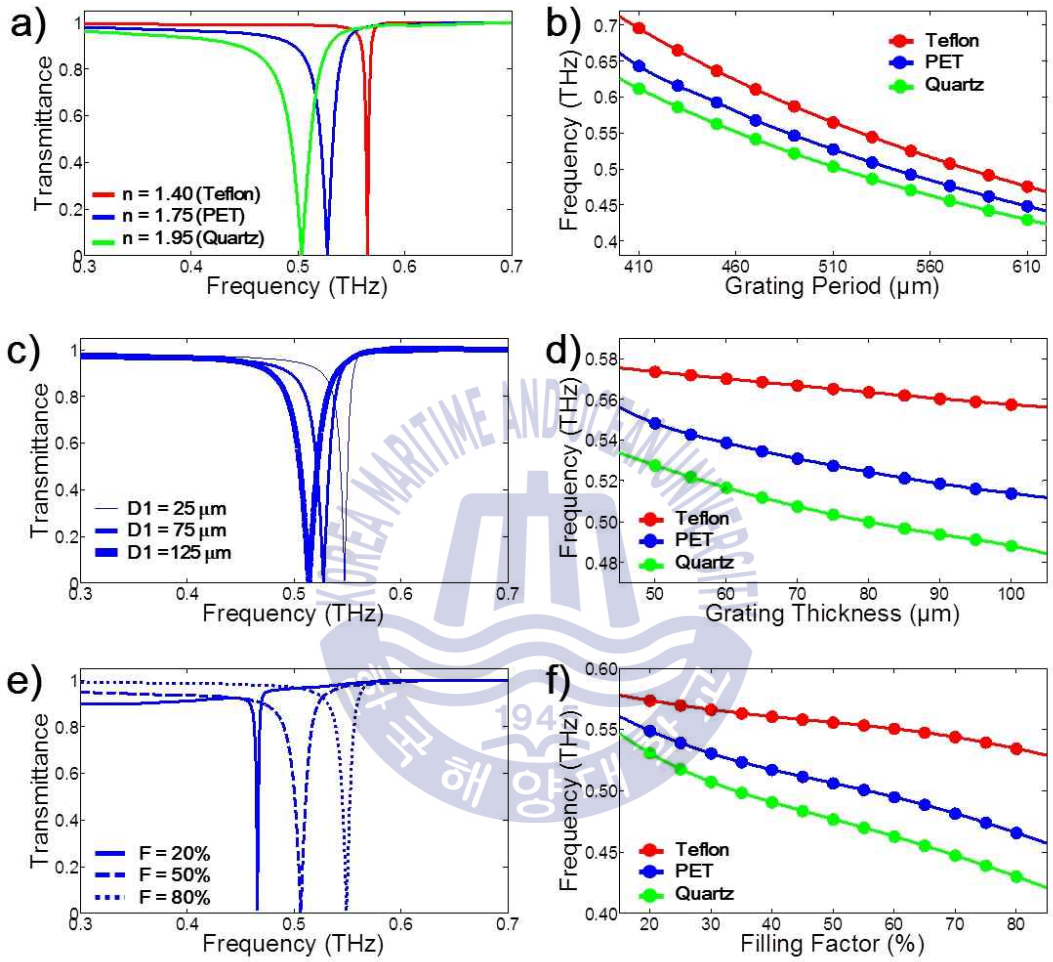

Fig. 5.10 CST simulation according to the structure change of GMR filter (grating period = 510 ㎛, D1 = 75 ㎛, filling factor = 32 %). (a) Transmittance characteristics according to refractive index change. The red line is 1.4 (Teflon), the blue line is 1.75 (PET) and the green line is 1.95 (quartz). (b) Resonance shift due to grating period variation (410 ~ 610 ㎛). (c) Transmittance characteristics according to grating thickness variation and (d) resonance shift. (e) Transmittance characteristics according to the change of filing factor and (f) resonance shift.

As shown in Fig. 6 (a), a non-polarized GMR filer (attached at right angles) was further simulated to investigate where the resonance occurred according to the echo index. In addition, the different film materials, grating period, lattice thickness, and fill factor of Teflon, PET and quartz are ordered in Fig. 6 (a, b, d, f) The process required to design a filter that can operate at the target frequency.

The data in Figure 6 (a) shows the resonance conversion and Q factor changes according to the exponents 1.4, 1.75 and 1.95 (quartz, PET and Teflon). When the refractive index difference (Δn) between the grating and the non-grating is small, resonance occurs at a high Q value and high frequency. Second, the data in Fig. 6 (b) shows that the diffraction direction is determined according to the grating period size and the wavelength size, and changes of the resonance wavelength. In order to generate strong resonances, a limited number of cycles must be included in the limited THz beam size [48], and a larger beam size is required to increase the cycle. Figure 6 (c, d) shows the thickness of the slab waveguide. As the thickness of the grating becomes thicker, the induced resonant wavelength increases and moves to lower frequencies. High Q value can be obtained with a small thickness. However, the high Q factor greatly affects the loss tangent of material and resonance, and the relationship between loss tangent and Q factor must be designed. Finally, in Fig. 6 (e, f), the change of filling factor affects the loss and transmissivity of the GMR filter. Higher filtering coefficients increase spatial density and lower frequency transmittance. Conversely, low filling factors result in lower spatial density, higher transmittance, and reduced loss effect.

5.5 Conclusion

The mGMR filter with the grating structure was designed. By combining two mGMR filters, it is possible to control the resonance depth change according to the THz beam polarization. The tilted angle of the two mGMR filters can be changed to a modulation filter and a polarization insensitive filter.

The modulation filter is represented by the tilted angle (α) along the direction of two GMR filter gratings and the sum of the resonance depth according to the polarization. (α) The resonance depth change width is determined by the magnitude at the angle, and all the magnitude change periods are. In addition, the relationship between two mGMR filters is formulated and agrees well with the measured values.

Polarization insensitive filter can obtain constant resonance depth and frequency change according to THz beam polarization when two mGMR filters are mutually according to grating direction. This phenomenon is explained by the equation of the electric field of the CST simulation and the principle of the polarization insensitive filter. At this time, when the two separated mGMR filters, deviation of the resonance depth is 5.0% and when the two mGMR filters are combined, the deviation of the resonance depth is measured as 0.16 %. The deviation range is reduced by 97 % and a stable polarization insensitive GMR filter combined with one is realized.

Chapter 6 Guided mode resonance film sensor

6.1 Introduction

The concept of guided-mode resonance (GMR) is widely used and applied in micro and optic wave fields. For example, polarizer [55], color filter [58], bandpass filter [58], GMR sensors [59, 60] and etc. However, in the terahertz region, it is difficult to find a study using the concept of GMR biased toward the study of MMs [104-108]. The electromagnetic spectrum including terahertz (0.1 ~ 5 THz) is part of the bandwidth between Microwave [49] and Optic wave [50]. Due to the overcoming of the THz gab [5] and the need for a new frequency domain, the technology in the micro and optic wave field is heading towards THz. This can lead to very exciting phenomena and new possibilities. Microwave Due to the shorter wavelength, the size of the GMR filter in THz is reduced according to the scale factor [1].

THz has been extensively investigated in the last few years using waveguide [8], MMs [18-24], absorber [2], image [27], sensor [18-20, 59, 60], and communications [28, 29]. THz proposed improved measurement methods using various structures to detect the properties of materials. The MMs [18-20] and parallel-plate waveguide (PPWG) [8], and resonance frequency shift [80].

Typical film measurement methods are waveguide (PPWG), MMs, and cylinder waveguide [81]. The film measurement method using the previously studied meta-material or PPWG can measure only a limited thickness. As the film thickness increases due to structural limitations,

the sensitivity can not be reduced or measured. The GMR filter, which is made of an all-dielectric structure, is capable of measuring the film thickness without any thickness limitation using the GMR filter, which is sensitive to the property of the material. The transmission characteristics of the GMR filter designed according to the thickness and loss tangent (δ) of the film were measured. The film thickness, refractive index, and loss tangent of the GMR filter were verified by simulation and measurement.

6.2 mGMR filter

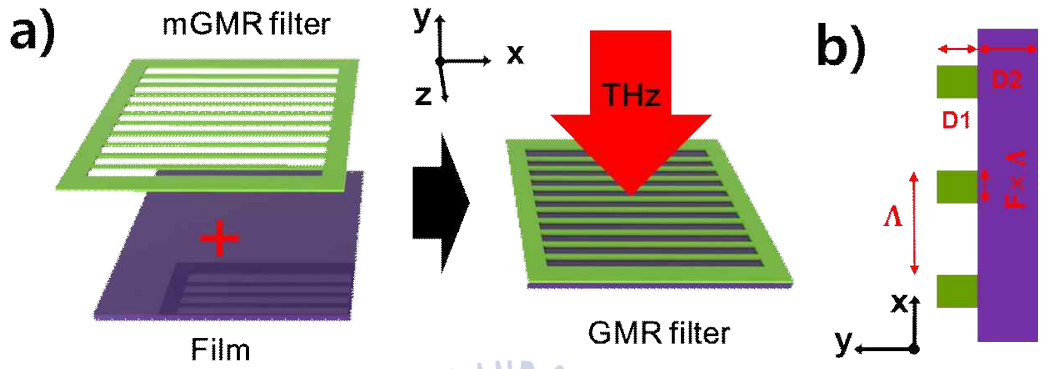

Fig. 6.1 (a) Schematic diagram describing a THz beam passing through GMR filters. GMR filter has a width of 30 mm and length of 30 mm. Grating and film combined each other. The linearly polarized THz beam enters the GMR filter to a diameter of 25 mm. The separation ($\Lambda \times F$) between each of the grooves is 163 ㎛, D1 = 75 ㎛, Refractive index = 1.75, Λ = 510 ㎛, and filing factor = 32 %.

Figure 6 (a) is a schematic diagram of a GMR filter completed by combining a designed mGMR filter with a film. The grating of the mGMR filter has a separation ($\Lambda \times F$) of 163 ㎛, D1 = 75 ㎛, refractive index = 1.75, Λ = 510 ㎛ and piling = 32%. The mGMR filter and film can be easily separated and attached without the empty space due to static electricity. A new GMR filter is completed according to the kind of film (quartz, PET, Teflon) and thickness of the mGMR filter. The difference in film thickness, refractive index and absorption rate can be measured by the resonance frequency and magnitude shift according to the characteristics of the GMR filter. The THz beams perpendicular to the + y axis pass through the GMR filter.

6.2.1 Resonance region

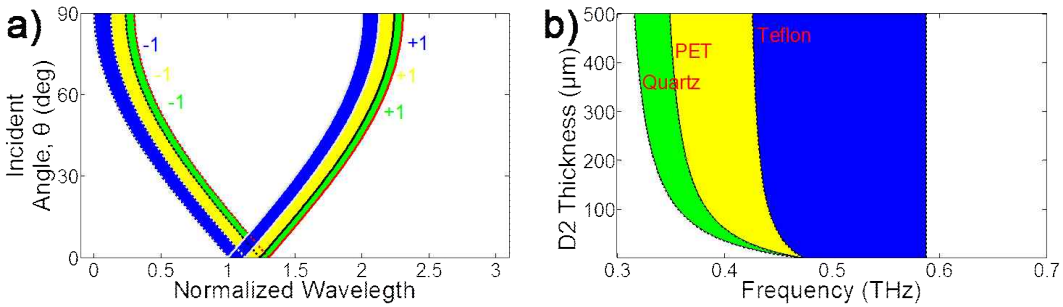

Fig. 6.2 (a) Resonance region according to the incident angle of the mGMR filter, The yellow, green, and blue areas represent Quartz, PET, and Teflon with D2 thickness 0 ㎛. (b) Resonance region according to thickness of film (D2). The yellow, green, and blue areas represent Quartz, PET, and Teflon films.

Figure 6.2 (a) shows the range of resonance occurrence for diffraction (m = ± 1) according to the angle of incidence and refractive index of the designed mGMR filter. The yellow, green and blue ranges refer to quartz, PET, and Teflon. When the film (D2) is quartz (n = 1.95), the resonance (± m) frequency range is 0.336 ~ 0.588 THz. If the film (D2) is PET and Teflon, the refractive index is 1.75, 1.4, and the frequency range of the first (± m) mode is 0.366 ~ 0.588 THz and 0.434 ~ 0.588 THz.

Figure 6.2 (b) shows the range of resonance according to the thickness and type of the film bonded to the mGMR filter fabricated with the PTE film. yellow, green and blue are resonance expected ranges according to Quartz, PET and teflon film combined with mGMR filter. The resonance occurrence range is determined by n_{avg} determined by

the thickness and the refractive index of the film. n_{avg} is the average refractive index of the mGMR filter and film.

6.2.2 Characteristics if GMR filter

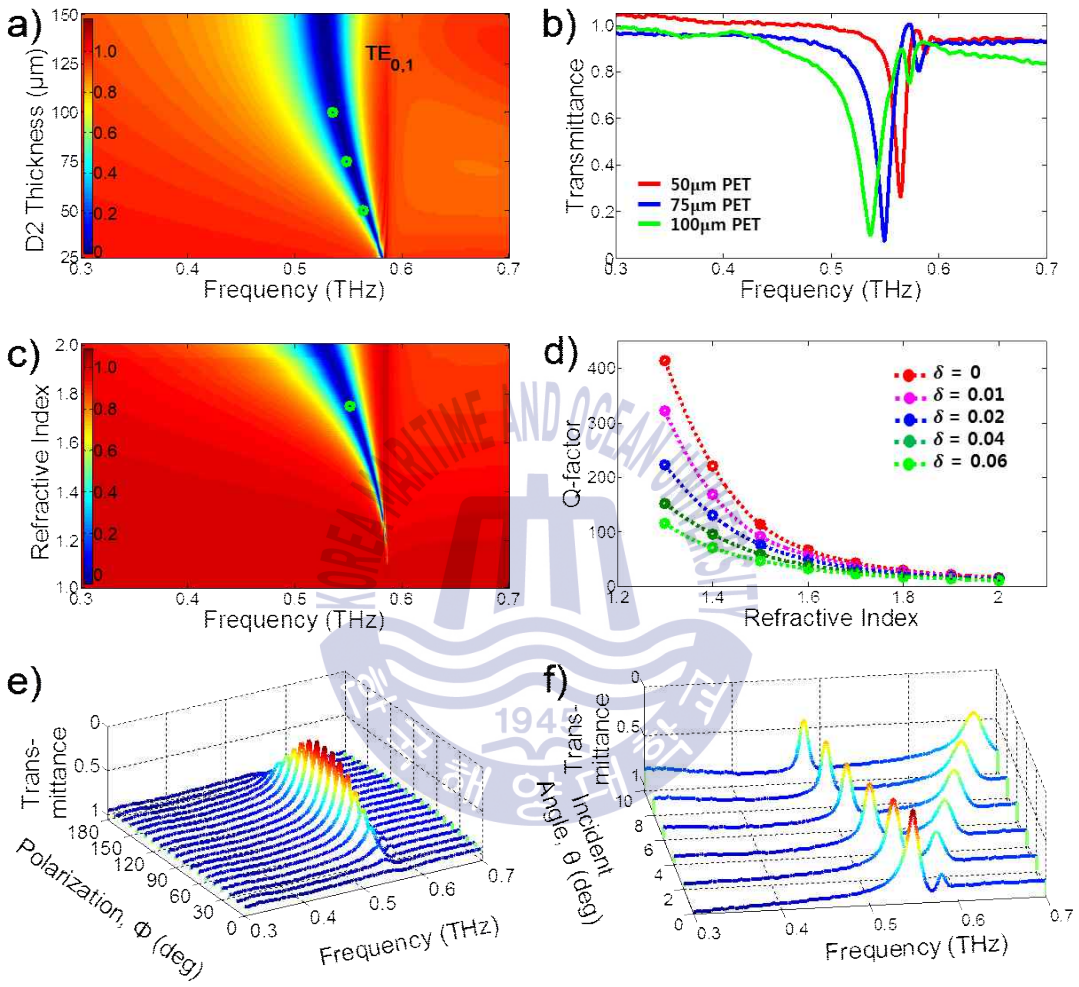

Fig. 6.3 (a) Simulation of transmittance characteristics according to lattice thickness (D1) in TE mode. Refractive index = 1.75, D1 = 25 ~ 150 ㎛, Λ = 510 ㎛, and filing factor = 32 %. (b) Measured transmittance of mGMR filter. The green, blue, and red lines have grating thicknesses of 100, 75, and 50 ㎛. (c) Simulation of transmittance characteristics according to refractive index of grating (1.0 ~ 2.0) in TE mode. (d) Change of Q-factor according to loss tangent and refractive index of mGMR filter. (e) Transmittance characteristics according to the measured polarization. (f) Transmittance

characteristics according to incident angle of THz beam.

Figure 6.3 shows the design characteristics of the mGMR filter. Figure 6.3 (a) shows the FDFD simulation according to the thickness variation of the mGMR filter. In Loss less, the grating (D1) refractive index is fixed at 1.75 and the change of resonance movement and resonance width (FWHM) according to the grating thickness change to the film thickness 25 ~ 150 ㎛.

Figure 6.3 (b) shows the transmittance characteristics of the mGMR filter designed with three different thicknesses. PET films with thicknesses of 100, 75 and 50 ㎛ were cut into 510 ㎛ periodic patterns using femto-second laser processing (FSLM). The grating's filing factor is 32%. Due to the femto-second laser focal distance, it is difficult to produce a pattern with a thickness of more than 100 ㎛ of PET film. Also, the Teflon film is difficult to cut due to warping when cutting the laser. The measured coupling agrees well with the FDFD simulation, and the resonant width (FWHM) decreases with decreasing grating (D1) thickness.

Figure 6.3 (c) shows the FDFD simulation with the refractive index change of the mGMR filter. In Loss less, The grating (D1) thickness is fixed at 75 ㎛, and the resonance shift and the resonance width (FWHM) change with grating refractive index change from 1.0 to 2.0. The smaller the difference in refractive index between the grating and the air, the narrower the resonance width. Resonance occurs at high frequencies and high Q-factor resonance occurs. The difference in refractive index between air and grating is an important factor in determining the width and Q-factor of resonance.

Figure 6.3 (d) is a simulation of the effect of loss tangent (δ). The loss tangent (δ) of a material is strongly affected by Q-factor and resonance. The resonance of high Q-factor increases the decrease of the resonance amplitude by the loss tangent (δ).

Figures 6.3 (e) and (f) show the transmission characteristics of the mGMR filter fabricated with a 75 ㎛ thick PET film. Figure 6.3 (e) shows resonance change due to the polarization change. The occurrence and disappearance of the resonance are repeated once every 180 degrees in the form of a cosine graph.

Figure 6.3 (f) shows the resonance divided into two according to the angle of incidence within the range of occurrence of the resonance according to Incident angle in Figure 6.2 (a).

6.3 Guided multi-mode resonance filter

6.3.1 TE mode fields

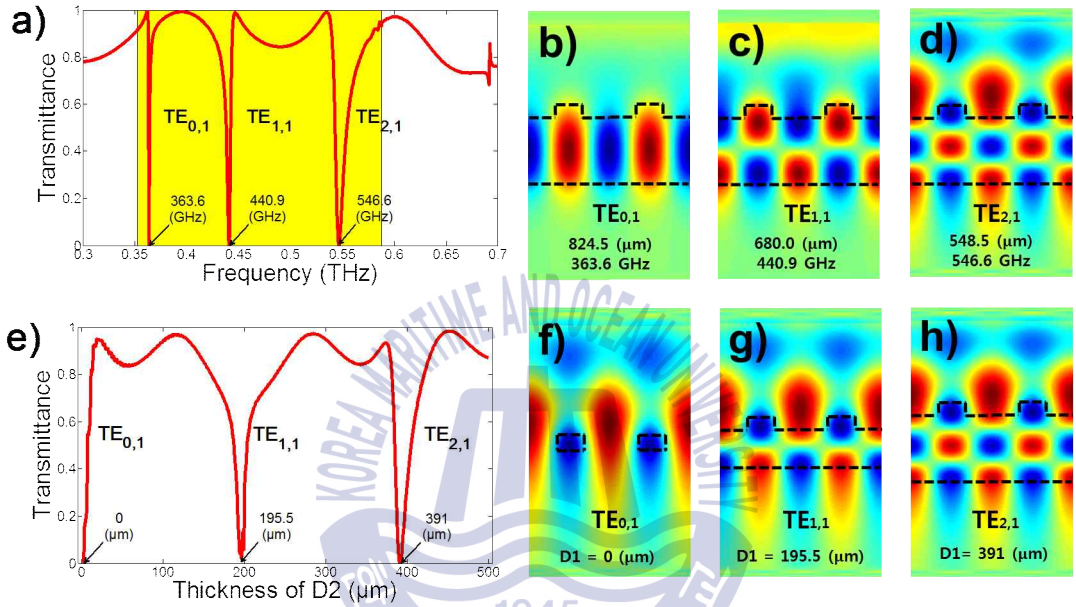

Fig. 6.4 (a) High-order mode resonance due to frequency variation when film thickness is 400 ㎛. Yellow area is the expected range of resonance occurrence. Field distribution at each mode resonance. (b) $TE_{0,1}$ mode. (c) $TE_{1,1}$ mode. (d) $TE_{2,1}$ mode. (e) Higher order mode with frequency 552 GHz thickness variation. Field distribution at each mode resonance. (f) $TE_{0,1}$ mode. (g) $TE_{1,1}$ mode. (h) $TE_{2,1}$ mode. The separation $\Lambda \times F$ is 148 ㎛, D1 = 60 ㎛, D2 = 168 ㎛, Λ = 460 ㎛, filing element = 32 %. The black dashed line is the out line of the structure, and the two unit cells are drawn as a picture.

Figure 6.6 (a) shows the transmittance characteristics of a GMR filter with fixed film (D2) thickness of 400 ㎛ coupled to mGMR filter in TE mode. Three strong resonances occur at 0.364, 0.441 and 0.547 THz,

respectively. Figures 6.6 (b-d) are electric filed distributions of GMR filters for three frequencies with a transmittance of 0 at 400 ㎛ thickness. Depending on the frequency, TE_0, TE_1 and TE_2 are induced in the GMR filter.

Figure 6.6 (e) shows the transmittance characteristics of the GMR filter when the thickness of the film (D2) changes from 0 to 500 ㎛ in the TE mode. Higher order mode resonance is induced as the film (D2) thickness increases at a fixed frequency of 0.552 THz. Three strong resonances occur at thicknesses of 0 ㎛, 196 ㎛ and 391 ㎛ for each film (D2) (0 ~ 500 ㎛). Figures 6.6 (f-h) are electric filed distributions of GMR filters at film thicknesses of three resonances with a transmittance of 0 at 0.552 THz. At a fixed frequency of 0.552 THz (544 ㎛), the half-wave, wave and 3/2 wavelengths are induced in the GMR filter for the thickness variation of the film (D1). These electric filed represent TE_0, TE_1 and TE_2 modes.

6.3.2 TM mode fields

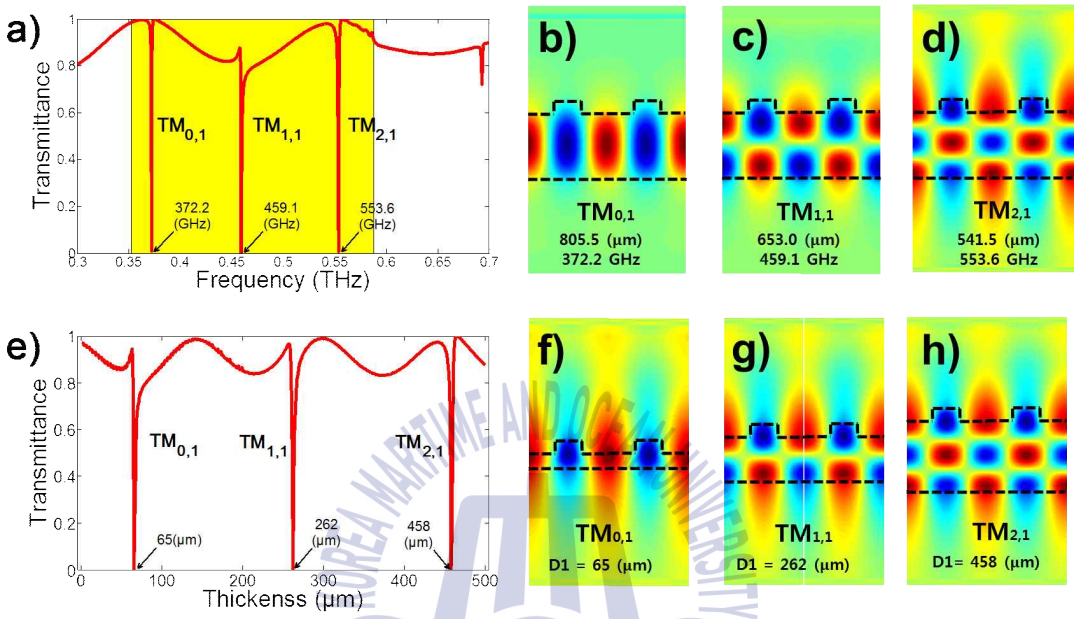

Fig. 6.5 (a) High-order mode resonance due to frequency variation when film thickness is 450 ㎛. Yellow area is the expected range of resonance occurrence. Field distribution at each mode resonance. (b) $TM_{0,1}$ mode. (c) $TM_{1,1}$ mode. (d) $TM_{2,1}$ mode. (e) Higher order mode with frequency 550 GHz thickness variation. Field distribution at each mode resonance. (f) $TM_{0,1}$ mode. (g) $TM_{1,1}$ mode. (h) $TM_{2,1}$ mode. The separation $\Lambda \times F$ is 148 ㎛, D1 = 60 ㎛, D2 = 168 ㎛, Λ = 460 ㎛, filing element = 32 %. The black dashed line is the out line of the structure, and the two unit cells are drawn as a picture.

Figure 6.5 (a) shows the transmittance characteristics of the GMR filter with a fixed film (D2) thickness of 450 ㎛ in the TM mode. Three strong resonances occur at 0.372, 0.459 and 0.554 THz, respectively. Figures 6.7 (b-d) show the electric filed distribution of the GMR filter for three frequencies with a transmittance of 0 at a thickness of 400

μm. Depending on the frequency, TM_0, TM_1 and TM_2 are induced in the GMR filter.

Figure 6.7 (e) shows the transmittance characteristics of the GMR filter when the thickness of the film (D2) changes from 0 to 500 μm in the TM mode. Higher order mode resonance is induced as the combined film (D2) thickness increases at a fixed frequency of 0.550 THz. Three strong resonances occur at thicknesses (0 ~ 500 μm) at thicknesses of 65 μm, 262 μm and 458 μm for each film (D2). Figures 6.7 (f-h) are electric filed distributions of GMR filters at film thicknesses of three resonances with a transmittance of 0 at 0.550 THz. Half, wave and 3/2 wavelengths are induced in the GMR filter for a change in the thickness of the film (D1) at a fixed frequency of 0.550 THz (544 μm). These H-fields represent the TM_0, TM_1 and TM_2 modes.

6.3.3 TE mode resonance depend on film thickness

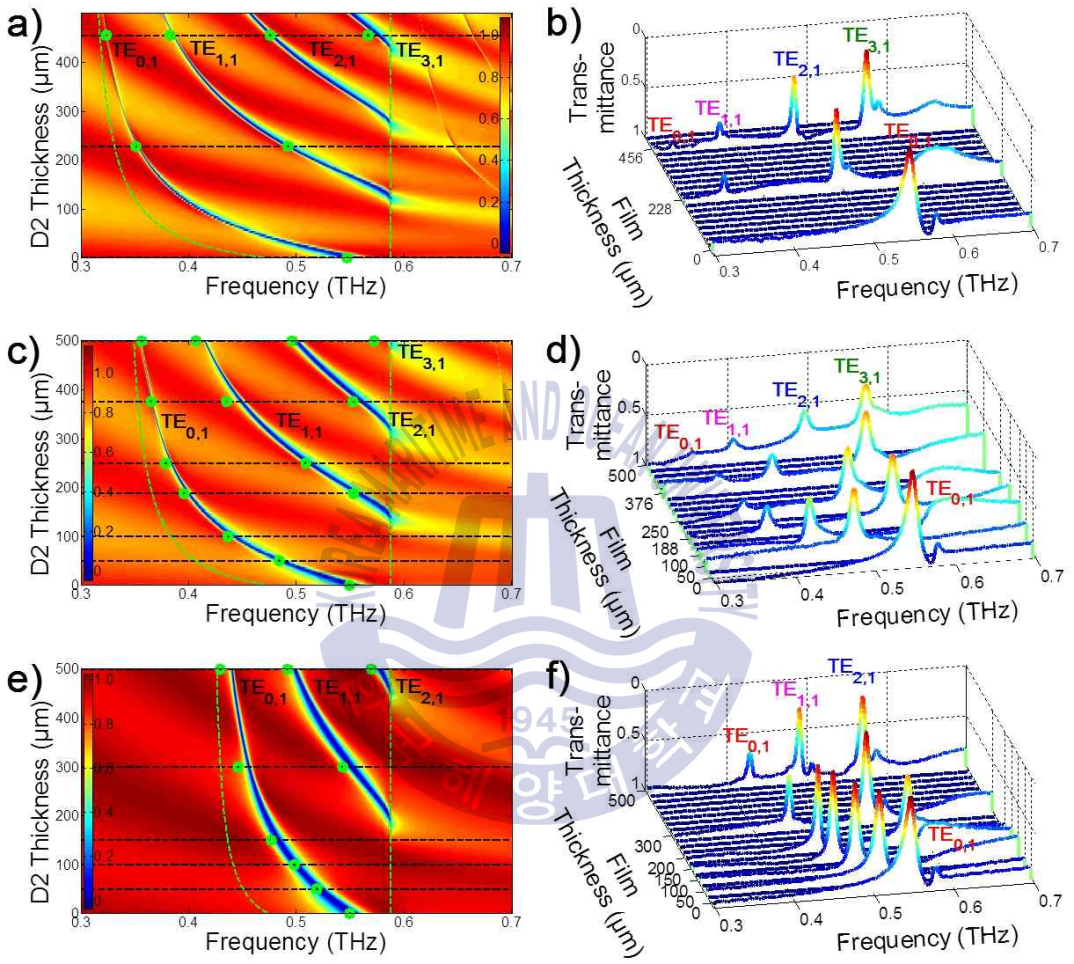

Fig. 6.6 2-D image of simulation and 3-D image of measurement for TE modes resonance frequency shift according to thickness changes of films (slab waveguide) for GMR filter; (a) Simulation of quartz; (b) Measurement of quartz; (c) Simulation of PET; (d) Measurement of PET; (e) Simulation of Teflon; (f) Measurement of Teflon. The green dot in (a), (c), and (e) indicate measured resonance frequencies. the green dotted lines represent the resonance range in Fig. 2 (b). The vertical color bars indicate the intensity of the electric field.

Figures 6.6 (a), 6 (c) and 6 (e) show the generation of the higher-order modes and the shift of the resonance frequency according to the film thickness in the TE mode using FDFD simulation. In the measurement, the resonance frequency shifts due to the refractive index and thickness of the film, and the resonance depth changes according to the loss tangent (δ) of the film. Figure 2 (b) shows the expected range of resonance frequency depending on the kind and thickness of the film. The green dash line shows the resonance frequency range in the simulation map. The resonance frequency of the $TE_{0,1}$, $TE_{1,1}$, and $TE_{2,1}$ ... modes of resonance occurs within the range calculated in Equation (1).

Figure 6.6 (b) shows the transmittance characteristics of GMR filter combined with mGMR filter and quartz film. To fabricate a thin 228 ㎛ thick quartz, it was fabricated by polishing (Co. Buysemi.). In order to measure the resonance of the higher-order mode caused by the increase in thickness, one and two layers were superimposed and measured. At 228 ㎛ thickness, resonance in two modes $TE_{0,1}$ and $TE_{1,1}$ modes was measured at 0.351 and 0.492 THz. At 456 ㎛ thickness, several resonances were measured at 0.324, 0.383, 0.476, and 0.567 THz from $TE_{0,1}$ to $TE_{3,1}$. As the thickness of the film becomes thicker, the resonance shift agrees well with the FDFD simulation. The resonance depth decreases as the loss tangent (δ) increases.

Figure 6.6 (d) shows the transmittance characteristics of a GMR filter combined with a PET film of the same material as the mGMR filter. The film thickness was 25, 75, 100, 188, 250, 376, and 500 ㎛, and mGMR filter was combined with various thickness films to make a new

GMR filter. As the thickness increased from 0 to 500 ㎛, the $TE_{0,1}$ mode resonance shifted from 0.549 to 0.357 THz and the $TE_{1,1}$ mode resonance shifted from 0.553 to 0.407 THz as the thickness increased from 188 to 500 ㎛.

PET film has the highest loss tangent (δ) value among the three materials. Although the refractive index is lower than that of Quartz, the resonant depth reduction is the largest measured on the measured film.

In Figure 6.6 (a), (c), and (e), $TE_{1,1}$ mode appears at film thicknesses of 123 ㎛, 139 ㎛, and 194 ㎛ for quartz, PET, and Teflon films. The high refractive index of the quartz film has a large resonance frequency shift. In addition, higher mode modes occur at thinner film thicknesses than Teflon and PET films with relatively lower refractive indices.

Figure 6.6 (f) shows the transmittance characteristics of a GMR filter coupled with a Teflon film bonded to mGMR. Higher order mode resonance was measured at film thickness variations. It shows the measured value of GMR filter with various thicknesses of films up to 50, 100, 150, 300 and 500 ㎛ thickness of Teflon film. Among three films, Teflon has the lowest loss tangent (δ) value. The decrease in the loss tangent (δ) effect was largely determined by the magnitude of the measured resonance. The refractive index, thickness, and loss tangent (δ) of the film affect the resonance occurrence.

6.3.4 TM mode resonance depend on film thickness

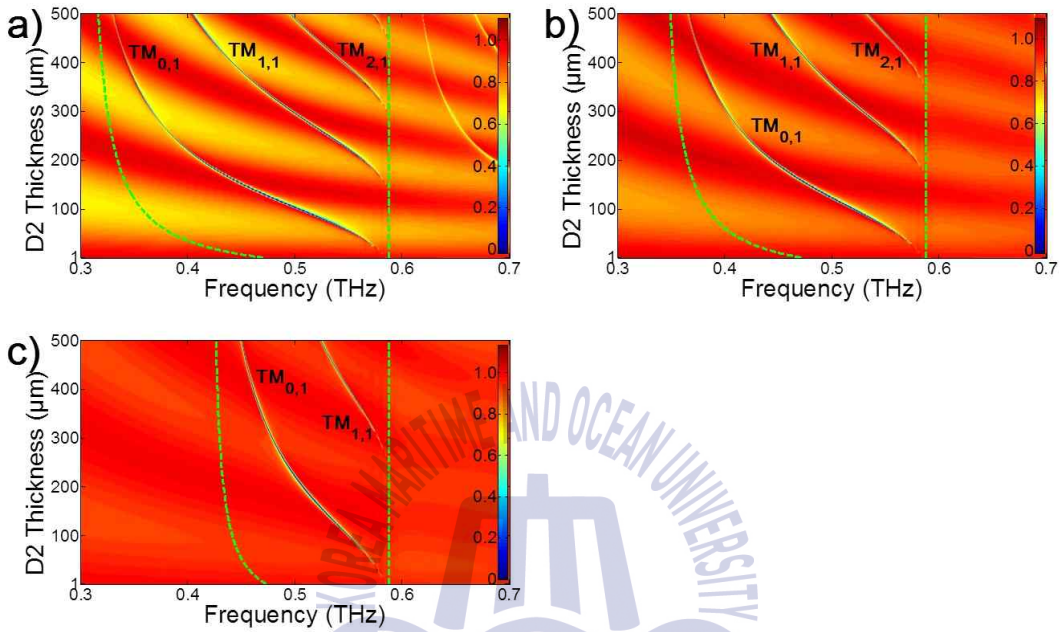

Fig. 6.7 2-D image of simulation for TM modes resonance frequency shift according to thickness changes of films (slab waveguide) for GMR filter; (a) Simulation of quartz; (b) Simulation of PET; (c) Simulation of Teflon; the green dotted lines represent the resonance frequency range in Fig. 2 (b). The vertical color bars indicate the intensity of the magnetic field.

Figures 6.7 (a), 7 (b) and 7 (c) use FDFD simulation to calculate the occurrence of higher modes and the shift of resonance frequency according to film thickness in TM mode. In the TM mode, the high Q-factor is greatly affected by the loss tangent (δ), and the measured resonance depth is not good. Further, as the thickness of the film becomes thick, the resonance disappears due to the influence of the loss and thickness. Simulated results are shown only under loss less

conditions. Figure 2 (b) shows the expected range of resonance depending on the type and thickness of the film. The green dash line shows the resonance range in the simulation map. Resonance frequencies of the $TE_{0,1}$, $TE_{1,1}$ and $TE_{2,1}$ ... modes were calculated within the calculated range.

6.4 Film sensor

6.4.1 Sensitivity

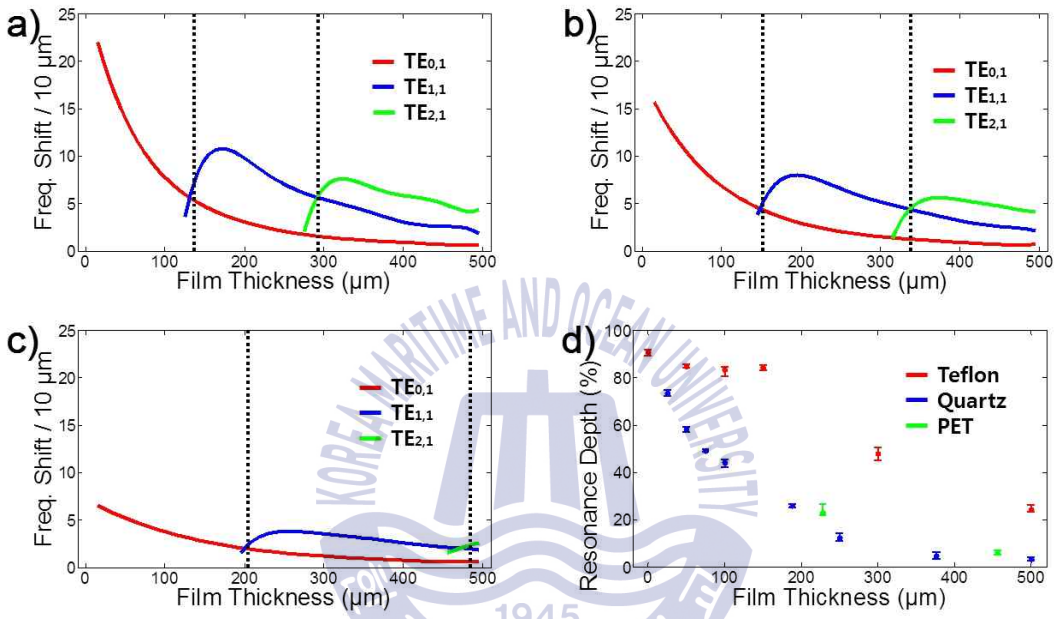

Fig. 6.8 (a) $TE_{0,1}$, $TE_{1,1}$, $TE_{2,1}$ and the rate of change of the resonance frequency of each mode depending on the film thickness of GMR filter. (a) mGMR filter with quartz films. (b) mGMR filter with PET films, (c) mGMR filter with Teflon films. (d) Measured resonance depth for $TE_{0,1}$ mode with different film thickness the dots indicate measured data.

Figure 6.8 shows the variation of the resonance frequency according to the film thickness of the GMR filter and the variation of the resonance depth with the loss tangent (δ) of the quartz, PET, and teflon films.

In Figure 6.8 (a), the quartz film with the highest refractive index (1.95) has the greatest variation rate of the resonant frequency shift

with thickness variation. The rate of the resonant frequency shift in the $TE_{0,1}$ mode sharply decreases with increasing film thickness and converges to zero. However, the $TE_{1,1}$ and $TE_{2,1}$ modes induced by the film thickness increased by the slab waveguide condition have a rate of the resonant frequency shift increased than that of the $TE_{0,1}$ mode. At 136 ㎛ and 293 ㎛ in film thickness, rate of the resonant frequency shift is increased compared to the low mode. Figure 6.8 (b) also shows the rate of the resonant frequency shift depending on the thickness of the PET film. $TE_{1,1}$ and $TE_{2,1}$ at 151 ㎛ and 338 ㎛ thickness of film maintain higher rate of the resonant frequency shift with increase of film thickness than previous mode. Figure 6.8 (c) shows the rate of the resonant frequency shift depending on the thickness of the Teflon film. $TE_{1,1}$ and $TE_{2,1}$ at 204 ㎛ and 484 ㎛ thickness of film keeps the rate of the resonant frequency shift higher than that of previous mode with increasing film thickness. The Teflon film has a low rate of the resonant frequency shift as a whole due to the lowest refractive index. The shift rate of the resonant frequency with increasing film thickness of the GMR filter is measured without limitation on the thickness of the film due to the further induced higher mode. Figure 6.8 (d) shows the loss tangent (δ) of the film and the depth variation of the resonance with increasing thickness. The depth of resonance was measured differently depending on the loss tangent (δ) of the three different materials (quartz, pet, teflon). The relationship between loss tangent (δ) and depth of resonance is shown clearly. Also, the thickness increase of the film is measured by reducing the magnitude of the resonance due to the loss tangent (δ) effect.

6.4.2 Film sensing

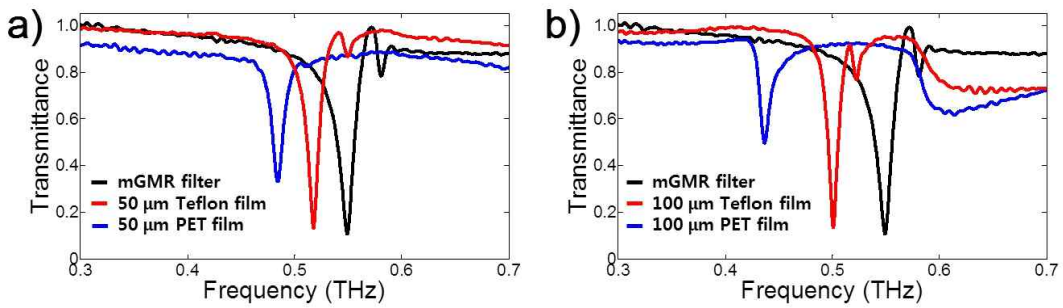

Fig. 6.9 Transmittance of GMR filter consisting of PET grating and dielectric thin films. (a) 50 ㎛ thick Teflon and PET film comparison; (b) 100 ㎛ thick Teflon and PET film comparison.

The special structure of the MMs [80] or PPWG [8] makes it possible to sensitively characterize the film. Structurally, as the film thickness increases, it blurs in the influence of the field, and the measurement sensitivity of the film has a limitation on the thickness of the film. Conversely, the film measurement method using the mGMR filter can measure the thickness of the film without light. Due to the film thickness, a thick film is also measured with a high sensitivity using a higher order mode.

Figure 6.9 (a) and (b) show the resonance shift and depth variation of a GMR filter combining 50 ㎛ and 100 ㎛ Teflon film and PET film of the same thickness. When the thickness of the film is 50 ㎛, the resonance shift difference between the Teflon film and the PET film is 33.3 GHz. When the thickness of the film is 100 ㎛, the resonance shift difference between the Teflon film and the PET film is 64.1 GHz.

It shows difference of refractive index and thickness of film. The resonant depth of Teflon film and PET film is represented by the loss tangent (δ) difference. When the thickness of the film is 50 ㎛, the resonance depth of the Teflon film and the PET film is 20 %. When the thickness of the film is 100 ㎛, the resonance depth of the Teflon film and the PET film is 36%. The difference in loss tangent (δ) of the film and the change in thickness are shown.

6.5 Conclusion

The GMR filter was designed by cutting the film at a low price and a universal film. The complicated process such as semiconductors is removed and the grating pattern is processed by simple FSLM method. In addition, the thickness of the structure, which is difficult to manufacture by mechanical processing, can be easily implemented using a film. In the mGMR filter, the resonance expected area was calculated according to the thickness and refractive index of the film. GMR filter was completed by combining mGMR filter structure on Quartz, PET and Teflon film. $TE_{0,1}$, $TE_{1,1}$, $TE_{2,1}$, $TE_{3,1}$ modes and resonance frequency shift were measured according to the refractive index and thickness of the film. The shift rate of the reduced resonance frequency of the $TE_{0,1}$ mode caused by the film thickness increase of the GMR filter is high from the measurement limit of the thickness by keeping the higher mode induced by the film thickness high.

The depth variation of the resonance due to the loss tangent (δ) of the material used in the GMR filter was measured. The difference between the refractive index and the loss tangent (δ) of the material in 50 ㎛ and 100 ㎛ PET and Teflon was measured by the resonance frequency shift and depth difference. The GMR filter fabricated by combining films can easily design various filters and can detect sensitive crab film using GMR filter structure. GMR filters can be applied to multi-mode resonance, polarizer, modulator, and film sensor

Chapter 7 Conclusion

7 Conclusion

GMR structure can design resonance occurrence range from equation. In addition, we analyzed the errors of the GMR structure, fabrication and experimental measurement of the GMR filter according to the number of gratings included in the THz beam, the inner corner curvature of the grating, the loss tangent (δ) of the material , the diffusion of the THz beam and the measurement time of the transmittance.

Designed as the first all-dielectric GMR filter has high transmittance and high Q-factor of 71, it has excellent characteristics as a tunable filter according to incident angle and a modulator according to polarization.

The TGMR filter, which is designed as a dielectric, has a tunable continuous resonance frequency. The tuning range can be adjusted according to the periodic rate of change of the grating period. Has potential for THz applications in spectroscopes, modulators, image sensors and filters for future THz communications.

We adjusted the change of resonance characteristics according to the tilted angle and polarization of two mGMR filters made of film. First, the modulated model according to the tilted angle and polarization of the GMR filter can change the magnitude of the resonance magnitude change. It can be used as a step attenuator. Second, when the tilted angle is 90, the magnitude of the resonance amplitude due to

polarization is minimized to 0.16 %. Polarization insensitive GMR filter.

It appears as a new GMR filter characteristic depending on the properties of the film attached to the mGMR filter. The resonance generated in the GMR filter is shifted by the thickness and refractive index of the film, and the magnitude of the resonance is sensed by the absorption. GMR filter multimode resonance can measure film without limitation of measurement thickness and can be applied to sensors such as liquid, gas, bio, and material.

The GMR structure can be designed for various purposes such as bandpass filter and reflector using high refractive index materials. In addition, studies on low-loss materials and structures to secure the performance of filters have been further studied. As a sensor, the special structure of the GMr filter is capable of developing a sensor that can measure materials sensitively by resonance change.

Reference

[1] J. H. Barton, R. C. Rumpf, R. W. Smith, C. Kozikowski & P. Zellner, "All-dielectric frequency selective surfaces with few number of periods," Progress In Electromagnetics Research B 41, 269-283 (2012).

[2] N. I. Landy, S. Sajuyigbe, J. J. Mock, D. R. Smith, & W. J. Padilla, "Perfect Metamaterial Absorber," Phys. Rev. Lett. 100, 207402 (2008).

[3] Nanfang Yu, Patrice Genevet, Mikhail A. Kats, Francesco Aieta, Jean-Philippe Tetienne, Federico Capasso & Zeno Gaburro1, "Light Propagation with Phase Discontinuities: Generalized Laws of Reflection and Refraction," Science 334(6054), 333-337 (2011).

[4] D. R. Smith, J. B. Pendry, & M. C. K. Wiltshire, "Metamaterials and Negative Refractive Index," Science 305, 788 (2004).

[5] Reinhold Kleiner, "Filling the Terahertz Gap," Science 318, 1254 (2007).

[6] Y. Kanamori, M. Shimono & K. Hane, "Fabrication of transmission color filters using silicon subwavelength gratings on quartz substrates," IEEE photonics Technol. Lett. 18(20), 2126-2128 (2006).

[7] J. H. Barton, C. R. Garcia, E. A. Berry, R. G.May, D. T. Gray & R. C. Rumpf, "All-dielectric frequency selective surface for high power microwaves," IEEE Transactions on Antennas and Propagation, 62(7), 3652-3656 (2014).

[8] E. S. Lee, S. G. Lee, C. S. Kee & T. I. Jeo, "Terahertz notch and low-pass filters based on band gaps properties by using metal slits in tapered parallel-plate waveguides," Opt. Express. 19, 14852-14859 (2011).

[9] T. D. Drysdale, R. J. Blaikie & D. R. S. Cumming, "Calculated and measured transmittance of a tunable metallic photonic crystal filter for terahertz frequencies," Appl. Phys. Lett. 83, 5362 (2003).

[10] Y. Zhu, S. Vegesna, Y. Zhao, V. Kuryatkov, M. Holtz, Z. Fan, M. Saed & A. A. Bernussi, "Tunable dual-band terahertz metamaterial bandpass filters," Opt. Lett. 38, 2382-2384 (2013).

[11] Lord Rayleigh, "On the Dynamical Theory of Gratings," Proceedings of the Royal Society of London. Series A, Containing Papers of a Mathematical and Physical Character 79(532), 399-416 (1907).

[12] S. S. Wang & R. Magnusson, "Theory and applications of guided-mode resonance filters," Appl. Opt. 32(14), 2606-2613 (1993).

[13] J. T. Murugan & T. R. S. Kumar, "Frequency selective transparent front door for microwave-oven," Hum. Nat. 3, 119-123 (2014).

[14] H. Chen, X. Hou, & L. Deng, "Design of frequency-selective surfaces radome for a planar slotted waveguide antenna," IEEE Antennas Wirel. Propag. Lett. 8, 1231-1233 (2009).

[15] B. A. Munk, "Frequency selective surface theory and design," John Wiley 11-44 (2005).

[16] S. S. Oh & C.-G. Choi, "Photonic-crystal-slab-type guided mode

resonance filters in infrared range," Photonics Technol. Lett. 21, 316-318 (2009).

[17] M. J. Uddin, T. Khaleque & R. Magnusson, "Guided-mode resonant polarization-controlled tunable color filters," Opt. Express 22, 12307-12315 (2014).

[18] Y. Chen, I. A. I. Al-Naib, J. Gu, M. Wang, T. Ozaki, R. Morandotti & W. Zhang, "Membrane metamaterial resonators with a sharp resonance: A comprehensive study towards practical terahertz filters and sensors," AIP Adv. 2, 022109 (2012).

[19] X. Hu, G. Xu, L. Wen, H. Wang, Y. Zhao, Y. Zhang, D. R. S. Cumming & Q. Chen, "Metamaterial absorber integrated microfluidic terahertz sensor," Laser Photonics Rev. 10, 962-969 (2016).

[20] C. Debus & P. H. Bolivar, "Frequency selective surfaces for high sensitivity terahertz sensing," Appl. Phys. Lett. 91, 184102 (2007).

[21] M. Liu, M. Susli, D. Silva, G. Putrino, H. Kala, S. Fan, M. Cole, L. Faraone, V. P. Wallace, W. J. Padilla, D. A. Powell, I. V. Shadrivov & M. Martyniuk, "Ultrathin tunable terahertz absorber based on mems-driven metamaterial," Microsystems & Nanoeng. 3, 17033 (2017).

[22] C. Jansen, I. A. I. Al-Naib, N. Born & M. Koch, "Terahertz metasurfaces with high Q-factors," Appl. Phys. Lett. 98, 051109 (2011).

[23] I. Al-Naib, Y. Yang, M. M. Dignam, W. Zhang & R. Singh, "Ultra-high Q even eigenmode resonance in terahertz metamaterials," Appl. Phys. Lett. 106, 011102 (2015).

[24] H. Hen, J. Liu & Z. Hong, "Guided mode resonance with extremely high Q-factors in terahertz metamaterials," Opt. Commun. 383, 508-512 (2017).

[25] R. Mendis, M. Nagai, W. Zhang & D. M. Mittleman, "Artificial dielectric polarizing beam splitter and isolator for the terahertz region," Sci. Rep. 7, 5909 (2017).

[26] P. K. Singh & S. Sonkusale, "High speed terahertz modulator on the chip based on tunable terahertz slot waveguide," Sci. Rep. 7, 40933 (2017).

[27] Y. Wen, D. Jia, W. Ma, Y. Feng, M. Liu, L. Dong, Y. Zhao & X. Yu, "Photomechanical meta-molecule array for real-time terahertz imaging," Microsystems & Nanoengineering 3, 17071 (2017).

[28] N. J. Karl, R. W. McKinney, Y. Monnai, R. Mendis & D. M. Mittleman, "Frequency-division multiplexing in the terahertz range using a leaky-wave antenna," Nat. Photonics 9, 717-721 (2015).

[29] J. Ma, N. J. Kar, S. Bretin, G. Ducournau & D. Mittleman, "Frequency-division multiplexer and demultiplexer for terahertz wireless links," Nat. Commun. 8, 729 (2017).

[30] L. Ren, C. L. Pint, L. G. Booshehri, W. D. Rice, X. Wang, D. J. Hilton, K. Takeya, I. Kawayama, M. Tonouchi, R. H. Hauge & J. Kono, "Carbon nanotube terahertz polarizer," J. Opt. Soc. Am. B 9, 2610-2613 (2009).

[31] J. Kyoung, E. Y. Jang, M. D. Lima, H. -R. Park, R. O. Robles, X. Lepro, Y. H. Kim, R. H. Baughman & D. -S. Kim, "A reel-wound carbon nanotube polarizer for terahertz frequencies," Nano Lett. 11, 4227-4231 (2011).

[32] A. Bingham, Y. Zhao, & D. Grischkowsky, "THz parallel plate photonic waveguides," Appl. Phys. Lett. 87, 051101 (2005).

[33] H. -T. Chen, W. J. Padilla, J. M. O. Zide, A. C. Gossard, A. J. Taylor & R. D. Averitt, "Active terahertz metamaterial devices," Nature 444, 597-600 (2006).

[34] S. Song, F. Sun, Q. Chen & Y. Zhang, "Narrow-linewidth and high-transmission terahertz bandpass filtering by metallic gratings," IEEE Transactions on THz Sci. Technol. 5, 131 - 136 (2015).

[35] E. S. Lee, J. -K. So, G. -S. Park, D. S. Kim, C. -S. Kee & T. -I. Jeon, "Terahertz band gaps induced by metal grooves inside parallel-plate waveguides," Opt. Express 20(6), 6116-6123 (2012).

[36] G. Gallot, S. P. Jamtson, R. mcGowan & D. Grischkowsky, "Terahertz waveguides," J. Opt. Soc. Am. B 17, 5909 (2000).

[37] D. Grischkowsky, & et al. "Far-infrared time-domain spectroscopy with terahertz beams of dielectrics and semiconductors," J. Opt. Soc. Am. B 7, 2006-2015 (1990).

[38] T. -I. Jeon & D. Grischkowsky, "Characterization of optically dense, doped semiconductors by reflection THz time domain spectroscopy," Appl. Phys. Lett. 72, 3032 (1998).

[39] R. R. Boye & R. K. Kostuk, "Investigation of the effect of finite grating size on the performance of guided-mode resonance filters," Appl. Opt. 39(21). 3649-3653 (2000).

[40] E. S. Lee & T. -I. Jeon, "THz filter using the transverse-electric (TE_1) mode of the parallel-plate waveguide," J. Opt. Soc. Kor. 13(4), 423-427 (2009)

[41] E. S. Lee & T. -I. Jeon, "Tunable THz notch filter with a single groove inside parallel-plate waveguides," Opt. Express 20(28), 29605-29612 (2012).

[42] M. Gil, J. Bonache & F. Martín, "Metamaterial filters: A review," Metamaterials 2, 186-197 (2008).

[43] H. -T. Chen, W. J. Padilla, J. M. O. Zide, A. C. Gossard, A. J. Taylor & R. D. Averitt, "Active terahertz metamaterial devices," Nature 444(30), 05343 (2006).

[44] H. -T. Chen, W. J. Padilla, M. J. Cich, A. K. Azad, R. D. Averitt & Antoinette J, "A metamaterial solid-state terahertz phase modulator," Nat. Photonics 3, 148-151 (2009).

[45] J. Li, C. M. Shah, W. Withayachumnankul, B. S. -Y. Ung & A. Mitchell, "Mechanically tunable terahertz metamaterials," Appl. Phys. Lett. 102, 121101 (2013).

[46] J. Han, & A. Lak, "Semiconductor split-ring resonators for thermally tunable, terahertz metamaterials," Journal of Modern Optics 56(4), 554-557 (2009).

[47] H. -T. Chen, J. F. O' hara, A. K. Azad, A. J. Taylor, R. D. Averitt, D. B. Shrekenhamer & W. J. Padilla, "Experimental demonstration of frequency-agile terahertz metamaterials," Nat. Photonics 2, 295-298 (2008).

[48] J. Han, A. Lakhtakia, & C. -W. Qiu, "Terahertz metamaterials with semiconductor split-ring resonators for magnetostatic tunability," Opt. Express 16(19), 14390-14396 (2008).

[49] K. Bi, W. Zhu, M. Lei & J. Zhou, "Magnetically tunable wideband microwave filter using ferrite-based metamaterials," Appl. Phys. Lett. 106, 173507 (2015).

[50] J.-B. Brückner, J. L. Rouzo, L. Escoubas, G. Berginc, O. Calvo-Perez, N. Vukadinovic & F. Flory, "Metamaterial filters at optical-infrared frequencies," Opt. Express 21(14), 16992-17006 (2011).

[51] J. P. Turpin, J. A. Bossard, K. L. Morgan, D. H. Werner & P. L. Werner, "Reconfigurable and tunable metamaterials: a review of the theory and applications" International Journal of Antennas and Propagation 2014, 429837 (2014).

[52] H. Tao, A. C. Strikwerda, K. Fan, C. M. Bingham, W. J. Padilla, X. Zhang & R. D. Averitt, "Terahertz metamaterials on free-standing highly-flexible polyimide substrates," J. Phys. D: Appl. Phys. 41, 232004 (2008).

[53] M. J. Uddin & R. Magnusson, "Efficient guided-mode-resonant tunable color filters," IEEE Photonics Technol. Lett. 24(17), 1552-1554 (2012).

[54] H. S. Bark, G. J. Kim & T. -I. Jeon, "Transmission characteristics of all-dielectric guided-mode resonance filter in the THz region," Sci. Rep. 8, 13570 (2018).

[55] M. J. Uddin, T. Khaleque & R. Magnusson, "Guided-mode resonant polarization-controlled tunable color filters," Opt. Express 22(10), 12307-12315 (2014).

[56] M. J. Uddin & R. Magnusson, "Guided-mode resonant thermo-optic tunable filters," IEEE Photonics Technol. Lett. 25(15), 1412-1415 (2013).

[57] D. W. Dobbs & B. T. Cunningham, "Optically tunable guided-mode resonance filter," Appl. Opt. 45(28), 7286-7293 (2006).

[58] M. Niraula, J. W. Yoon, and R. Magnusson, "Single-layer optical bandpass filter technology," Opt. Lett. 40(21) 5062-5065 (2015).

[59] G. Xiao, Q. Zhu, Y. Shen, K. Li, M. Liu, Q. Zhuang and C. Jin, "A tunable submicro-optofluidic polymer filter based on guided-mode resonance," Nanoscale 7(8), 3429-34 (2015).

[60] J. -R. Lee, N. Sato, D. J. B. Bechstein, S. J. Osterfeld, J. Wang, A. W. Gani, D. A. Hall & S. X. Wang, "Experimental and theoretical investigation of the precise transduction mechanism in giant magneto resistive biosensors," Sci. Rep. 6, 18692 (2016).

[61] Jae W. Yoon, K. J. Lee & R. Magnusson, "Ultra-sparse dielectric nanowire grids as wideband reflectros and polarizers," Opt. Express 23(22), 28849-28856 (2015).

[62] Y. Zhong, Z. Goldenfeld, K. Li, W. Streyer, L. Yu, L. Nordin, N. Murphy & D. Wasserman, "Mid-wave infrared narrow bandwidth guided mode resonance notch filter," Opt. Lett. 42(2), 223-226 (2017).

[63] S. Boonruang, A. Greenwell & M. G. Moharam, "Broadening the angular tolerance in two-dimensional grating resonance structures at oblique incidence," Appl. Opt. 46(33), 7982 (2017).

[64] A D. Lacour, G. Granet & J.-P. Plumey, "Polarization independence of a one-dimensional grating in conical mount," J. Opt. Soc. Am. A 20(8), 1546-1551 (2003).

[65] G. Niederer, W. Nakagawa & H. P. Herzig, "Design and characterization of a tunable polarization-independent resonant grating filter," Opt. Express 13(6), 2196- 2200 (2005).

[66] X. Fu, K. Yi, J. Shao & Z. Fanl, "Nonpolarizing guided-mode resonance filt," Opt. Lett. 34(2), 124- 126 (2009).

[67] D. Wu, X. Sui, J. Yang & Z. Zhou, "Binary blazed grating-based polarization-independent filter on silicon on insulator," Frontiers of Optoelectgronics 5(1), 78-81 (2012).

[68] T. Alasaarela, D. Zheng, L. Huang, A. Priimagi, B. Bai, A. Tervonen, S. Honkanen, M. Kuittinen & J. Turunen, "Single-layer one-dimensional nonpolarizing guided-mode resonance filters under normal incidence," Opt. Lett. 36(13), 2411-2413 (2011).

[69] K. Kintaka, T. Majima, K. Hatanaka, J. Inoue & S. Ura, "Polarization-independent guided-mode resonance filter with cross-integrated waveguide resonators," Opt. Lett. 37(15), 3264- 3266 (2012).

[70] S. Peng & G. M. Morris, "Resonant scattering from two-dimensional gratings," J. Opt. Soc. Am. A 13(5), 993-1004 (1996).

[71] C. -H. Park, Y. -T. Yoon & S. -S. Lee, "Polarization-independent visible wavelength filter incorporating a symmetric metal-dielectric resonant structure," Opt. Express 20(21), 23769-23777 (2012).

[72] T. Clausnitzer, A. V. Tishchenko, E.-B. Kley, H.-J. Fuchs, and D. Schelle, O. Parriaux & U. Kroll, "Narrowband, polarization-independent free-space wave notch filter," J. Opt. Soc. Am. A 22(12), 2799-2803 (2005).

[73] S. Peng & G. M. Morris, "Experimental demonstration of resonant anomalies in diffraction from two-dimensional gratings," Opt. Lett. 21(8), 549-551 (1996).

[74] A. -L. Fehrembach, A. Talneau, O. Boyko, F. Lemarchand & A. Senten, "Experimental demonstration of a narrowband, angular tolerant, polarization independent, doubly, periodic resonant grating filter," Opt. Lett. 32(15), 2269-2271 (2007).

[75] O. Boyko, F. Lemarchand, A. Talneau, A. -L. Fehrembach & A. Sentenac, "Experimental demonstration of ultrasharp unpolarized filtering by resonant gratings at oblique incidence," J. Opt. Soc. Am. 26(3), 676 -679 (2009).

[76] A. -L. Fehrembach & A. Sentenac, "Study of waveguide grating eigenmodes for unpolarized filtering applications," J. Opt. Soc. Am. A 20(3), 481-487 (2003).

[77] A. Mizutani, H. Kikuta, K. Nakajima & K. Iwat, "Nonpolarizing guided-mod resonant grating filter for oblique incidence," J. Opt. Soc. Am. A 18(6), 1261-1266 (2001).

[78] W. Wang, G. Zhu, Q. Liu, X. Li, T. Sa, X. Fang, H. Zhu & Y. Wang,

"Angle- and polarization-dependent spectral characteristics of circular grating filters," Opt. Express 24(10), 11033-11042 (2016).

[79] W. Wang, Q. Liu, G. Zhu, X. Li, S. He, T. Sa, X. Gao & Y. Wang, "Polarization-Insensitive concentric circular grating filters featuring a couple of resonant peaks," IEEE Photon. J. 7(5), 7102010 (2015).

[80] J. F. O' Hara, R. Singh, I. Brener, E. Smirnova, J. Han, A. J. Taylor & W. Zhang, "Thin-film sensing with planar terahertz metamaterials: sensitivity and limitations reosnance shift sensing," Opt. Express 16(3) 1786-1795 (2008).

[81] M. Theuer, R. Beigang & D. Grischkowsky, "Highly sensitive terahertz measurement of layer thickness using a two-cylinder waveguide sensor," Appl. Phys. Lett. 97, 071106 (2010).